Masterthesis: Continuous Time - Quantum Monte Carlo impurity solver for the Hubbard model

Version:[1] July 2, 2014

Masterarbeit im Fach Physik
vorgelegt der Mathematisch-Naturwissenschaflichen Fakultät
der Universität Augsburg

angefertigt von Markus Dutschke

Juni 2014

angefertigt am Lehrstuhl für Theoretische Physik III
Zentrum für Elektronische Korrelationen und Magnetismus
Institut für Physik der Universität Augsburg
bei Prof. Dr. L. Chioncel
Zweitprüfer: Prof. Dr. T. Kopp

[1] This version was modified subsequently to correct typos and formatting issues. The nummeration of formulas may differ.
Die hier vorliegende Version, wurde im nachhinein angepasst um Tippfehler und falsche Formatierungen zu korrigieren. Die Numerierung von Formeln kann abweichen.

$$\left\langle \begin{array}{c} \textit{"Alea iacta est"} \\ \text{Julius Caesar, January 10, 49 BC} \end{array} \right\rangle_{\text{MC}}$$

Program code

In the following the program code, which was written in the context of this Masterthesis, is listed and differentiated from the programs, which were used but not programmed by the author:

written by Markus Dutschke in the context of this Masterthesis:

- DMFT loop: as described in 1.4
- CT-QMC solver: as described in 3
- different shell scripts used for job handling on ALCC and on local computers

written by others:

- fast Fourier transformation: written by Junya Otsuki, 2009, Dept. of Physics, Tohoku University, Sendai, Japan
- analytic continuation (maxent): implemented by Mark Jarrell and J.E. Gubernatis, 1990 following [5, 27]

Contents

Abstract

Strongly correlated electron systems provide a large variety of interesting phenomena including superconductivity, quantum information or quantum computing that triggers an intense interest towards correlated electron materials. The prototype models of correlated electron systems are the Hubbard and the Kondo models and it is known that these models are in general not solvable analytically. The difficulty steam from the none perturbative nature of these problems, and existing analytical solutions are always bases on serious simplifications [9, 11]. A very efficient method, suitable to describe these kind of systems is the so called Dynamical Mean Field Theory (DMFT). DMFT is based on the mapping of the many-particles/orbitals Hubbard model into a single impurity Anderson Model. In the pioneering work of Metzner and Vollhardt [24] it is shown that the Hubbard model is exactly solvable in the limit of infinite coordination number z. For the Hubbard model in a face-centered cubic lattice at three dimensions the number of nearest neighbours is $z = 12$ and even though z is finite DMFT provides a useful solution. The systematic increase in computational power contributed significantly to the development and the success of DMFT.

A recent development in the field of correlated electrons materials is the combination of DMFT with the Density Functional Theory (DFT) [18]. DFT provides the realistic materials input while the problem of the interactions between electrons is solved within DMFT. In such a combined approach the weakly coupled/correlated electrons (on s,p orbitals) are treated using DFT and the strongly correlated electrons (on d or f orbitals) are treated using DMFT.

This work will focus on the description of strongly correlated electrons using DMFT. From a technical point of view DMFT was formulated in a close set of self-consistent equations, in which the most important step - the impurity solver - is non trivial. There are several impurity solvers available, which use different methods and are efficient in different parameter regimes. In the followings a brief list of different solvers is presented:

- Iterative Perturbation Theory (IPT): historically one of the first solvers, that implements the computation of the second-order self-energy.

- Numerical Renormalization Group (NRG): is an accurate and broadly used zero temperature solver, extension for finite temperatures being available.

- Hirsch-Fye Quantum Monte Carlo (HF-QMC): very extensively used solver for models with few orbitals, prior to the invention of the continuous time version. Its computational complexity increases for multiband systems and low temperatures considerably.

- Continuous-time Quantum Monte Carlo (CT-QMC): an improved solver using QMC. Low temperatures and multi-orbitals are accessible. Runtime and precision continuously adjustable.

- Exact Diagonalisation (ED): exact solver, but limited due to the dimension of the Hilbert space. efficient and precise for small systems

More recent solvers implement DMRG, PEPS....

The usual QMC procedure consists in statistical sampling of terms derived from a perturbative expansion. There are several ways to perform the perturbative expansion. Expanding upon the interaction gives rise to the method called interaction expansion CT-QMC(-INT). Another option is the auxiliary field expansion which is a technique developed starting from the HF-QMC. The present work deals with the technicalities, fundamental concepts and the implementation of a Continuous-Time Quantum Monte Carlo (CT-QMC) solver in hybridisation expansion (CT-HYB), together with the application of the Hubbard model in magnetic field at half-filling. The thesis is structured as follows:

In the **1. Chapter**, the cavity construction is discussed as the key concept used for the mapping of the lattice model into a single impurity. The formulation of the effective action is given and the concepts of bath green's function/Weiss field, local Green's function are introduced. These quantities are essential for the derivation of the self-consistent set of Dynamical Mean Field Theory equations. The consequence of a finite number of Matsubara frequencies is the presence of high energy tails of the Green's function and/or self-energy. This problem is also discussed in this chapter in connection to the computation of the number of particles.

In the **2. Chapter** the solution of the single Anderson impurity model is presented. For the analytic solution the equation of motion technique is used. For the sake of simplicity the hybridization expansion is illustrated on the spinless single impurity Anderson model using the technique called the segment picture. The corresponding extension including spin and magnetic field is also presented. At the end of the chapter the evaluation of the one particle (Green's function) and two particle (susceptibility) correlation function is discussed.

Chapter 3 deals with the practical implementation of CT-QMC algorithm. The essentials of the Monte Carlo scheme are introduced the metropolis and the detailed balance condition are discussed. The updating processes are described in detail, such as the fast update scheme together with many computational details and testing aspects of the code. The analytic solution from Chapter 2 as well as the technicalities turned out to be essential for testing purposes.

The numerical results for the Hubbard model in magnetic field at half-filling are presented in **Chapter 4**. These are the original results of the thesis and are compared with the paper of Bauer et. al. [3]. The effective mass enhancement as a function of the applied field is discussed. A good agreement with the results using the NRG method of Bauer et. al. [3] is obtained.

1. Introduction to DMFT

The Hubbard model is a quantum mechanical model to describe interacting electrons on a lattice. In its simple form it describes the competition between the kinetic energy corresponding to the hopping and a local interaction. The kinetic energy corresponds to the hopping process from one lattice site to another. Suppressing the interaction-term, the Hubbard model becomes the usual tight binding model known from solid state physics, characterized by the hopping amplitude t. The hopping amplitude between neighbouring sites represents physically the overlap between the atomic orbitals, centered on the neighbouring sites. The electronic interaction in the Hubbard model is modelled by the so-called on-site repulsion U, when two electrons happen to be on the same lattice site. For fermionic systems, due to the Pauli principle, there can only be 2 electrons with opposite spins per lattice site. So in the single band Hubbard model electrons with the same spin can never interact while in the multiband Hubbard models such interaction is present.

The Hubbard model can only be solved analytically in special limits and in one dimension [9]. Being a lattice model the number of sites considered on the lattice is limited by the dimension of the Hilbert space. Stochastic methods, based on Monte Carlo sampling for the lattice problem, exist and may provide exact solutions. However for very low temperatures and large system sizes the computational effort increases siginificantly. Alternatively, the Hubbard model can also be studied using Dynamical Mean Field Theory (DMFT) which becomes exact in the limit of infinite connectivity z [10]. The DMFT scheme maps self-consistently the lattice problem into a single site Anderson impurity model (SIAM), and in this way simplifies the problem considerably. The SIAM consists of only one lattice site (the impurity) and a non interacting bath coupled to it. The impurity is one of the lattice sites of the lattice model. The bath models the presence of all lattice sites and the hopping into and outof the impurity. Particles can jump from the bath on the lattice site with a hybridisation term V and interact there with a particle with opposite spin (single orbital case). The interaction is again represented by the same U parameter. The Pauli principle holds here as well and restricts the maximum number of particles on this impurity to one, for each spin in the single orbital case.

As the impurity model is in general easier to solve using numerical methods (this is called the impurity solver), one can calculate the Green function on this impurity. The local approximation of DMFT states that this impurity Green function is equal to the local Green function of the lattice.

In many examples the single orbital Hubbard model is considered on a Bethe lattice. The Bethe lattice, also called "Cayley tree", is a lattice with infinite connectivity, which results in

a semicircular non interacting density of states with bandwidth $D = 2t$. The non-interacting density of states serves as an input parameter for the simulations performed.

1.1. Cavity method

The following derivation is similar to [11–13, 15, 17, 28]. The cavity method describes the mapping of a lattice problem to a single site in a mean field. The basic idea is, that we take one special lattice site (site 0) and integrate out all other degrees of freedom in the partition function. By this we derive an effective action and the "Weiss field".

First we start with the Hubbard Hamiltonian

$$\hat{H} = -\sum_{<i,j>,\sigma} t_{i,j}\hat{c}^{\dagger}_{i,\sigma}\hat{c}_{j,\sigma} + \sum_{i} U\hat{n}_{i,\uparrow}\hat{n}_{i,\downarrow} - \sum_{i}\mu\left(\hat{n}_{i,\uparrow} + \hat{n}_{i,\downarrow}\right). \tag{1.1}$$

with

$$t_{i,j} = t_{j,i} \in \mathbb{R} \tag{1.2}$$

(needed for a hermitian Hamiltonian, $t_{i,j} \in \mathbb{C}$ is only needed if a magnetic vector potential is included into the Hamiltonian) and $\sum_{<i,j>}$ denoting the sum over all pairs of lattice sites (counting each pair only once in contrast to $\sum_{i,j}$).

The partition function then writes

$$Z = \int \prod_{i} \mathrm{D}c^{*}_{i,\sigma}\mathrm{D}c_{i,\sigma}e^{-S} \tag{1.3}$$

(where c and c^{*} are Grassmann numbers) with the corresponding action [6]

$$S = \int_{0}^{\beta} \mathrm{d}\tau \left[\sum_{i,\sigma} c^{*}_{i,\sigma}(\tau)\left(\frac{\partial}{\partial\tau} - \mu\right)c_{i,\sigma}(\tau) - \sum_{i,j,\sigma} t_{i,j}c^{*}_{i,\sigma}(\tau)c_{j,\sigma}(\tau) + \sum_{i} U n_{i,\uparrow}(\tau)n_{i,\downarrow}(\tau)\right]. \tag{1.4}$$

Now we split the contributions to the action up into 3 parts:

$$S = S_0 + \Delta S + S^{(0)}. \tag{1.5}$$

S_0 is called the cavity part, ΔS is called the exchange part and $S^{(0)}$ is called the **cavity-lattice** part (which **is the lattice with the cavity removed**).

$$S_0 = \int_{0}^{\beta} \mathrm{d}\tau \left[\sum_{\sigma} c^{*}_{0,\sigma}(\tau)\left(\frac{\partial}{\partial\tau} - \mu\right)c_{0,\sigma}(\tau) + U n_{0,\uparrow}(\tau)n_{0,\downarrow}(\tau)\right] \tag{1.6}$$

describes all processes, which are restricted to site 0,

$$\Delta S = -\int_0^\beta \mathrm{d}\tau \left[\sum_{i,\sigma} t_{i,0} c^*_{i,\sigma}(\tau) c_{0,\sigma}(\tau) + t_{0,i} c^*_{0,\sigma}(\tau) c_{i,\sigma}(\tau) \right] \tag{1.7}$$

describes all exchange processes between site 0 and the other sites,

$$\begin{aligned} S^{(0)} = \int_0^\beta \mathrm{d}\tau \Bigg[& \sum_{i\neq 0,\sigma} c^*_{i,\sigma}(\tau) \left(\frac{\partial}{\partial \tau} - \mu \right) c_{i,\sigma}(\tau) - \sum_{i\neq 0, j\neq 0,\sigma} t_{i,j} c^*_{i,\sigma} c_{j,\sigma}(\tau) + \\ & + \sum_{i\neq 0} U n_{i,\uparrow}(\tau) n_{i,\downarrow}(\tau) \Bigg] \end{aligned} \tag{1.8}$$

describes all processes, which are not related to site 0. Further we define the ensemble average (of the cavity-lattice) as

$$\langle X \rangle_{(0)} \equiv \frac{1}{Z_{(0)}} \int \prod_{i\neq 0,\sigma} \mathrm{D}c^*_{i,\sigma} \mathrm{D}c_{i,\sigma} X e^{-S^{(0)}}; \quad Z_{(0)} = \int \prod_{i\neq 0,\sigma} \mathrm{D}c^*_{i,\sigma} \mathrm{D}c_{i,\sigma} e^{-S^{(0)}}. \tag{1.9}$$

To get now the effective action S_{eff}, we integrate out all the cavity-lattice degrees of freedom. We start with the definition of the effective action by the ensemble averager and introduce a random expression X, which only depends on $c^*_{0,\sigma}$ and $c_{0,\sigma}$:

$$\langle X \rangle_{\text{eff}} \stackrel{!}{=} \langle X \rangle \text{ with } X = X(c^*_{0,\sigma}, c_{0,\sigma}) \Leftrightarrow \tag{1.10}$$

$$\frac{1}{Z_{\text{eff}}} \int \prod_{\sigma} \mathrm{D}c^*_{0,\sigma} \mathrm{D}c_{0,\sigma} X e^{-S_{\text{eff}}} \stackrel{!}{=} \frac{1}{Z} \int \prod_{i,\sigma} \mathrm{D}c^*_{i,\sigma} \mathrm{D}c_{i,\sigma} X e^{-S} \tag{1.11}$$

$$= \frac{1}{Z} \int \prod_{\sigma} \mathrm{D}c^*_{0,\sigma} \mathrm{D}c_{0,\sigma} X e^{-S_0} \int \prod_{i\neq 0,\sigma} \mathrm{D}c^*_{i,\sigma} \mathrm{D}c_{i,\sigma} e^{-\Delta S - S^{(0)}} \tag{1.12}$$

$$= \frac{Z_{(0)}}{Z} \int \prod_{\sigma} \mathrm{D}c^*_{0,\sigma} \mathrm{D}c_{0,\sigma} X e^{-S_0} \langle e^{-\Delta S} \rangle_{(0)}. \tag{1.13}$$

The effective action follows as

$$S_{\text{eff}} = S_0 + \ln \langle e^{-\Delta S} \rangle_{(0)}. \tag{1.14}$$

We express $\langle e^{-\Delta S} \rangle_{(0)}$ by its Taylor series. The odd powers of the Taylor expansion of $e^{-\Delta S}$ do not contribute, as we have an odd number of cavity-lattice operators (i.e. $c^*_{i,\sigma}$ or $c_{i,\sigma}$). The ensemble average for odd parameters hence yields 0.

$$\langle e^{-\Delta S} \rangle_{(0)} = \sum_{n=0}^{\infty} \frac{\langle (-\Delta S)^n \rangle_{(0)}}{n!} = \sum_{n=0}^{\infty} \frac{\langle (\Delta S)^{2n} \rangle_{(0)}}{(2n)!}. \tag{1.15}$$

Further we use the following statement:

$$\begin{aligned}\mathbb{A}: \quad (\Delta S)^{2n} = &\sum_{m=0}^{2n} \binom{2n}{m} (-1)^{n-m} \int \mathrm{d}\tau_1 \dots \mathrm{d}\tau_m \mathrm{d}\tau'_1 \dots \mathrm{d}\tau'_{2n-m} \sum_{i_1,\dots,i_m,j_1,\dots,j_{2n-m}} \\ &\times t_{0,i_1} \dots t_{0,i_m} t_{j_1,0} \dots t_{j_{2n-m},0} \\ &\times c_0^*(\tau_1) \dots c_0^*(\tau_m)\, c_0(\tau'_1) \dots c_0(\tau'_{2n-m}) \\ &\times c_{i_1}(\tau_1) \dots c_{i_m}(\tau_m) c_{j_1}^*(\tau'_1) \dots c_{j_{2n-m}}^*(\tau'_{2n-m}) \qquad (1.16) \\ \equiv &\sum_{m=0}^{2n} \binom{2n}{m} (-1)^{n-m} F_m^{2n}. \qquad (1.17)\end{aligned}$$

Here F_m^{2n} is used as an abbreviating notation, which will only be used in the proof of this statement.
For simplicity we dropped the spin index σ. This can be done, as the hopping is spin independent. This convention will hold until equation (1.24), where we reintroduce σ again.

This statement can be shown via induction. For clearness lengthly proofs are written with a margin and in a smaller font size.
First we show the $n = 1$ case:

$$\begin{aligned}&(-\Delta S)^2 \\ &= \int_0^\beta \mathrm{d}\tau_i \left[\sum_i t_{i,0} c_i^*(\tau_i) c_0(\tau_i) + t_{0,i} c_0^*(\tau_i) c_i(\tau_i)\right] \int_0^\beta \mathrm{d}\tau_j \left[\sum_j t_{j,0} c_j^*(\tau_j) c_0(\tau_j) + t_{0,j} c_0^*(\tau_j) c_j(\tau_j)\right] \\ &= \int_0^\beta \mathrm{d}\tau_i \mathrm{d}\tau_j \sum_{i,j} \big[t_{i,0} t_{j,0} c_i^*(\tau_i) c_0(\tau_i) c_j^*(\tau_j) c_0(\tau_j) + t_{i,0} t_{0,j} c_i^*(\tau_i) c_0(\tau_i) c_0^*(\tau_j) c_j(\tau_j) \\ &\quad + t_{0,i} t_{j,0} c_0^*(\tau_i) c_i(\tau_i) c_j^*(\tau_j) c_0(\tau_j) + t_{0,i} t_{0,j} c_0^*(\tau_i) c_i(\tau_i) c_0^*(\tau_j) c_j(\tau_j)\big] \\ &= -F_0^2 + 2F_1^2 - F_2^2.\end{aligned}$$

For the induction step we use the following relations:

$$F_m^{2n} \cdot F_0^2 = F_m^{2(n+1)}; \quad F_m^{2n} \cdot F_1^2 = F_{m+1}^{2(n+1)}; \quad F_m^{2n} \cdot F_2^2 = F_{m+2}^{2(n+1)},$$

which are easily verifiable. Now, we can proof the assumption.

$$
\begin{aligned}
(-\Delta S)^{2(n+1)} =& (-\Delta S)^{2n}(-\Delta S)^2 \overset{\mathbb{A}}{=} \sum_{m=0}^{2n} \binom{2n}{m} (-1)^{n-m} F_m^{2n} \cdot \left(-F_0^2 + 2F_1^2 - F_2^2\right) \\
=& \sum_{m=0}^{2n} \binom{2n}{m} (-1)^{n+1-m} F_m^{2(n+1)} + \sum_{m=0}^{2n} \binom{2n}{m} (-1)^{n-m} 2F_{m+1}^{2(n+1)} \\
&+ \sum_{m=0}^{2n} \binom{2n}{m} (-1)^{n+1-m} F_{m+2}^{2(n+1)} \\
=& \sum_{m=0}^{2n} \binom{2n}{m} (-1)^{n+1-m} F_m^{2(n+1)} + \sum_{m=1}^{2n} \binom{2n}{m-1} (-1)^{n-(m-1)} 2F_m^{2(n+1)} \\
&+ \sum_{m=2}^{2n} \binom{2n}{m-2} (-1)^{n-(m-2)} F_m^{2(n+1)} \\
=& \binom{2n}{0} (-1)^{n+1-0} F_0^{2(n+1)} + \left[\binom{2n}{1} + 2\binom{2n}{0}\right] (-1)^{n+1-1} F_1^{2(n+1)} \\
&+ \sum_{m=2}^{2n} \left[\binom{2n}{m} + 2\binom{2n}{m-1} + \binom{2n}{m-2}\right] (-1)^{n+1-m} F_m^{2(n+1)} \\
&+ \left[\binom{2n}{2n} + \binom{2n}{2n-1}\right] (-1)^{n+1-(2n+1)} F_{2n+1}^{2(n+1)} + \left[\binom{2n}{2n}\right] (-1)^{n-2(n+1)} F_{2(n+1)}^{2(n+1)} \\
=& \binom{2(n+1)}{0} (-1)^{n+1-0} F_0^{2(n+1)} + \left[\binom{2(n+1)}{1}\right] (-1)^{n+1-1} F_1^{2(n+1)} \\
&+ \sum_{m=2}^{2n} \left[\binom{2(n+1)}{m}\right] (-1)^{n+1-m} F_m^{2(n+1)} + \left[\binom{2(n+1)}{2n+1}\right] (-1)^{n+1-(2n+1)} F_{2n+1}^{2(n+1)} \\
&+ \left[\binom{2(n+1)}{2(n+1)}\right] (-1)^{n+1-2(n+1)} F_{2(n+1)}^{2(n+1)} \\
=& \sum_{m=0}^{2(n+1)} \binom{2(n+1)}{m} (-1)^{n+1-m} F_m^{2(n+1)}
\end{aligned}
$$

If we take the ensemble average, only the term with $m = n$ survives. Note again, that τ_n, τ_n' denote imaginary times and i_n,j_n denote lattice sites and the spin on those lattice sites. These quantities are independent of each other even if they have the same index.

$$
\begin{aligned}
\langle e^{-\Delta S} \rangle_{(0)} =& \sum_{n=0}^{\infty} \frac{(-1)^n}{(n!)^2} \int \mathrm{d}\tau_1 \ldots \mathrm{d}\tau_n \mathrm{d}\tau_1' \ldots \mathrm{d}\tau_{j_n} \sum_{i_1,\ldots,i_n,j_1,\ldots,j_n} \\
&\times t_{0,i_1} \ldots t_{0,i_n} \cdot t_{j_1,0} \ldots t_{j_n,0} \cdot c_0^*(\tau_1) \ldots c_0^*(\tau_n) \cdot c_0(\tau_1') \ldots c_0(\tau_n') \\
&\times G^{(0)}_{i_1,\ldots,i_n,j_1,\ldots,j_n}(\tau_1, \ldots, \tau_n, \tau_1', \ldots, \tau_n')
\end{aligned} \tag{1.18}
$$

with

$$
G^{(0)}_{i_1,\ldots,i_n,j_1,\ldots,j_n}(\tau_1, \ldots, \tau_n, \tau_1', \ldots, \tau_n') \equiv (-1)^n \langle c_{i_1}(\tau_1) \ldots c_{i_n}(\tau_n) c_{j_1}^*(\tau_1') \ldots c_{j_n}^*(\tau_n') \rangle_{(0)}. \tag{1.19}
$$

$G^{(0)}$ is the n particle Green function of the system with the cavity excluded.

According to the the linked cluster theorem [1, 23] it follows:

$$\begin{aligned} S_{eff} =& S_0 - \sum_{n=1}^{\infty} \sum_{i_1,\ldots,j_n} \int \mathrm{d}\tau_1 \ldots \mathrm{d}\tau_n \mathrm{d}\tau_1' \ldots \mathrm{d}\tau_n' \\ & \times t_{0,i_1} \ldots t_{0,i_n} t_{j_1,0} \ldots t_{j_n,0}\, c_0^*(\tau_1) \ldots c_0^*(\tau_n)\, c_0(\tau_1') \ldots c_0(\tau_n') \\ & \times (-1)^n G^{(0),c}_{i_1,\ldots,i_n,j_1,\ldots,j_n}(\tau_1,\ldots,\tau_n,\tau_1',\ldots,\tau_n') \end{aligned} \tag{1.20}$$

where $G^{(0),c}_{\ldots}$ denotes the connected n particle Greensfunction on the cavity-lattice.

1.2. Limit of infinite dimensions

The non-trivial scaling of the hopping parameter was first found by Metzner and Vollhardt in 1989 [24]. According to [11,28] the hopping parameter $t_{i,j}$ scales with $t_{i,j} \propto \frac{1}{\sqrt{2d}^{|i-j|}}$, where d is the number of dimensions.
An argument for that scaling works as follows: Let P be the probability, that an electron hops on site x (it does not matter from where). We can split P up in different hopping processes, according to the number of lattice sites Δi, that have to be passed. In the following we consider only hopping processes of order Δi:

$$P = \sum_{\Delta i} P_{\Delta i}. \tag{1.21}$$

Each $P_{\Delta i}$ combines the hopping processes from all the neighbours with distance Δi to site x (we will call those neighbouring sites $i(\Delta i)$). Because of translation invariance all hopping amplitudes are the same. We call the hopping amplitude $t_{\Delta i}$. The number of neighbours is of order $(2d)^{\Delta i}$. So it follows

$$P_{\Delta i} = \sum_{i(n)} |t_{i(n),x}|^2 \propto (2d)^{\Delta i} |t_{\Delta i}|^2 \tag{1.22}$$

With $P_{\Delta i}$ being of order 1 we get directly:

$$t_{\Delta i} \propto (2d)^{-\frac{\Delta i}{2}}. \tag{1.23}$$

From that other scaling properties follow:

- $\sum_{i_x} \propto d^{\Delta i}$; $\sum_{j_x} \propto d^{\Delta i}$; i_x, j_x are site indices, because these are the number of neighbors in the considered distance.

- $G^{(0)}_{i_1,\ldots,j_n} = (-1)^n \langle c_{i_1}(\tau_1) \ldots c^*_{j_n}(\tau_n') \rangle_{(0)} \propto \frac{1}{(2d)^{\Delta i(2(n-1)+1)}}$ with every index a different lattice site.
  This follows from the fact, that for every c/c^* in the average, there has to be a c^*/c

from the expansion of the exponential function $e^{-S^{(0)}}$. Otherwise the term would vanish in the cavity-lattice average. With every set of $c_i^* c_j$ from the expansion, there also gets a factor $t_{i,j}$ into the term. In the case with the highest contribution to S_{eff} (i.e. lowest number of $t_{...}$ factors), i and j are both nearest neighbours to site 0. [1] The power of $2(n-1)+1$ is a combinatoric issue, because we consider connected Green functions here. $2(n-1)+1$ is the minimal number of terms, which is needed from the expansion of $e^{-S^{(0)}}$ to produce a connected Green function, as illustrated in figure 1.1.

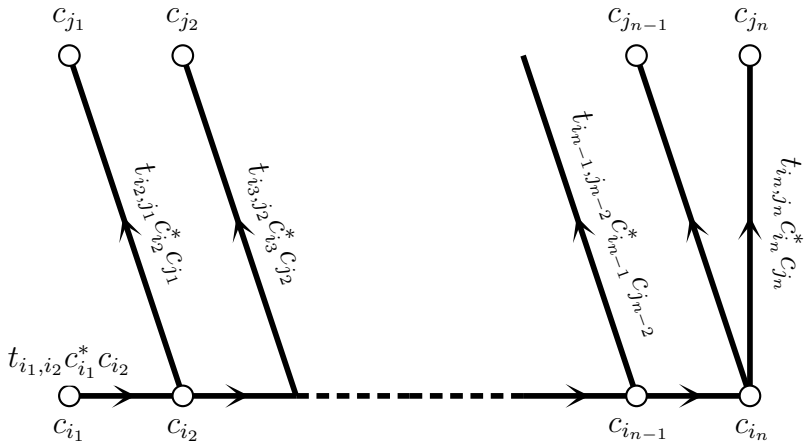

Figure 1.1.: Schematic picture of the lowest-order (in $t_{i,j}$) connected diagram. Each of the $2(n-1)+1$ lines contributes a factor $t_{i,j}$ as well as a c_a^* and a c_b to get an even number of operators for each lattice site.

From that it follows, that the contribution to S_{eff}, which has a n-particle Green function, is proportional to $d^{\Delta i(1-n)}$.

For the case, that two lattice sites are equal, this result stays the same, as there is a factor $d^{\Delta i}$ from the sums and a factor $\frac{1}{d^{\Delta i}}$ from the Green function less. The argument for more than two lattice sites being the same works analogue.

We see, that in the limit of infinite dimensions only the $n = 1$ contribution survives and the effective action results to:

$$S_{eff} = -\sum_{\sigma} \int_0^\beta \mathrm{d}\tau_1 \mathrm{d}\tau_2 \, c^*_{0,\sigma}(\tau_1) \mathcal{G}^{-1}_{\sigma}(\tau_1 - \tau_2) c_{0,\sigma}(\tau_2) + \int_0^\beta \mathrm{d}\tau \, U n_{0,\uparrow}(\tau) n_{0,\downarrow}(\tau) \tag{1.24}$$

$$\begin{aligned} \mathcal{G}^{-1}_{\sigma}(\tau_1 - \tau_2) &= -\left(\frac{\mathrm{d}}{\mathrm{d}\tau_1} - \mu\right) \delta_{\tau_1,\tau_2} - \sum_{i,j} t_{i,0} t_{0,j} G^{(0)}_{i,j,\sigma}(\tau_1 - \tau_2) \\ &\equiv -\left(\frac{\mathrm{d}}{\mathrm{d}\tau_1} - \mu\right) \delta_{\tau_1,\tau_2} - \Delta(\tau_1 - \tau_2). \end{aligned} \tag{1.25}$$

[1] Therefore they have Manhattan distance 2 to each other (the case, that i and j denote the same lattice site is discussed later). This is the reason, why the square root is missing.

$\mathcal{G}_\sigma^{-1}$ is called the Weiss field. We also reintroduced the spin index σ. We have now an 1-particle Green function included. As we have spin conservation at every vertex, we get the condition $\sigma_i = \sigma_j$. Hence we introduce just one index σ for that.

1.3. Local approximation

So far we derived an effective action S_{eff} equation (1.25), which contains only a single particle Green function. Unfortunately the effective action depends on the cavity-lattice Green function $G^{(0)}$.The problem with the cavity-lattice Green function is, that it represents the lattice without the cavity and still does not allow to solve the problem. The task is now, to express the cavity-lattice Green function by better accessible quantities. In the limit of infinite dimensions the cavity Green function can also be expressed as

$$G^{(0)}_{i,j,\sigma} = G_{i,j,\sigma} - \frac{G_{i,0,\sigma} G_{0,j,\sigma}}{G_{0,0,\sigma}}. \tag{1.26}$$

This expression was derived by Hubbard [15, 17]. [2] So the difference between the Green function of the lattice without the cavity and the lattice with the cavity, are all paths which go through site 0. Because of the $d \to \infty$ limit only paths are considered, which pass site 0 once. To avoid counting the paths entering and leaving site 0 twice, we need the factor $\frac{1}{G_{0,0,\sigma}}$.

We Fourier transform the Weiss field (equation (1.25)) with respect to the time domain [3]

$$f(\tau) = \sum_{\omega_n} f(i\omega_n) e^{-i\omega_n \tau};\ \delta_{\tau_1,\tau_2} = \sum_{\omega_n} e^{-i\omega_n(\tau_1-\tau_2)}. \tag{1.27}$$

The Weiss field in Matsubara domain hence reads

$$\mathcal{G}_\sigma^{-1}(i\omega_n) = i\omega_n + \mu - \sum_{i,j} t_{i,0} t_{0,j} G^{(0)}_{i,j,\sigma}(i\omega_n) \tag{1.28}$$

$$= F^{-1}(i\omega_n) + \Sigma_\sigma(i\omega_n) - \Delta(i\omega_n) \tag{1.29}$$

with

$$F^{-1}(i\omega_n) \equiv i\omega_n + \mu - \Sigma_\sigma(i\omega_n) \tag{1.30}$$

$$\Delta(i\omega_n) \equiv \sum_{i,j} t_{i,0} t_{0,j} G^{(0)}_{i,j,\sigma}(i\omega_n). \tag{1.31}$$

[2] The proof is based on the key points:
a) the Green function can be expressed in terms of an inverse Hamilton matrix
b) the equation hence becomes a matrix equation, where the index $^{(0)}$ means, that a row and a column are set to zero
c) a similar method like the one to derive (3.34) can be used.

[3] Here we have a discrete Fourier series, due to the fact, that the Green function is only defined on the interval $\tau_1 - \tau_2 \in [-\beta; \beta]$. The discrete set of Matsubara frequencies ($\omega_n = 2n\pi/\beta$ (bosons); $\omega_n = (2n+1)\pi/\beta$ (fermions)) follows from the symmetry $G(\tau + \beta) = \pm G(\tau)$ [4].

We note that the Weiss field does not depend on the self-energy Σ, as this is added and subtracted at the same time. Δ has already been defined in imaginary time domain (1.25); for reasons of simplicity the definition is repeated.

A crucial point here is that we assumed the self-energy to be local (i.e. momentum $\boldsymbol{k}$ -independent)

$$\Sigma_\sigma(\boldsymbol{k},i\omega_n) = \Sigma_\sigma(i\omega_n). \tag{1.32}$$

This, so called **local approximation**, holds in the limit $d \to \infty$ for any order of perturbation [11, 28].

With (1.26) we can express $\Delta(i\omega_n)$ in terms of lattice Green functions instead of cavity-lattice Green functions:

$$\Delta(i\omega_n) = \sum_{i,j} t_{i,0}t_{0,j}G_{i,j,\sigma}(i\omega_n) - \frac{\left(\sum_i t_{i,0}G_{i,0,\sigma}(i\omega_n)\right)\left(\sum_j t_{0,j}G_{0,j,\sigma}(i\omega_n)\right)}{G_{0,0,\sigma}(i\omega_n)}. \tag{1.33}$$

We will express the terms of this equation in dependence of $F^{-1}(i\omega_n)$ and $G_{0,0,\sigma}(i\omega_n)$. We do so by switching to $\boldsymbol{k}$-space, as the Green function $G_{\boldsymbol{k},\sigma}(i\omega_n)$ just depends on $F^{-1}(i\omega_n)$ and $\epsilon_{\boldsymbol{k}}$ in this space (L represents the number of possible momenta): [4]

$$G_{i,j,\sigma}(i\omega_n) = \frac{1}{L}\sum_k e^{i\boldsymbol{k}(\boldsymbol{R_i}-\boldsymbol{R_j})}G_{\boldsymbol{k},\sigma}(i\omega_n) \tag{1.34}$$

$$G_{\boldsymbol{k},\sigma}(i\omega_n) = \frac{1}{F^{-1}(i\omega_n) - \epsilon_{\boldsymbol{k}}} \tag{1.35}$$

$$\epsilon_{\boldsymbol{k}} = \sum_i t_{i,0}e^{-i\boldsymbol{k}\boldsymbol{R_i}} = \sum_j t_{0,j}e^{i\boldsymbol{k}\boldsymbol{R_j}} \tag{1.36}$$

$$\epsilon_{-\boldsymbol{k}} = \sum_i t_{i,0}e^{-i(-\boldsymbol{k})\boldsymbol{R_i}} = \sum_i t_{0,i}e^{i\boldsymbol{k}\boldsymbol{R_i}} = \epsilon_{\boldsymbol{k}} \quad \text{using (1.2)} \tag{1.37}$$

$$t_{i,j} = \frac{1}{L}\sum_{\boldsymbol{k}} \epsilon_{\boldsymbol{k}}e^{i\boldsymbol{k}(\boldsymbol{R}_i-\boldsymbol{R}_j)} \tag{1.38}$$

[4] We remember the following relations: $\frac{1}{L}\sum_{\boldsymbol{k}} 1 = 1$ and $\sum_{\boldsymbol{k}} \epsilon_{\boldsymbol{k}} = 0$.

$$\begin{aligned}
\sum_i t_{i,0} G_{i,0,\sigma}(i\omega) =& \sum_i \left(\frac{1}{L} \sum_{\boldsymbol{k}_i} \epsilon_{\boldsymbol{k}_i} e^{i\boldsymbol{k}_i \boldsymbol{R}_i} \right) \left(\frac{1}{L} \sum_{\boldsymbol{k}_j} G_{\boldsymbol{k}_j,\sigma} e^{i\boldsymbol{k}_j \boldsymbol{R}_i} \right) \\
=& \frac{1}{L^2} \sum_{i,\boldsymbol{k}_i,\boldsymbol{k}_j} \epsilon_{\boldsymbol{k}_i} G_{\boldsymbol{k}_j} e^{i(\boldsymbol{k}_i+\boldsymbol{k}_j)\boldsymbol{R}_i} = \frac{1}{L^2} \sum_{\boldsymbol{k}_i,\boldsymbol{k}_j} \epsilon_{\boldsymbol{k}_i} G_{\boldsymbol{k}_j} \delta_{\boldsymbol{k}_i,-\boldsymbol{k}_j} \\
=& \frac{1}{L} \sum_{\boldsymbol{k}_j} \epsilon_{-\boldsymbol{k}_j} G_{\boldsymbol{k}_j} = \frac{1}{L} \sum_{\boldsymbol{k}} \epsilon_{\boldsymbol{k}} G_{\boldsymbol{k},\sigma} \qquad (1.39) \\
=& \frac{1}{L} \sum_{\boldsymbol{k}} \left(\frac{\epsilon_{\boldsymbol{k}} - F^{-1}(i\omega_n)}{F^{-1}(i\omega_n) - \epsilon_{\boldsymbol{k}}} + \frac{F^{-1}(i\omega_n)}{F^{-1}(i\omega_n) - \epsilon_{\boldsymbol{k}}} \right) \\
=& -1 + F^{-1}(i\omega_n) \frac{1}{L} \sum_{\boldsymbol{k}} G_{\boldsymbol{k},\sigma}(i\omega_n) \qquad (1.40) \\
=& -1 + F^{-1}(i\omega_n) G_{0,0,\sigma}(i\omega_n) \qquad (1.41)
\end{aligned}$$

$$\begin{aligned}
\sum_j t_{0,j} G_{0,j,\sigma}(i\omega) =& \sum_j \left(\frac{1}{L} \sum_{\boldsymbol{k}_i} \epsilon_{\boldsymbol{k}_i} e^{i\boldsymbol{k}_i(-\boldsymbol{R}_j)} \right) \left(\frac{1}{L} \sum_{\boldsymbol{k}_l} G_{\boldsymbol{k}_l,\sigma} e^{i\boldsymbol{k}_l(-\boldsymbol{R}_j)} \right) \\
=& \ldots \text{analogue} \ldots = -1 + F^{-1}(i\omega_n) G_{0,0,\sigma}(i\omega_n) \qquad (1.42)
\end{aligned}$$

$$\begin{aligned}
\sum_{i,j} t_{i,0} t_{0,j} G_{i,j}(i\omega_n) =& \sum_j t_{0,j} \sum_i t_{i,0} \left(\frac{1}{L} \sum_{\boldsymbol{k}_i} G_{\boldsymbol{k}_i,\sigma} e^{i\boldsymbol{k}_i(\boldsymbol{R}_i - \boldsymbol{R}_j)} \right) \\
=& \frac{1}{L} \sum_{\boldsymbol{k}_i} G_{\boldsymbol{k}_i,\sigma}(i\omega_n) \sum_j t_{0,j} e^{i\boldsymbol{k}_i(-\boldsymbol{R}_j)} \sum_i t_{i,0} e^{i\boldsymbol{k}_i \boldsymbol{R}_i} \qquad (1.43) \\
=& \frac{1}{L} \sum_{\boldsymbol{k}_i} G_{\boldsymbol{k}_i,\sigma}(i\omega_n) \epsilon_{\boldsymbol{k}_i} \epsilon_{\boldsymbol{k}_i} \qquad (1.44) \\
=& \frac{1}{L} \sum_{\boldsymbol{k}} \frac{\epsilon_{\boldsymbol{k}}(\epsilon_{\boldsymbol{k}} - F^{-1}(i\omega_n))}{F^{-1}(i\omega_n) - \epsilon_{\boldsymbol{k}}} + \frac{F^{-1}(i\omega_n)\epsilon_{\boldsymbol{k}}}{F^{-1}(i\omega_n) - \epsilon_{\boldsymbol{k}}} \qquad (1.45) \\
=& 0 + F^{-1}(i\omega_n) \frac{1}{L} \sum_{\boldsymbol{k}} \epsilon_{\boldsymbol{k}} G_{\boldsymbol{k},\sigma} \\
\overset{(1.41)}{=}& -F^{-1}(i\omega_n) + F^{-1}(i\omega_n)^2 G_{0,0,\sigma}(i\omega_n) \qquad (1.46)
\end{aligned}$$

and get

$$\begin{aligned}
\Delta(i\omega_n) =& -F^{-1}(i\omega_n) + F^{-1}(i\omega_n)^2 G_{0,0,\sigma}(i\omega_n) - \frac{\left(-1 + F^{-1}(i\omega_n) G_{0,0,\sigma}(i\omega_n)\right)^2}{G_{0,0,\sigma}(i\omega_n)} \qquad (1.47) \\
=& F^{-1}(i\omega_n) - G^{-1}_{0,0,\sigma}(i\omega_n). \qquad (1.48)
\end{aligned}$$

It follows the **Dyson-like equation** for the Weiss field:

$$\mathcal{G}^{-1}_\sigma(i\omega_n) = G^{-1}_{0,0,\sigma}(i\omega_n) + \Sigma_\sigma(i\omega_n). \qquad (1.49)$$

We managed in this way, to express the Weiss field in terms of the local lattice Green function and the self-energy. Equation (1.49) relates these three quantities in exactly the same way to each other, like the Dyson equation does.

$$G^{\text{non int.}\,-1}_{0,0,\sigma}(i\omega_n) = G^{-1}_{0,0,\sigma}(i\omega_n) + \Sigma_\sigma(i\omega_n). \qquad (1.50)$$

We introduced the Weiss field to subsume the contributions to the effective action by propagation processes on the cavity; now we can deduce, that the Weiss field is the non-interacting local lattice Green function of the Hubbard model

$$G^{\text{non int.}}_{0,0,\sigma}(i\omega_n) = \mathcal{G}_\sigma(i\omega_n). \tag{1.51}$$

1.4. DMFT scheme

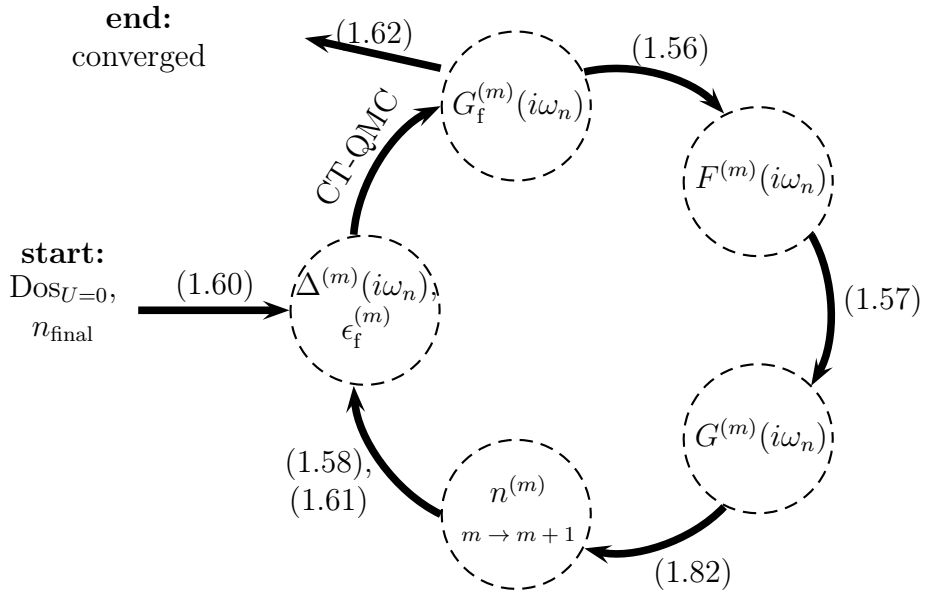

Figure 1.2.: numerical scheme of the implementation of the DMFT loop.

1.4.1. Set of self-consistent equations

In the following all impurity quantities are denoted by an index $\ldots_{\mathrm{f}}$ the lattice quantities have no additional index. $\mathcal{G}_{(\mathrm{f})}$ denotes the non-correlated ($U = 0$) Green function on the cavity (impurity).

To achieve a self consistent DMFT loop, we start with an initial guess for the hybridisation function in the lattice model (1.60). The effective action, we achieve

$$S_{eff} = -\sum_{\sigma} \int_0^{\beta} \mathrm{d}\tau_1 \mathrm{d}\tau_2 c^*_{0,\sigma}(\tau_1) \mathcal{G}^{-1}_{\sigma}(\tau_1 - \tau_2) c_{0,\sigma}(\tau_2) + \sum_{\sigma} \int_0^{\beta} \mathrm{d}\tau U n_{0,\uparrow}(\tau) n_{0,\downarrow}(\tau) \tag{1.52}$$

$$\mathcal{G}^{-1}_{\sigma}(i\omega_n) = i\omega_n + \mu - \Delta(i\omega_n) \tag{1.53}$$

is the same as in the Single Impurity Anderson Model (SIAM) with the Hamiltonian (1.1) with integrated out bath degrees of freedom. The comparison of S_{eff} of both models yield the following relation between the parameters of the Hubbard model and the SIAM:

$$\epsilon_{\mathrm{f},\sigma} = -\mu \tag{1.54}$$

$$|V|^2 = \int \omega^2 \mathrm{Dos}(\omega)\,\mathrm{d}\omega - \left(\int \omega \mathrm{Dos}(\omega)\,\mathrm{d}\omega\right)^2, \tag{1.55}$$

where we used $\mathrm{Dos}(\omega') = \sum_{\boldsymbol{k}} \delta(\omega' - \epsilon_{\boldsymbol{k}})$. The hybridisation function Δ_{f} of the SIAM, as defined in (2.55), is then equal to the hybridisation function of the Hubbard model Δ.

The next step is called the "impurity solver". [5] The purpose of all impurity solvers is to derive some correlated quantity (G_{imp} or Σ) from some non-correlated quantity (like Δ_{f} or $\mathcal{G}_{\mathrm{f}}$) in the impurity model.

To show how F_{f} is constructed from the impurity Green function and the hybridisation function, we start with the definition of $F_{\mathrm{f},\sigma}(i\omega_n) \equiv \frac{1}{i\omega_n + \mu - \Sigma_{\mathrm{f},\sigma}(i\omega_n)}$. We put in there the Dyson equation, which defines the self-energy $\Sigma \equiv \mathcal{G}^{-1} + G_{\mathrm{f}}^{-1}$. Then we use the analytic solution of the non-interacting SIAM $\mathcal{G}^{-1} = i\omega_n + \mu - \Delta$ (proven in equation (2.24)[6]) and yield

$$F_{\mathrm{f},\sigma}(i\omega_n) = \frac{1}{G^{-1}_{\mathrm{f},\sigma}(i\omega_n) + \Delta(i\omega_n)}. \tag{1.56}$$

The problem is now, that we have to get back to the lattice quantities. This can be done by the local approximation of the self-energy $\Sigma_{\mathrm{f},\sigma}(i\omega_n) \equiv \Sigma_\sigma(i\omega_n)$, which is demonstrated in perturbation theory in [11,25,28] As a consequence the quantity $F(i\omega_n) = i\omega_n + \mu - \Sigma_\sigma(i\omega_n) = i\omega_n + \mu - \Sigma_{\mathrm{f},\sigma}(i\omega_n) = F_{\mathrm{f}}(i\omega_n)$ is now the same in both models. According to (1.48) the lattice Green function is

$$G_\sigma(i\omega_n) \equiv G_{0,0,\sigma}(i\omega_n) = \int \frac{\mathrm{Dos}(\omega)}{F^{-1}_\sigma(i\omega_n) - \omega} \mathrm{d}\omega. \tag{1.57}$$

The hybridisation function now follows from (1.48)

$$\Delta(i\omega_n) = F^{-1}_\sigma(i\omega_n) - G^{-1}_\sigma(i\omega_n). \tag{1.58}$$

Now we arrived back at the beginning and have the necessary input for the impurity solver again.

[5] There are several impurity solvers available like IPT, NRG, HF-QMC, CT-QMC, exact diagonalisation, ... Those are usable for different parameter regimes like, zero or finite temperature, etc. (for details compare 1). We will later use a CT-QMC solver, which derives the correlated impurity Green function $G_{\mathrm{f}}(i\omega_n)$ from the hybridisation function $\Delta(i\omega_n)$.

[6] $\mathcal{G}_{\mathrm{f}} = G_{\mathrm{f}}$ as this prove is based on a non-interacting Hamiltonian

1.4.2. Initialisation

To begin the self consistency loop, we have to choose a suitable starting point. According to equation (1.44), we choose the hybridisation function to be

$$\Delta(i\omega_n) = \frac{1}{L}\sum_{\boldsymbol{k}_i} \epsilon_{\boldsymbol{k}_i} G_{\boldsymbol{k}_i,\sigma}(i\omega_n)\epsilon_{\boldsymbol{k}_i} \approx \frac{1}{L}\sum_{\boldsymbol{k}_i} \epsilon^2_{\boldsymbol{k}_i} G_\sigma(i\omega_n) \tag{1.59}$$

$$= \int \mathrm{Dos}(\omega)\omega^2 \mathrm{d}\omega\, G_\sigma(i\omega_n) \approx \int \mathrm{Dos}(\omega)\omega^2 \mathrm{d}\omega\, g_\mathrm{c}(i\omega_n), \tag{1.60}$$

where the interaction lattice Green function G is approximated by the non interacting one g_c (for details compare 2.55). We remember, that the purpose of this is not to do an accurate approximation, but to find a casual initial value for the hybridisation function.

1.4.3. Mixing

To stabilize this self consistent loop, we use something called mixing. The use of this is to prevent the system from diverging immediately and to support convergence. This is done by mixing the old and the new hybridisation function to achieve the hybridisation function for the next iteration.

$$\Delta^{(m)}(i\omega_n) = \mathfrak{m}\Delta^{(\mathrm{new})} + (1-\mathfrak{m})\Delta^{(m-1)} \tag{1.61}$$

1.4.4. Convergence

Convergence is established, if there is no more significant change in $G_\mathrm{f}(i\omega_n)$ and $G(i\omega_n)$ compared to the run before. For the results presented in this thesis the convergence criteria

$$||G_\mathrm{f}^{(m)} - G_\mathrm{f}^{(m-1)}|| \equiv \sum_{n=0}^{\infty} |G_\mathrm{f}^{(m)}(i\omega_n) - G_\mathrm{f}^{(m-1)}(i\omega_n)| = \mathcal{O}(10^{-4}) \tag{1.62}$$

was used.

The whole scheme for the implementation of the DMFT loop can be seen in figure 1.2.

1.5. Particle number

To perform computations away from half filling (compare sec. 1.6), it is important to calculate the average occupation number $\langle n\rangle$ on the lattice. We can adjust the chemical potential afterwards in such a way, that we achieve the wanted filling. We are going to

derive $\langle n \rangle$ from the Green function in the Matsubara domain $\bar{G}(i\omega_n)$, which is already computed in the DMFT self consistency loop. We begin with the definition of the counting operator and switch to its representation in imaginary time. η denotes a sufficiently small finite number [7] .

$$\langle n \rangle = \langle \hat{c}^\dagger \hat{c} \rangle = -\langle \mathrm{T}_\tau \hat{c}(-\eta) \hat{c}^\dagger(0) \rangle \equiv \bar{G}(\tau = -\eta) = \frac{1}{\beta} \sum_n \bar{G}(i\omega_n) e^{i\omega_n \eta} \tag{1.63}$$

In general the problem is solved at this point already, but from a numerical point of view some issues remain open. The first is, that we store only positive Matsubara frequencies but have to sum up over all Matsubara frequencies. This can be cured by the relation

$$\bar{G}(z) = \bar{G}^*(z^*) \Rightarrow \tag{1.64}$$

$$\mathfrak{Re}\left\{\bar{G}(i\omega_n)\right\} = \mathfrak{Re}\left\{\bar{G}(-i\omega_n)\right\} \tag{1.65}$$

$$\mathfrak{Im}\left\{\bar{G}(i\omega_n)\right\} = -\mathfrak{Im}\left\{\bar{G}(-i\omega_n)\right\}. \tag{1.66}$$

So we change the summation to positive n. The reason for the addition and subtraction of $\frac{1}{\omega_n} i$ will become important later, as this is the high frequency limit of the Green function.

$$\langle n \rangle = \frac{1}{\beta} \sum_n \left(\bar{G}(i\omega_n) + \frac{1}{\omega_n} i \right) e^{i\omega_n \eta} + \frac{1}{\beta} \sum_n \frac{1}{i\omega_n} e^{i\omega_n \eta} \tag{1.67}$$

$$= \frac{1}{\beta} \sum_{n \geq 0} \left[\left(\bar{G}(i\omega_n) + \frac{1}{\omega_n} i \right) e^{i\omega_n \eta} + \left(\bar{G}(-i\omega_n) + \frac{1}{-\omega_n} i \right) e^{-i\omega_n \eta} \right] + \frac{1}{\beta} \sum_n \frac{1}{i\omega_n} e^{i\omega_n \eta} \tag{1.68}$$

$$= \frac{1}{\beta} \sum_{n \geq 0} \left[\mathfrak{Re}\left\{\bar{G}(i\omega_n)\right\} \left(e^{i\omega_n \eta} + e^{-i\omega_n \eta} \right) + i \left(\mathfrak{Im}\left\{\bar{G}(i\omega_n)\right\} + \frac{1}{\omega_n} \right) \left(e^{i\omega_n \eta} - e^{-i\omega_n \eta} \right) \right] + \frac{1}{\beta} \sum_n \frac{1}{i\omega_n} e^{i\omega_n \eta} \tag{1.69}$$

A more subtle point is that we can sum up only over a finite number of Matsubara frequencies N_{Mats}. As η is very small and N_{Mats} is finite, it follows [8] :

$$e^{i\omega_n \eta} \approx 1 \approx e^{-i\omega_n \eta} \text{ for } n \leq N_{\mathrm{Mats}}. \tag{1.71}$$

Unfortunately the Green function does not vanish fast enough for large n, so that the contribution of the parts we can not store numerically, is not negligible. For $n > N_{\mathrm{Mats}}$ we can express the Green function by its high frequency limit

$$\bar{G}(i\omega_{n > N_{\mathrm{Mats}}}) \approx -\frac{1}{\omega_n} i. \tag{1.72}$$

[7] The limes $\lim_{\eta \to 0}$ is not performed here.

[8] the following condition is fulfilled if

$$0 < \eta \ll \frac{\beta}{(2N_{\mathrm{Mats}} + 1)\pi} = \frac{1}{\omega_{N_{\mathrm{Mats}}}}. \tag{1.70}$$

This is always guaranteed, as we choose η to be sufficiently small.

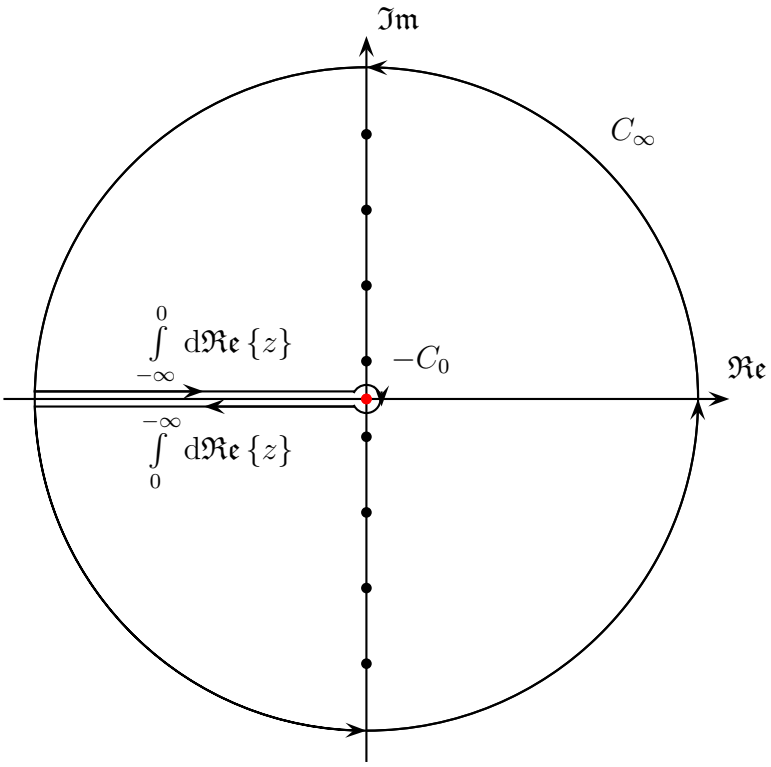

This is the **high energy tail** of the Green function. Because η is finite, for very large $|n|$ the tails of negative and positive $i\omega_n$ do not cancel out

$$n \to \infty : \qquad \bar{G}(i\omega_n) = -\frac{1}{\omega_n} i e^{i\omega_n \eta} \neq -\left(-\frac{1}{-\omega_n} i e^{-i\omega_n \eta}\right) = -\bar{G}(-i\omega_n). \tag{1.73}$$

To handle this issue we subtracted and added the high energy tail in (1.69) before. So we achieved, that the first summand in (1.69) vanishes for large n and the tail handling is treated separately in the second summand.

The second term can be shown to give $-\frac{1}{2}$:
Therefore we use Cauchy's integral formula and get

$$\frac{1}{\beta} \sum_n \frac{1}{i\omega_n} e^{i\omega_n \eta} = -\frac{1}{2\pi i} \oint_{\mathcal{C}} \frac{1}{1+e^{\beta z}} \frac{1}{z} e^{\eta z} \mathrm{d}z, \tag{1.74}$$

where $\mathcal{C}$ denotes a complex integration contour, which includes all Matsubara frequencies but not the point $z = 0$. [9]. We then simplify the integration contour to a counterclockwise circle $\mathcal{C}_\infty$ with infinite radius and a clockwise circle $-\mathcal{C}_0$ with infinitely small radius around 0.

[9] This formula can be proven by the Cauchy theorem and L'Hospital's rule. An introduction, how to handle summation over Matsubara frequencies can be found in [4]

$$= -\frac{1}{2\pi i}\left(\oint\limits_{\mathcal{C}_\infty} + \oint\limits_{-\mathcal{C}_0}\right)\frac{1}{1+e^{\beta z}}\frac{1}{z}e^{\eta z}\,\mathrm{d}z \tag{1.75}$$

$$= -\frac{1}{2\pi i}\left(\lim_{r\to\infty}\int\limits_{-\pi}^{\pi} + \lim_{r\to 0}\int\limits_{\pi}^{-\pi}\right)\frac{ie^{\eta r\cos\phi}e^{i\eta r\sin\phi}}{1+e^{\beta r\cos\phi}e^{i\beta r\sin\phi}}\,\mathrm{d}\phi. \tag{1.76}$$

In the limes $r\to\infty$ the integrand converges to [10]

$$\lim_{r\to\infty}\frac{ie^{\eta r\cos\phi}e^{i\eta r\sin\phi}}{1+e^{\beta r\cos\phi}e^{i\beta r\sin\phi}} \propto \begin{cases} \lim\limits_{r\to\infty}\frac{1}{e^{(\beta-\eta)r\cos\phi}} = 0 & \text{for } \cos\phi > 0 \\ \lim\limits_{r\to\infty} e^{\eta r\cos\phi} = 0 & \text{for } \cos\phi < 0. \end{cases} \tag{1.77}$$

Hence the $\oint\limits_{\mathcal{C}_\infty}$ contour yields no contribution. The limes $r\to 0$ converges to

$$\lim_{r\to 0}\frac{ie^{\eta r\cos\phi}e^{i\eta r\sin\phi}}{1+e^{\beta r\cos\phi}e^{i\beta r\sin\phi}} = \frac{i}{1+1} \tag{1.78}$$

So the integration yields in the end

$$\frac{1}{\beta}\sum_n \frac{1}{i\omega_n}e^{i\omega_n\eta} = -\frac{1}{2\pi i}\int\limits_{\pi}^{-\pi} i\frac{1}{2} = +\frac{1}{2}. \tag{1.79}$$

With that result we can go back to the average occupation. We split the sum up into a into a part $\leq N_{\text{Mats}}$ and a part $> N_{\text{Mats}}$:

$$\langle n\rangle \tag{1.80}$$

$$= \frac{1}{\beta}\sum_{n\geq 0}^{N_{\text{Mats}}}\left[\mathfrak{Re}\left\{\bar{G}(i\omega_n)\right\}\underbrace{\left(e^{i\omega_n\eta}+e^{-i\omega_n\eta}\right)}_{=2} + i\left(\mathfrak{Im}\left\{\bar{G}(i\omega_n)\right\}+\frac{1}{\omega_n}\right)\underbrace{\left(e^{i\omega_n\eta}-e^{-i\omega_n\eta}\right)}_{=0}\right]$$

$$+\frac{1}{\beta}\sum_{n\geq N_{\text{Mats}}}\left[\underbrace{\mathfrak{Re}\left\{\bar{G}(i\omega_n)\right\}}_{=0}\left(e^{i\omega_n\eta}+e^{-i\omega_n\eta}\right) + i\underbrace{\left(\mathfrak{Im}\left\{\bar{G}(i\omega_n)\right\}+\frac{1}{\omega_n}\right)}_{=0}\left(e^{i\omega_n\eta}-e^{-i\omega_n\eta}\right)\right]$$

$$-\frac{1}{2} \tag{1.81}$$

$$= \frac{2}{\beta}\sum_{n\leq N_{\text{Mats}}}\mathfrak{Re}\left\{\bar{G}(i\omega_n)\right\}+\frac{1}{2}. \tag{1.82}$$

1.6. Particle-hole symmetry transformation for the Hubbard Hamiltonian

In this section, we will show, that for a Hubbard model a chemical potential of $\mu = \frac{U}{2}$ always leads to half filling.

[10] This limes is the reason, why η is set to a small but finite number.

We repeat the used Hubbard Hamiltonian from (1.1).

$$\hat{H}_{\text{Hub}} = -\sum_{i,j,\sigma} t_{i,j}\hat{c}^{\dagger}_{i,\sigma}\hat{c}_{j,\sigma} + \sum_{i} U\hat{n}_{i,\uparrow}\hat{n}_{i,\downarrow} - \sum_{i}\mu\left(\hat{n}_{i,\uparrow}+\hat{n}_{i,\downarrow}\right). \tag{1.83}$$

Now we do a particle-hole transformation on this Hamiltonian. From a physical point of view we replace now the empty states by occupied states and the other way round. From a mathematical point of view we exchange creation and annihilation operators $\hat{c}^{\dagger}_{\dots} \leftrightarrow \hat{c}_{\dots}$ (and hence $n_{i,\sigma} \leftrightarrow 1 - n_{i,\sigma}$). From that follows a particle-hole transformed Hamiltonian

$$\begin{aligned}
\hat{H}_{\text{ph}} =& -\sum_{i,j,\sigma} t_{i,j}\hat{c}_{i,\sigma}\hat{c}^{\dagger}_{j,\sigma} + \sum_{i} U(1-\hat{n}_{i,\uparrow})(1-\hat{n}_{i,\downarrow}) - \sum_{i}\mu\left(2-\hat{n}_{i,\uparrow}-\hat{n}_{i,\downarrow}\right) && (1.84)\\
=& \sum_{i,j,\sigma} t_{j,i}\hat{c}^{\dagger}_{i,\sigma}\hat{c}_{j,\sigma} + \sum_{i} U n_{i,\uparrow}\hat{n}_{i,\downarrow} - \sum_{i}\mu\left(\hat{n}_{i,\uparrow}+\hat{n}_{i,\downarrow}\right) && (1.85)\\
&+ \sum_{i} U(1-n_{i,\uparrow}-n_{i,\downarrow}) - \sum_{i}\mu\left(2-2n_{i,\uparrow}-2n_{i,\downarrow}\right). && (1.86)
\end{aligned}$$

In the second step we used the relation (1.2) in the hopping term. We notice now that due to the symmetry in the hopping parameters, we can express the particle-hole transformed Hamiltonian by the original one with $t_{i,j} \to -t_{i,j}$. This transformation yields only one additional term

$$\hat{H}_{\text{ph}} = \hat{H}_{\text{Hub}}(t_{i,j} \to -t_{i,j}) + (U-2\mu)\sum_{i}\left(1-n_{i,\uparrow}-n_{i,\downarrow}\right), \tag{1.87}$$

which can be set to zero easily. For $\mu = \frac{U}{2}$ it follows $\hat{H}_{\text{ph}} = \hat{H}_{\text{Hub}}(t_{i,j} \to -t_{i,j})$. Both Hamiltonians $\hat{H} \in \left\{\hat{H}_{\text{Hub}}, \hat{H}_{\text{Hub}}(t_{i,j} \to -t_{i,j})\right\}$ describe the same filling. The sign of the hopping parameter is not relevant, as the filling is defined by

$$\langle n_{\sigma}\rangle = \text{Tr}\left(\hat{n}_{\sigma}e^{-\beta\hat{H}}\right). \tag{1.88}$$

When we expand the exponential function and calculate the trace only terms with even powers of $t_{i,j}$ remain, as an odd number of creators or annihilators on any lattice site yields zero. So the actual result of $\langle n\rangle$ is the same for the Hubbard Hamiltonian and its particle-hole transformed. This means the system is half filled for $\mu = \frac{U}{2}$.

2. Single impurity Anderson model and the segment picture

In this chapter we will explain the analytic foundations of the CT-QMC solver for the SIAM. We will derive an analytic solution for the non-interacting case, which is important for testing purposes, We will calculate the partition function and introduce a new mathematical formalism called "segment picture" based on the partition function. The we will explain how to calculate the Green function and the susceptibility in the segment picture formalism. The simple nature of the segment picture will enable us to evaluate indefinite sums of configurations by the Methods presented in chapter 3.

2.1. Analytic solution of the non-interacting SIAM

In the following we will derive an analytic expression for the Greens function on the impurity $G_{\mathrm{ff}}(i\omega_n)$ of the non-interacting SIAM. This helps us to ensure the validity of the numeric results of the CT-QMC impurity solver without interaction. As will turn out, the interaction in the CT-QMC algorithm has only influence on minor parts of the whole code. This makes the analytic result as an important tool for testing.

We begin with some basic operator relations and the Hamiltonian $\hat{H}$ of the non-interacting SIAM.

$$[\hat{a}\hat{b},\hat{c}] = \hat{a}\{\hat{b},\hat{c}\} - \{\hat{a},\hat{c}\}\hat{b} \tag{2.1}$$

$$\hat{H} = \epsilon_{\mathrm{f}}\hat{f}^\dagger\hat{f} + \sum_{\boldsymbol{k}} \epsilon_{\boldsymbol{k}}\hat{c}^\dagger_{\boldsymbol{k}}\hat{c}_{\boldsymbol{k}} + \frac{1}{\sqrt{N}}\sum_{\boldsymbol{k}}\left(V_{\boldsymbol{k}}\hat{f}^\dagger\hat{c}_{\boldsymbol{k}} + V^*_{\boldsymbol{k}}\hat{c}^\dagger_{\boldsymbol{k}}\hat{f}\right) \tag{2.2}$$

$$[\hat{H},\hat{f}] = -\epsilon_{\mathrm{f}}\hat{f} - \frac{1}{\sqrt{N}}\sum_{\boldsymbol{k}} V_{\boldsymbol{k}}\hat{c}_{\boldsymbol{k}} \tag{2.3}$$

$$[\hat{H},\hat{f}^\dagger] = \epsilon_{\mathrm{f}}\hat{f}^\dagger + \frac{1}{\sqrt{N}}\sum_{\boldsymbol{k}'} V^*_{\boldsymbol{k}'}\hat{c}^\dagger_{\boldsymbol{k}'} \tag{2.4}$$

$$[\hat{H},\hat{c}^\dagger_{\boldsymbol{k}'}] = \epsilon_{\boldsymbol{k}'}\hat{c}^\dagger_{\boldsymbol{k}'} + \frac{V_{\boldsymbol{k}'}}{\sqrt{N}}\hat{f}^\dagger\,, \tag{2.5}$$

where N denotes the number of $\boldsymbol{k}$-points. We will use the explicit form of the commutator relations $[\hat{H},\hat{.}\,.]$ later.

Further we introduce the definitions of the Greens functions

$$G_{\mathrm{ff}}(\tau,\tau') \equiv -\langle \mathrm{T}_\tau \hat{f}(\tau)\hat{f}^\dagger(\tau')\rangle = \Theta(\tau-\tau')\langle -\hat{f}(\tau)\hat{f}^\dagger(\tau')\rangle + \Theta(\tau'-\tau)\langle \hat{f}^\dagger(\tau')\hat{f}(\tau)\rangle \tag{2.6}$$

$$G_{\boldsymbol{k}\mathrm{f}}(\tau,\tau') \equiv -\langle \mathrm{T}_\tau \hat{c}_{\boldsymbol{k}}(\tau)\hat{f}^\dagger(\tau')\rangle \tag{2.7}$$

$$G_{\boldsymbol{k}\boldsymbol{k}'}(\tau,\tau') \equiv -\langle \mathrm{T}_\tau \hat{c}_{\boldsymbol{k}}(\tau)\hat{c}^\dagger_{\boldsymbol{k}'}(\tau')\rangle\,. \tag{2.8}$$

G_{ff} describes the propagation on the impurity, $G_{\boldsymbol{k}\mathrm{f}}$ describes the propagation from the bath into the impurity (part of the hybridisation processes) and $G_{\boldsymbol{k}\boldsymbol{k}'}$ describes the propagation in the bath.

We continue by equation of motion of G_{ff}:

$$\frac{\mathrm{d}}{\mathrm{d}\tau}G_{\mathrm{ff}}(\tau,\tau') = -\left[\delta(\tau-\tau')\langle \hat{f}(\tau)\hat{f}^\dagger(\tau')\rangle + \delta(\tau'-\tau)\langle \hat{f}^\dagger(\tau')\hat{f}(\tau)\rangle\right] - \langle \mathrm{T}_\tau \frac{\mathrm{d}\hat{f}(\tau)}{\mathrm{d}\tau}\hat{f}^\dagger(\tau')\rangle \tag{2.9}$$

$$= -\delta(\tau-\tau')\langle\left\{\hat{f}(\tau),\hat{f}^\dagger(\tau')\right\}\rangle - \langle \mathrm{T}_\tau \frac{\mathrm{d}\hat{f}(\tau)}{\mathrm{d}\tau}\hat{f}^\dagger(\tau')\rangle\,. \tag{2.10}$$

Then we express the time derivative of the $\hat{f}$ operator by its commutator with the Hamiltonian

$$\frac{\mathrm{d}\hat{f}(\tau)}{\mathrm{d}\tau} = \frac{\mathrm{d}(e^{\tau\hat{H}}\hat{f}e^{-\tau\hat{H}})}{\mathrm{d}\tau} = e^{\tau\hat{H}}\left[\hat{H},\hat{f}\right]e^{-\tau\hat{H}}. \tag{2.11}$$

Inserting this into the equation of motion of the Greens function yields

$$\frac{\mathrm{d}}{\mathrm{d}\tau}G_{\mathrm{ff}}(\tau,\tau') = -\delta(\tau-\tau') - \epsilon_{\mathrm{f}}G_{\mathrm{ff}}(\tau,\tau') - \frac{1}{\sqrt{N}}\sum_{\boldsymbol{k}} V_{\boldsymbol{k}}G_{\boldsymbol{k}\mathrm{f}}(\tau,\tau')\,. \tag{2.12}$$

Fourier transformation as defined in (2.48) and comparing the coefficients of $e^{i\omega_n}$ leads us to the first equation of motion in the Matsubara domain:

$$-i\omega_n G_{\mathrm{ff}}(i\omega_n) = -1 - \epsilon_{\mathrm{f}}G_{\mathrm{ff}}(i\omega_n) - \frac{1}{\sqrt{N}}\sum_{\boldsymbol{k}} V_{\boldsymbol{k}}G_{\boldsymbol{k}\mathrm{f}}(i\omega_n), \tag{2.13}$$

where we used $G(\tau,\tau') = G(\tau-\tau')$.

The equations of motion for $G_{\boldsymbol{k}\mathrm{f}}$ and $G_{\boldsymbol{k}\boldsymbol{k}'}$ follow in an similar way. Because of that the reader may follow the description for G_{ff} and use the following formulas for $G_{\boldsymbol{k}\mathrm{f}}$:

$$\frac{\mathrm{d}}{\mathrm{d}\tau'}G_{\boldsymbol{k}\mathrm{f}}(\tau,\tau') = \delta(\tau-\tau')\langle\left\{\hat{c}_{\boldsymbol{k}},\hat{f}^\dagger(\tau')\right\}\rangle - \langle \mathrm{T}_\tau \hat{c}_{\boldsymbol{k}}(\tau)\frac{\mathrm{d}\hat{f}^\dagger(\tau')}{\mathrm{d}\tau'}\rangle \tag{2.14}$$

$$\frac{\mathrm{d}\hat{f}^\dagger(\tau)}{\mathrm{d}\tau} = \frac{\mathrm{d}(e^{\tau\hat{H}}\hat{f}^\dagger e^{-\tau\hat{H}})}{\mathrm{d}\tau} = e^{\tau\hat{H}}\left[\hat{H},\hat{f}^\dagger\right]e^{-\tau\hat{H}} \tag{2.15}$$

$$\frac{\mathrm{d}}{\mathrm{d}\tau'}G_{\boldsymbol{k}\mathrm{f}}(\tau,\tau') = \epsilon_{\mathrm{f}}G_{\boldsymbol{k}\mathrm{f}}(\tau,\tau') + \frac{1}{\sqrt{N}}\sum_{\boldsymbol{k}'} V^*_{\boldsymbol{k}'}G_{\boldsymbol{k}\boldsymbol{k}'}(\tau,\tau') \tag{2.16}$$

$$i\omega_n G_{\boldsymbol{k}\mathrm{f}}(i\omega_n) = \epsilon_{\mathrm{f}}G_{\boldsymbol{k}\mathrm{f}}(i\omega_n) + \frac{1}{\sqrt{N}}\sum_{\boldsymbol{k}'} V^*_{\boldsymbol{k}'}G_{\boldsymbol{k}\boldsymbol{k}'}(i\omega_n) \tag{2.17}$$

and for $G_{\boldsymbol{k}\boldsymbol{k}'}$:

$$\frac{\mathrm{d}}{\mathrm{d}\tau'}G_{\boldsymbol{k}\boldsymbol{k}'}(\tau,\tau') = \delta(\tau-\tau')\langle\left\{\hat{c}_{\boldsymbol{k}}(\tau),\hat{c}^\dagger_{\boldsymbol{k}'}(\tau')\right\}\rangle - \langle \mathrm{T}_\tau \hat{c}_{\boldsymbol{k}}(\tau)\frac{\mathrm{d}\hat{c}^\dagger_{\boldsymbol{k}'}(\tau')}{\mathrm{d}\tau'}\rangle \tag{2.18}$$

$$\frac{\mathrm{d}\hat{c}^\dagger_{\boldsymbol{k}'}(\tau)}{\mathrm{d}\tau} = \frac{\mathrm{d}(e^{\tau\hat{H}}\hat{c}^\dagger_{\boldsymbol{k}'}e^{-\tau\hat{H}})}{\mathrm{d}\tau} = e^{\tau\hat{H}}\left[\hat{H},\hat{c}^\dagger_{\boldsymbol{k}'}\right]e^{-\tau\hat{H}} \tag{2.19}$$

$$\frac{\mathrm{d}}{\mathrm{d}\tau'}G_{\boldsymbol{k}\boldsymbol{k}'}(\tau,\tau') = \delta(\tau-\tau')\langle\left\{\hat{c}_{\boldsymbol{k}}(\tau),\hat{c}^\dagger_{\boldsymbol{k}'}(\tau')\right\}\rangle + \epsilon_{\boldsymbol{k}'}G_{\boldsymbol{k}\boldsymbol{k}'}(\tau,\tau') + \frac{1}{\sqrt{N}}V_{\boldsymbol{k}'}G_{\boldsymbol{k}\mathrm{f}}(\tau,\tau') \tag{2.20}$$

$$i\omega_n G_{\boldsymbol{k}\boldsymbol{k}'}(i\omega_n) = \delta_{\boldsymbol{k},\boldsymbol{k}'} + \epsilon_{\boldsymbol{k}'}G_{\boldsymbol{k}\boldsymbol{k}'}(i\omega_n) + \frac{1}{\sqrt{N}}V_{\boldsymbol{k}'}G_{\boldsymbol{k}\mathrm{f}}(i\omega_n) \tag{2.21}$$

Now we derived a system of three equations of motion (2.13), (2.17) and (2.21). Each equation describes the time evolution of a Greens function in the Matsubara domain. Those can be solved by first solving equations (2.17) and (2.21), which leads to:

$$G_{\boldsymbol{k}\mathrm{f}}(i\omega_n) = \frac{\frac{V_{\boldsymbol{k}}}{\sqrt{N}}\frac{1}{i\omega_n-\epsilon_{\boldsymbol{k}}}}{i\omega_n - \epsilon_\mathrm{f} - \sum_{\boldsymbol{k}'}\frac{V_{\boldsymbol{k}'}V^*_{\boldsymbol{k}'}}{N}\frac{1}{i\omega_n-\epsilon_{\boldsymbol{k}'}}}\,. \tag{2.22}$$

By using that with (2.13), we easily get the analytic expression for the Greens function on the impurity of the non-interacting SIAM.

$$G_{\mathrm{ff}}(i\omega_n) = \frac{1}{i\omega_n - \epsilon_\mathrm{f} - \sum_{\boldsymbol{k}'}\frac{V_{\boldsymbol{k}'}V^*_{\boldsymbol{k}'}}{N}\frac{1}{i\omega_n-\epsilon_{\boldsymbol{k}'}}} \tag{2.23}$$

For a momentum independent hybridisation $V_{\boldsymbol{k}} = V$ follows further

$$G_{\mathrm{ff}}(i\omega_n) = \frac{1}{i\omega_n - \epsilon_\mathrm{f} - |V|^2 g_\mathrm{c}(i\omega_n)} \text{ with } \Delta(i\omega_n) = |V|^2 g_\mathrm{c}(i\omega_n) = \frac{|V|^2}{N}\sum_{\boldsymbol{k}'}\frac{1}{i\omega_n-\epsilon_{\boldsymbol{k}'}}\,. \tag{2.24}$$

This result will be used later to check the validity of the results of the CT-QMC solver without interaction $U = 0$.

2.2. Hybridisation expansion of the spinless SIAM

2.2.1. Hybridisation expansion

First we introduce another way of writing the partition function. We start with a Hamiltonian of the form

$$\hat{H} = \hat{H}_0 + \hat{H}_\mathrm{hyb}. \tag{2.25}$$

We will split up $e^{-\beta\hat{H}}$ by going to the interaction picture and show, that

$$e^{-\beta\hat{H}} = \mathrm{T}_\tau e^{-\beta\hat{H}_0}e^{-\int_0^\beta \hat{H}_\mathrm{hyb}(\tau)\mathrm{d}\tau} \tag{2.26}$$

$$\text{with } \hat{H}_\mathrm{hyb}(\tau) = e^{-\tau\hat{H}_0}\hat{H}_\mathrm{hyb}e^{\tau\hat{H}_0}. \tag{2.27}$$

We start with

$$e^{-\beta\hat{H}} = e^{-\beta(\hat{H}_0+\hat{H}_{\mathrm{hyb}})} \tag{2.28}$$

We introduce time ordering T_τ:
This operator changes the order of he following creation and annihilation operators in such a way, that a time-wise rising order of the time arguments / indices is established from right to left. As we describe a fermionic model every permutation of two operators ($\hat{c}$ or $\hat{c}^\dagger$) contributes an additional factor $\times(-1)$. As the terms $\hat{H}_{0,\tau}$ and $\hat{H}_{0,\mathrm{hyb}}$ consist of an even number of operators, there does not arise any minus sign from time ordering.

T_τ is the reason for introducing new indices τ_i on the operators. These indices have no physical meaning. Their only purpose is to tag, how the time order operator has to act.

$$e^{-\beta\hat{H}} = \mathrm{T}_\tau e^{-\int_0^\beta \hat{H}_{0,\tau}+\hat{H}_{\mathrm{hyb},\tau}\mathrm{d}\tau} = \mathrm{T}_\tau e^{-\int_0^\beta \hat{H}_{0,\tau}\mathrm{d}\tau} e^{-\hat{\int}_0^\beta H_{\mathrm{hyb},\tau}\mathrm{d}\tau} \tag{2.29}$$

Now we expand in $\hat{H}_{\mathrm{hyb}}$ and yield

$$e^{-\beta\hat{H}} = \mathrm{T}_\tau e^{-\int_0^\beta H_{0,\tau}\mathrm{d}\tau} \sum_{n=0}^{\infty} \frac{(-1)^n}{n!} \int_0^\beta \mathrm{d}\tau_1 \ldots \int_0^\beta \mathrm{d}\tau_n \, \hat{H}_{\mathrm{hyb},\tau_n} \ldots \hat{H}_{\mathrm{hyb},\tau_1} \tag{2.30}$$

$$\stackrel{*}{=} \mathrm{T}_\tau e^{-\left(\int_0^{\tau_1}+\int_{\tau_1}^{\tau_2}+\ldots+\int_{\tau_n}^{\beta}\right)\hat{H}_{0,\tau}\mathrm{d}\tau} \sum_{n=0}^{\infty}(-1)^n \int_0^\beta \mathrm{d}\tau_1 \int_{\tau_1}^\beta \mathrm{d}\tau_2 \ldots \int_{\tau_{n-1}}^\beta \mathrm{d}\tau_n \times \hat{H}_{\mathrm{hyb},\tau_n} \ldots \hat{H}_{\mathrm{hyb},\tau_1}. \tag{2.31}$$

The last step (*) is proven in [8] and [14].[1] By time ordering everything by hand, the time order operator is not necessary anymore. We first put the $e^{-\int_{\tau_i}^{\tau_{i+1}} \hat{H}_{0,\tau}\mathrm{d}\tau}$ in order and calculate the integral afterwards to get $e^{-\tau_{i+1}\hat{H}_0}e^{\tau_i\hat{H}_0}$ instead. Further we define $\hat{H}_{\mathrm{hyb}}(\tau) = e^{\tau\hat{H}_0}\hat{H}_{\mathrm{hyb}}e^{-\tau\hat{H}_0}$.

$$e^{-\beta\hat{H}} = \sum_{n=0}^{\infty}(-1)^n \int_0^\beta \mathrm{d}\tau_1 \int_{\tau_1}^\beta \mathrm{d}\tau_2 \ldots \int_{\tau_{n-1}}^\beta \mathrm{d}\tau_n \times e^{-\beta\hat{H}_0}e^{\tau_n\hat{H}_0}\hat{H}_{\mathrm{hyb},\tau_n}e^{-\tau_n\hat{H}_0}e^{\tau_{n-1}\hat{H}_0} \ldots e^{-\tau_2\hat{H}_0}e^{\tau_1\hat{H}_0}\hat{H}_{\mathrm{hyb},\tau_1}e^{-\tau_1\hat{H}_0} \tag{2.32}$$

$$= \mathrm{T}_\tau \sum_{n=0}^{\infty} \frac{(-1)^n}{n!} \int_0^\beta \mathrm{d}\tau_1 \hat{H}_{\mathrm{hyb}}(\tau_1) \ldots \int_0^\beta \mathrm{d}\tau_n \hat{H}_{\mathrm{hyb}}(\tau_n) \tag{2.33}$$

$$= \mathrm{T}_\tau e^{-\beta\hat{H}_0} e^{-\int_0^\beta \hat{H}_{\mathrm{hyb}}(\tau)\mathrm{d}\tau} \tag{2.34}$$

[1] One may notice at this point, that the contribution for $\tau_i = \tau_j$ to the integral is infinitely small (for the finite hybridisation function we will use later) and hence not counted, as the time order operator is not defined then.

2.2.2. Spinless SIAM

The Hamiltonian of the spinless Anderson model is given by

$$\hat{H} = \underbrace{\epsilon_{\mathrm{f}} \hat{f}^\dagger \hat{f} + \sum_{\boldsymbol{k}} \epsilon_{\boldsymbol{k}} \hat{c}^\dagger_{\boldsymbol{k}} \hat{c}_{\boldsymbol{k}}}_{\hat{H}_0} + \underbrace{\frac{1}{\sqrt{N}} \sum_{\boldsymbol{k}} V \hat{f}^\dagger \hat{c}_{\boldsymbol{k}} + \frac{1}{\sqrt{N}} \sum_{\boldsymbol{k}} V^* \hat{c}^\dagger_{\boldsymbol{k}} \hat{f}}_{\hat{H}_{\mathrm{hyb}}} . \tag{2.35}$$

We dropped the index of V because we will only work with a momentum independent hybridisation in the following. $\hat{H}$ can be split up in a local part $\hat{H}_{\mathrm{loc}}$, a bath part $\hat{H}_{\mathrm{bath}}$, a hybridisation part $\hat{H}_{\mathrm{hyb}}$ and a on-site part $\hat{H}_0$:

$$\hat{H}_{\mathrm{loc}} = \epsilon_{\mathrm{f}} \hat{f}^\dagger \hat{f}; \quad \hat{H}_{\mathrm{bath}} = \sum_{\boldsymbol{k}} \epsilon_{\boldsymbol{k}} \hat{c}^\dagger_{\boldsymbol{k}} \hat{c}_{\boldsymbol{k}}; \tag{2.36}$$

$$\hat{H}_{\mathrm{V}} = \frac{1}{\sqrt{N}} \sum_{\boldsymbol{k}} V \hat{f}^\dagger \hat{c}_{\boldsymbol{k}} \equiv V \hat{f}^\dagger \hat{c}; \quad \hat{H}^\dagger_{\mathrm{V}} = \frac{1}{\sqrt{N}} \sum_{\boldsymbol{k}} V^* \hat{c}^\dagger_{\boldsymbol{k}} \hat{f} \equiv V^* \hat{c}^\dagger \hat{f}; \tag{2.37}$$

$$\hat{H}_0 = \hat{H}_{\mathrm{loc}} + \hat{H}_{\mathrm{bath}}; \quad \hat{H}_{\mathrm{hyb}} = \hat{H}_{\mathrm{V}} + \hat{H}^\dagger_{\mathrm{V}}. \tag{2.38}$$

Then we expand the partition function in the hybridisation term. It is necessary to have an even number of $\hat{H}_{\mathrm{hyb}}$, because the trace gives zero, otherwise.

$$Z_0 \equiv \mathrm{Tr}\{e^{-\beta \hat{H}_0}\} \tag{2.39}$$

$$\frac{Z}{Z_0} = \frac{\mathrm{Tr}\left\{e^{-\beta \hat{H}}\right\}}{Z_0} = \frac{\mathrm{Tr}\left\{\mathrm{T}_\tau e^{-\beta \hat{H}_0} e^{-\int_0^\beta \mathrm{d}\tau \hat{H}_{\mathrm{hyb}}(\tau)}\right\}}{Z_0} \quad \left(\equiv \langle e^{-\int_0^\beta \mathrm{d}\tau \hat{H}_{\mathrm{hyb}}(\tau)} \rangle_0\right) \tag{2.40}$$

$$= \frac{1}{Z_0} \mathrm{Tr}\left\{ \mathrm{T}_\tau e^{-\beta \hat{H}_0} \frac{1}{(2k)!} \sum_{k=0}^{\infty} \int_0^\beta \mathrm{d}\tilde{\tau}_{2k} \ldots \mathrm{d}\tilde{\tau}_1 \left(\hat{H}_{\mathrm{V}}(\tilde{\tau}_{2k}) + \hat{H}^\dagger_{\mathrm{V}}(\tilde{\tau}_{2k})\right) \ldots \left(\hat{H}_{\mathrm{V}}(\tilde{\tau}_1) + \hat{H}^\dagger_{\mathrm{V}}(\tilde{\tau}_1)\right) \right\}$$

As the integrand has to consist of the same number of $\hat{H}_{\mathrm{V}}$ as $\hat{H}^\dagger_{\mathrm{V}}$, there are $\begin{pmatrix} 2k \\ k \end{pmatrix}$ terms, which give a contribution. The resulting pre factor $\frac{1}{(2k)!} \begin{pmatrix} 2k \\ k \end{pmatrix} = \frac{1}{(k!)^2}$ is replaced by the new (ordered) integration intervals [2] . Further we renumber the integration indices, so that the primed indices belong to the annihilation operators on the impurity and get

$$\frac{Z}{Z_0} = \sum_{k=0}^{\infty} \int_0^\beta \mathrm{d}\tau_1 \int_{\tau_1}^\beta \mathrm{d}\tau_2 \ldots \int_{\tau_{k-1}}^\beta \mathrm{d}\tau_k \int_0^\beta \mathrm{d}\tau'_1 \int_{\tau'_1}^\beta \mathrm{d}\tau'_2 \ldots \int_{\tau'_{k-1}}^\beta \mathrm{d}\tau'_k \, w(q_k) \equiv \sum_{q_k} w(q_k). \tag{2.41}$$

with q_k denoting the manifold of all integration / summation variables

$$(q_k) \equiv (k, \tau_1, \tau_2, \ldots, \tau_k, \tau'_1, \tau'_2, \ldots, \tau'_k). \tag{2.42}$$

[2] Compare again: [8] and [14].

The weight $w(q_k)$ dependent of those variables is

$$w(q_k) = \frac{1}{Z_0}\mathrm{Tr}\left\{\mathrm{T}_\tau e^{-\beta\hat{H}_0}\hat{H}_\mathrm{V}^\dagger(\tau_k')\hat{H}_\mathrm{V}(\tau_k)\dots\hat{H}_\mathrm{V}^\dagger(\tau_1')\hat{H}_\mathrm{V}(\tau_1)\right\} \tag{2.43}$$

$$\equiv \left\langle \mathrm{T}_\tau \hat{H}_\mathrm{V}^\dagger(\tau_k')\hat{H}_\mathrm{V}(\tau_k)\dots\hat{H}_\mathrm{V}^\dagger(\tau_1')\hat{H}_\mathrm{V}(\tau_1)\right\rangle_0 \tag{2.44}$$

$$= |V|^{2k}\left\langle \mathrm{T}_\tau\, \hat{c}^\dagger(\tau_k')\hat{f}(\tau_k')\hat{f}^\dagger(\tau_k)\hat{c}(\tau_k)\dots\hat{c}^\dagger(\tau_1')\hat{f}(\tau_1')\hat{f}^\dagger(\tau_1)\hat{c}(\tau_1)\right\rangle_0 \tag{2.45}$$

$$= |V|^{2k}\frac{\mathrm{Tr}\left\{e^{-\beta\hat{H}_\mathrm{bath}}\mathrm{T}_\tau\hat{c}^\dagger(\tau_k')\hat{c}(\tau_k)\dots\hat{c}^\dagger(\tau_1')\hat{c}(\tau_1)\right\}}{\mathrm{Tr}\left\{e^{-\beta\hat{H}_\mathrm{bath}}\right\}}\cdot\frac{\mathrm{Tr}\left\{e^{-\beta\hat{H}_\mathrm{loc}}\mathrm{T}_\tau\hat{f}(\tau_k')\hat{f}^\dagger(\tau_k)\dots\hat{f}(\tau_1')\hat{f}^\dagger(\tau_1)\right\}}{\mathrm{Tr}\left\{e^{-\beta\hat{H}_\mathrm{loc}}\right\}}$$

$$\equiv |V|^{2k}\left\langle \mathrm{T}_\tau\hat{c}^\dagger(\tau_k')\hat{c}(\tau_k)\dots\hat{c}^\dagger(\tau_1')\hat{c}(\tau_1)\right\rangle_\mathrm{c}\left\langle \mathrm{T}_\tau\hat{f}(\tau_k')\hat{f}^\dagger(\tau_k)\dots\hat{f}(\tau_1')\hat{f}^\dagger(\tau_1)\right\rangle_\mathrm{f} \tag{2.46}$$

The trace was split up by inserting a sum over all possible many particle states. With the finite temperature Wick theorem [31] [3] the first part can be expressed as

$$|V|^{2k}\left\langle \mathrm{T}_\tau\hat{c}^\dagger(\tau_k')\hat{c}(\tau_k)\dots\hat{c}^\dagger(\tau_1')\hat{c}(\tau_1)\right\rangle_\mathrm{c} = \det(\Delta)$$
$$\text{with } \Delta_{i,j} \equiv -|V|^2\left\langle \mathrm{T}_\tau\hat{c}(\tau_i)\hat{c}^\dagger(\tau_j')\right\rangle_\mathrm{c} \equiv \Delta(\tau_i-\tau_j'). \tag{2.47}$$

Δ is a matrix of dimension $k\times k$, the matrix elements are denoted by $\Delta_{i,j}$. A Fourier transformation

$$f(\tau) = \frac{1}{\beta}\sum_n f(i\omega_n)e^{-i\omega_n\tau} \tag{2.48}$$

$$f(i\omega_n) = \int_0^\beta \mathrm{d}\tau f(\tau)e^{+i\omega_n\tau} \tag{2.49}$$

of $\Delta(\tau)$ yields

$$\Delta(i\omega_n) \equiv \int_0^\beta e^{i\omega_n\tau}\Delta(\tau)\mathrm{d}\tau = -\int_0^\beta e^{i\omega_n\tau}\frac{|V|^2}{N}\sum_{\boldsymbol{k},\boldsymbol{k'}}\left\langle \hat{c}_{\boldsymbol{k}}(\tau)\hat{c}_{\boldsymbol{k'}}^\dagger(0)\right\rangle_\mathrm{c}\mathrm{d}\tau \tag{2.50}$$

$$= -\frac{|V|^2}{N}\sum_{\boldsymbol{k}}\int_0^\beta e^{i\omega_n\tau}\frac{\mathrm{Tr}\left\{e^{-\beta\hat{H}_\mathrm{bath}}e^{\tau\hat{H}_\mathrm{bath}}c_{\boldsymbol{k}}e^{-\tau\hat{H}_\mathrm{bath}}\hat{c}_{\boldsymbol{k}}^\dagger\right\}}{\mathrm{Tr}\left\{e^{-\beta\hat{H}_\mathrm{bath}}\right\}}\mathrm{d}\tau. \tag{2.51}$$

We use the definition of time dependent operators (compare equation 2.27) $A(\tau) = e^{\tau\hat{H}_0}Ae^{-\tau\hat{H}_0}$ with $A\in\{\hat{c}_{\boldsymbol{k}},\hat{c}_{\boldsymbol{k}}^\dagger\}$. Because $\left[A,\hat{f}^\dagger\hat{f}\right]=0$, it follows $A(\tau)=e^{\tau\hat{H}_\mathrm{bath}}Ae^{-\tau\hat{H}_\mathrm{bath}}$. As we evaluate the trace of the creation / annihilation operators of the impurity, we can insert the projection on special states on the left and the right side of every operator. $|k=0\rangle$ means "state with momentum $\boldsymbol{k}$ not occupied", $|k=1\rangle$ means "state with momentum $\boldsymbol{k}$ occupied".

$$\hat{c}_{\boldsymbol{k}} \to |k=0\rangle\langle k=0|\hat{c}_{\boldsymbol{k}}|k=1\rangle\langle k=1| \tag{2.52}$$

$$\hat{c}_{\boldsymbol{k}}^\dagger \to |k=1\rangle\langle k=1|\hat{c}_{\boldsymbol{k}}^\dagger|k=0\rangle\langle k=0| \tag{2.53}$$

[3] The Wick theorem holds because the bath of the SIAM is non-interacting.

This leads us to

$$\Delta(i\omega_n) = -\frac{|V|^2}{N}\sum_{\boldsymbol{k}}\frac{\int_0^\beta e^{i\omega_n\tau}e^{-\tau\epsilon_{\boldsymbol{k}}}\mathrm{d}\tau}{e^{-\beta\epsilon_{\boldsymbol{k}}}+1} = \frac{|V|^2}{N}\sum_{\boldsymbol{k}}\frac{1}{i\omega_n-\epsilon_{\boldsymbol{k}}} = |V|^2\int\frac{\mathrm{Dos}(\epsilon)}{i\omega_n-\epsilon}\mathrm{d}\epsilon \tag{2.54}$$

$$\equiv |V|^2 g_{\mathrm{c}}(i\omega_n). \tag{2.55}$$

The $\langle\ldots\rangle_{\mathrm{f}}$ can be evaluated accordingly to the calculation of $\Delta(i\omega_n)$, by projecting on the occupation number basis. For $A\in\{\hat{f},\hat{f}^\dagger\}$ it follows $A(\tau)=e^{\tau\hat{H}_0}Ae^{-\tau\hat{H}_0}=e^{\tau\hat{H}_{\mathrm{loc}}}Ae^{-\tau\hat{H}_{\mathrm{loc}}}$, as $\left[A,c^\dagger_{\boldsymbol{k}}c_{\boldsymbol{k}}\right]=0$. We insert projections on both sides of every operator again, whereupon $|f=0\rangle$ means "impurity not occupied" and $|f=1\rangle$ means "impurity occupied".

$$\hat{f}\to|f=0\rangle\langle f=0|\hat{f}|f=1\rangle\langle f=1| \tag{2.56}$$

$$\hat{f}^\dagger\to|f=1\rangle\langle f=1|\hat{f}^\dagger|f=0\rangle\langle f=0| \tag{2.57}$$

With those two relations we get

$$\begin{aligned}
&\langle \mathrm{T}_\tau \hat{f}(\tau_k')\hat{f}^\dagger(\tau_k)\ldots\hat{f}(\tau_1')\hat{f}^\dagger(\tau_1)\rangle_{\mathrm{f}}\\
&=\begin{cases}
\left.\begin{aligned}&\langle\hat{f}(\tau_k')\hat{f}^\dagger(\tau_k)\ldots\hat{f}(\tau_1')\hat{f}^\dagger(\tau_1)\rangle_{\mathrm{f}}\\&=\frac{1}{1+e^{-\beta\epsilon_{\mathrm{f}}}}\prod_{m=1}^{n}e^{-(\tau_m'-\tau_m)\epsilon_{\mathrm{f}}}\end{aligned}\right\} & \text{for } \tau_k'>\tau_1(\text{no wind})\\
\left.\begin{aligned}&\langle-\hat{f}^\dagger(\tau_k)\hat{f}(\tau_{k-1}')\hat{f}^\dagger(\tau_{k-1})\ldots\hat{f}(\tau_1')\hat{f}^\dagger(\tau_1)\hat{f}(\tau_k')\rangle_{\mathrm{f}}\\&=-\frac{e^{-\beta\epsilon_{\mathrm{f}}}}{1+e^{-\beta\epsilon_{\mathrm{f}}}}\prod_{m=1}^{n}e^{-(\tau_m'-\tau_m)\epsilon_{\mathrm{f}}}\end{aligned}\right\} & \text{for } \tau_1\geq\tau_k'(\text{wind})\\
\frac{1}{1+e^{-\beta\epsilon_{\mathrm{f}}}} & \text{for } n=0(\text{no wind})\\
0 & \text{for non alternating } \hat{f} \text{ and } \hat{f}^\dagger.
\end{cases}
\end{aligned} \tag{2.58}$$

In the wind case $\tau_1\geq\tau_k'$, hence the time order operator shifts τ_k' about $2k-1$ positions and we get the additional minus sign. When executing the time ordering operator the index space of the imaginary timepoints $\tau_{\ldots}$ and $\tau'_{\ldots}$ has been renamed. After timeordering the condition $\tau_{i+1}\geq\tau_i'>\tau_i\ \forall i\in[1,n)$ is valid. To summarize (2.47) and (2.58) we get

$$w(q_k)=\frac{\det(\Delta)}{1+e^{-\beta\epsilon_{\mathrm{f}}}}\prod_{m=1}^{n}e^{-(\tau_m'-\tau_m)\epsilon_{\mathrm{f}}}\times\begin{cases}1 & \text{for no wind case}\\ -e^{-\beta\epsilon_{\mathrm{f}}} & \text{for wind case}\end{cases} \tag{2.59}$$

2.2.3. Segment picture

This section describes how we translate the imaginary time configurations q_k into **segment pictures**. By doing so, we can easily calculate the partition function (2.41). The advantage is, that the segment picture provides a simple way to evaluate the weight of a configuration. To translate a weight $w(q_k)$ into a segment picture, we have to draw the imaginary time scale from 0 to β. In analogy to the operator order of the trace, β is equal to the left handside

of the timescale and 0 is equal to the right handside of the timescale. According to this, we read the segment picture from right to left. In the next step we replace every pair of creation and annihilation operators on the impurity with a box on the imaginary time scale. This box is called a segment. The beginning of the box is the position of the creator $f^\dagger(\ldots)$ and the end is the position of the annihilator $f(\ldots)$ (keep in mind, that we read from right to left). We yield the transformation

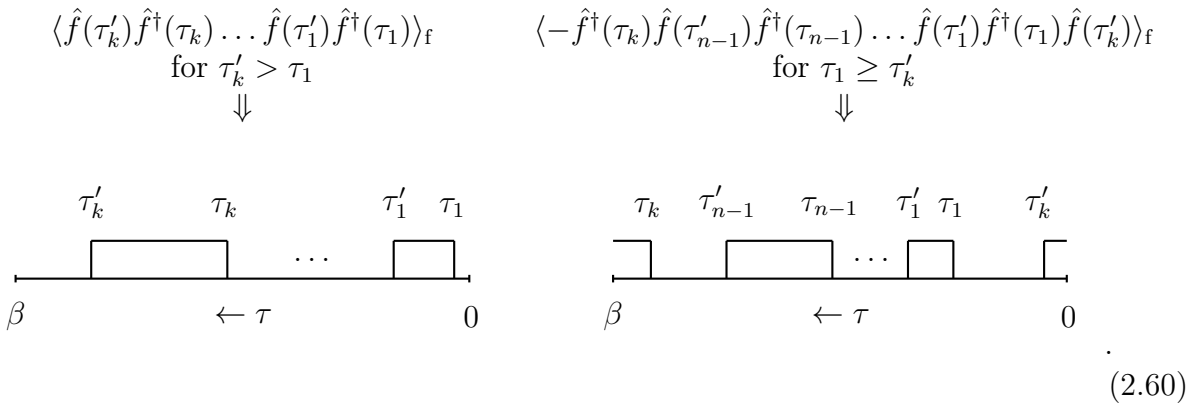

(2.60)

Figure 2.1.: Illustration of the transformation from ensemble averages to segment pictures.

According to (2.47) and (2.58) we can determine $w(q_k)$ directly from the segment picture.

$$w(q_k) = \mathrm{sign}_\mathrm{wind}\det(\Delta)\frac{e^{-L\epsilon_\mathrm{f}}}{1+e^{-\beta\epsilon_\mathrm{f}}} \tag{2.61}$$

Here $\mathrm{sign}_\mathrm{wind}$ is $+1$ for the no wind case and -1 for the wind case. L is the sum of the length of all segments, whereby the lenght of the n-th segment of the wind case is just $\beta+\tau_k'-\tau_k$.

All possible configurations for one spin direction:

note: half open segments

Further we remember that the time order operator in 2.2 was not defined for two equal time points. Therefore we introduce the convention, that the creator position is included and the annihilator position is excluded from the segment. In this way segments are allowed to touch each other $\tau_n' = \tau_{n+1}$, because the physical meaning of the endpoint τ_n' is, that the corresponding annihilator acts an infinitely small imaginary time unit before. In the segment picture this means, that the left edge of every segment has to be shifted an infinitesimal distance to the right.

According to this convention a configuration with $n = 1, \tau_1 = \tau_1'$ means full occupation on the whole imaginary time span (with the impurity being not occupied only in the infinitely small timespan at τ_1). A wrong interpretation would be, that the impurity is empty all the time, but at τ_1 it is shortly occupied.

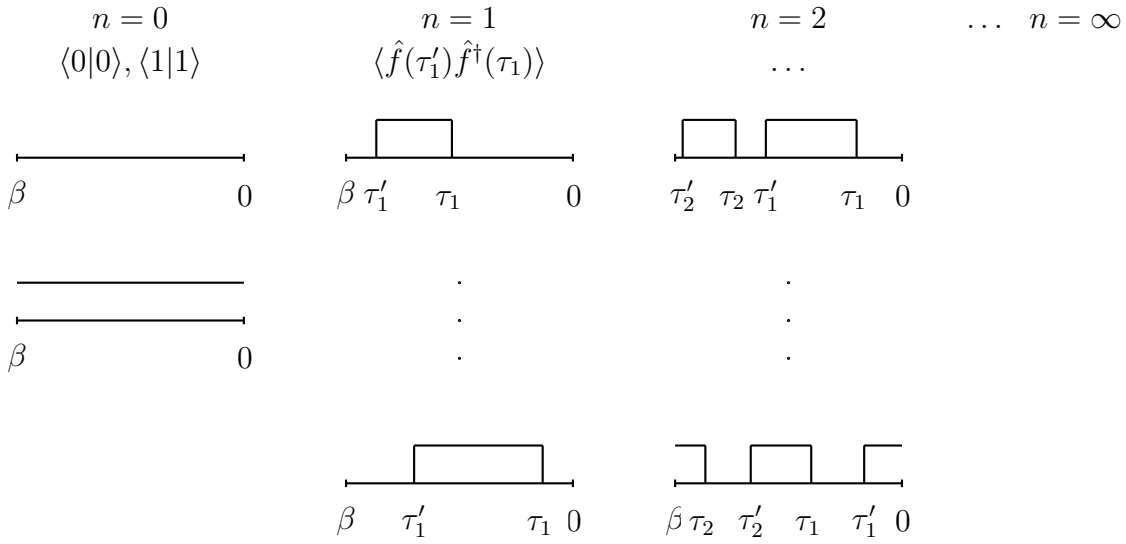

Figure 2.2.: Schematic illustration of the phase space of all possible configurations q_k.

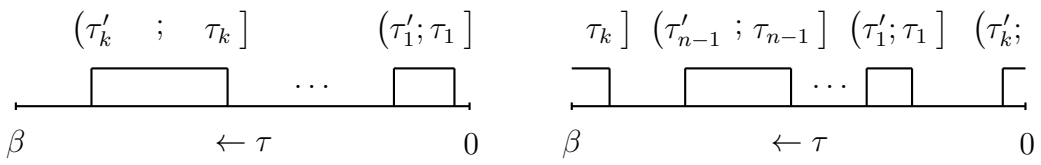

Figure 2.3.: Illustration of half open segments

2.3. Single Impurity Anderson Model with spin in a magnetic field

2.3.1. Incorporation of the spin

The Hamiltonian of the interacting single impurity Anderson model is given by

$$\hat{H}_{\text{spin}} = \underbrace{\sum_\sigma \epsilon_{\text{f},\sigma}\hat{f}_\sigma^\dagger\hat{f}_\sigma + \sum_{\boldsymbol{k},\sigma}\epsilon_{\boldsymbol{k},\sigma}\hat{c}_{\boldsymbol{k},\sigma}^\dagger\hat{c}_{\boldsymbol{k},\sigma}}_{\sum_\sigma \hat{H}_{0,\sigma}} + \underbrace{\frac{1}{\sqrt{N}}\sum_{\boldsymbol{k},\sigma} V\hat{f}_\sigma^\dagger\hat{c}_{\boldsymbol{k},\sigma} + \frac{1}{\sqrt{N}}\sum_{\boldsymbol{k},\sigma} V^*\hat{c}_{\boldsymbol{k},\sigma}^\dagger\hat{f}_\sigma}_{\sum_\sigma \hat{H}_{\text{hyb},\sigma}} + \underbrace{U\hat{n}_{\text{f},\uparrow}\hat{n}_{\text{f},\downarrow}}_{\hat{H}_{\text{int}}}. \tag{2.62}$$

So far the on-site energy on the impurity is the same for both spins: $\epsilon_{\text{f},\sigma} = \epsilon_{\text{f}}$

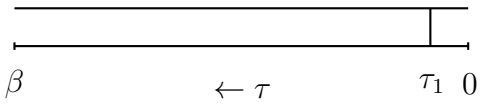

Figure 2.4.: segment picture for $n = 1; \tau_1 = \tau_1'$ (winded)

If we follow the derivation of section 2.2, we just have to replace:

$$\begin{aligned} \hat{H}_0 \ &\to \sum_\sigma \hat{H}_{0,\sigma} + \hat{H}_{\text{int}} \\ \hat{H}_{loc} &\to \sum_\sigma \hat{H}_{loc,\sigma} + \hat{H}_{\text{int}} \end{aligned} \tag{2.63}$$

Further we have to add a spin index to every operator and every imaginary time point. The only part that changes is the imaginary time average on the impurity $\langle \mathrm{T}_\tau \hat{f}(\tau_k')\hat{f}^\dagger(\tau_k)\dots\hat{f}(\tau_1')\hat{f}^\dagger(\tau_1)\rangle_{\mathrm{f}}$. We get an additional factor $e^{-Ul_{\text{ov}}}$ for the result, with l_{ov} being the imaginary time span of the impurity being doubly occupied. The reason for that is, that an additional operator $e^{-\left(\tau_1^*-\tau_2^*\right)\hat{H}_{\text{int}}}$ ($\tau_{\dots}^*$ are the imaginary time arguments of the neighbouring operators) appears between the $\hat{f}$ and $\hat{f}^\dagger$ operators, when we resolve the time dependence. This term yields $e^{-\left(\tau_1^*-\tau_2^*\right)U}$ in case of double occupancy and 1 otherwise.

With the incorporation of the spin, we need to adjust the definition of the configuration q_k (2.42):

$$q_{k,\sigma} \equiv (k,\sigma,\tau_{1,\sigma},\tau_{2,\sigma},\dots,\tau_{k,\sigma},\tau_{1,\sigma}',\tau_{2,\sigma}',\dots,\tau_{k,\sigma}') \tag{2.64}$$

$$q_k \equiv (q_{k_1,\uparrow}, q_{k_2,\downarrow}) \tag{2.65}$$

with $k_1 + k_2 = k$.

2.3.2. Incorporation of a magnetic field

We implement now an additional term in our Hamiltonian, which represents a magnetic field h.

$$\hat{H}_{\text{spin, h}} = \hat{H}_{\text{spin}} + \sigma h \hat{f}_\sigma^\dagger \hat{f}_\sigma \tag{2.66}$$

Comparing this with (2.62), we recognize, that the additional therm can be easily included in the existing Hamiltonian by adjusting the on-site energy

$$\epsilon_{\mathrm{f},\sigma} = \epsilon_{\mathrm{f}} + \sigma h. \tag{2.67}$$

2.3.3. Generalized weights

This leads us to the following formula for the weight of a configuration with respect to the spin [29].

$$w(q_k) = \text{sign}_{\text{wind},\sigma}\text{sign}_{\text{wind},-\sigma}\det(\Delta)\frac{e^{-L_\sigma\epsilon_{\text{f},\sigma}}}{1+e^{-\beta\epsilon_{\text{f},\sigma}}}\frac{e^{-L_{-\sigma}\epsilon_{\text{f},-\sigma}}}{1+e^{-\beta\epsilon_{\text{f},-\sigma}}}e^{-l_{\text{ov}}U} \tag{2.68}$$

with l_{ov} being the imaginary time span of the impurity being doubly occupied. Due to the overlap, the weight depends on $q_{k,\uparrow}$ and $q_{k,\downarrow}$. Because of the (2.47) matrix elements of Δ, which refer to different spins, give zero. Δ has a block diagonal form in the spin sectors and hence factorizes

$$\det(\Delta) = \det(\Delta_\uparrow)\det(\Delta_\downarrow). \tag{2.69}$$

In practice we will usually consider the ratio of the weights of two configurations. One spin channel $(-\sigma)$ of those configurations will be identical. For this reason we introduce a abbreviating definition:

$$w_\sigma(q_k) \equiv \text{sign}_{\text{wind},\sigma}\det(\Delta_\sigma)\frac{e^{-L_\sigma\epsilon_{\text{f},\sigma}}}{1+e^{-\beta\epsilon_{\text{f},\sigma}}}e^{-l_{\text{ov}}U} \tag{2.70}$$

$$\text{with } \frac{w(q_k)}{w(p_l)} = \frac{w_\sigma(q_k)}{w_\sigma(p_l)} \text{ if } q_{k,-\sigma} = p_{l,-\sigma}. \tag{2.71}$$

The weights according to the configuration shown in 2.5 would hence be:

$$w_\uparrow\left((1,\uparrow,\tau_{1,\uparrow},\tau'_{1,\uparrow}),(1,\downarrow,\tau_{1,\downarrow},\tau'_{1,\downarrow})\right) = \det\left(\Delta(\tau_{1,\uparrow}-\tau'_{1,\uparrow})\right)\frac{e^{-(\tau'_{1,\uparrow}-\tau_{1,\uparrow})(\epsilon_\text{f}+h)}}{1+e^{-\beta(\epsilon_\text{f}+h)}}e^{-(\tau'_{1,\downarrow}-\tau_{1,\uparrow})U} \tag{2.72}$$

$$w_\downarrow\left((1,\uparrow,\tau_{1,\uparrow},\tau'_{1,\uparrow}),(1,\downarrow,\tau_{1,\downarrow},\tau'_{1,\downarrow})\right) = \det\left(\Delta(\tau_{1,\downarrow}-\tau'_{1,\downarrow})\right)\frac{e^{-(\tau'_{1,\downarrow}-\tau_{1,\downarrow})(\epsilon_\text{f}-h)}}{1+e^{-\beta(\epsilon_\text{f}-h)}}e^{-(\tau'_{1,\downarrow}-\tau_{1,\uparrow})U}. \tag{2.73}$$

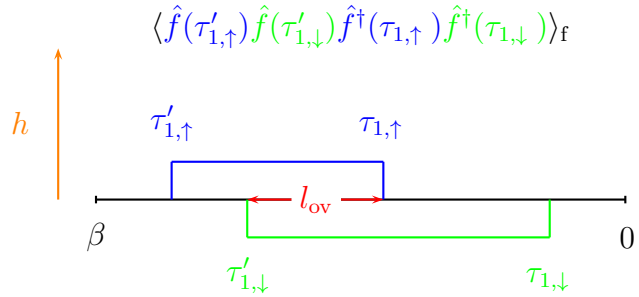

Figure 2.5.: Illustration of the segment picture with spin in a magnetic field.

2.4. Green function

According to [29, 30], the Green function on the impurity can be evaluated directly from these weights $w(q_k)$. Therefore we first introduce the Matrix M, which is the inverse and transposed of the Matrix Δ defined in (2.47).

$$M = \left(\Delta^{-1}\right)^{\mathrm{T}} \tag{2.74}$$

The Green function is then

$$G_\sigma(\tau) = \frac{\sum\limits_{q_{k,\sigma}} -\frac{1}{\beta}\sum_{n,m} M^{q_{k,\sigma}}_{n,m}\, d(\tau,\tau'_m-\tau_n) w_\sigma(q_{k,\sigma})}{\sum\limits_{q_{k,\sigma}} w_\sigma(q_k)} \equiv \left\langle -\frac{1}{\beta}\sum_{n,m} M^{q_{k,\sigma}}_{n,m}\, d(\tau,\tau'_m-\tau_n)\right\rangle_\sigma$$

$$d(\tau,\tau'_m-\tau_n) = \begin{cases} \delta(\tau-(\tau'_m-\tau_n)) & , \quad (\tau'_m-\tau_n)>0, \\ -\delta(\tau-(\tau'_m+\beta-\tau_n)), & (\tau'_m-\tau_n)<0. \end{cases} \tag{2.75}$$

To evaluate the impurity Green Function, hence means to sum up over all possible (infinitely many) configurations q_k. This problem is faced in 3.1.

As the Green function is discontinuous at $\tau = 0$ and $\tau = \beta$, we use an alternative way of measurement at these points. The Green function at $\tau = 0+\epsilon \equiv 0^+$ and $\tau = \beta - \epsilon \equiv \beta^-$ with $\epsilon \to 0$ can be expressed by the average occupation number n. From the definition

$$G_\sigma(\tau) = -\frac{1}{\beta}\int_0^\beta \mathrm{d}\tilde{\tau}\langle \mathrm{T}_\tau \hat{f}_\sigma(\tau+\tilde{\tau})\hat{f}^\dagger_\sigma(\tilde{\tau})\rangle \tag{2.76}$$

$$\tag{2.77}$$

follows

$$G(0^+) = -\langle \hat{f}\hat{f}^\dagger\rangle = -\langle 1-\hat{f}^\dagger\hat{f}\rangle = -1+n \tag{2.78}$$

$$G(\beta^-) = -G(0^-) = -\langle \hat{f}^\dagger\hat{f}\rangle = -n. \tag{2.79}$$

In the following we will see the derivation of equation (2.75). This formula is also derived in [16]. [4]

proof of Green function formula

For simplicity, we drop the index σ at all operators. We keep in mind, that every pair of creation and annihilation operators at imaginary time points has a additional spin. So τ_k/τ'_k is just an abbreviating version of $(\tau_k,\sigma_k)/(\tau'_k,\sigma_k)$. τ'_{new} and τ_{new} obviously have spin σ.

[4] The additional minus sign compared to these papers arises from the different definition of $F(\tau)$ and $\Delta(\tau)$, respectively.

Lets start with the definition of the Green function [5]

$$G_\sigma(\tau'_{\rm new},\tau_{\rm new}) \equiv -\langle \mathrm{T}_\tau \hat{f}(\tau'_{\rm new})\hat{f}^\dagger(\tau_{\rm new})\rangle = -\frac{Z_0}{Z}\langle \mathrm{T}_\tau \hat{f}(\tau'_{\rm new})\hat{f}^\dagger(\tau_{\rm new}) e^{-\int_0^\beta \mathrm{d}\tau \hat{H}_{\rm hyb}(\tau)}\rangle_0, \quad (2.80)$$

with $\tau_{\rm new}, \tau'_{\rm new} \in (0,\beta)$. We introduced the $\langle \ldots \rangle_0$-average using 2.34 and 2.40. Then we follow the arguments leading from 2.40 to 2.46 to do the first transformation:

$$-\frac{Z}{Z_0} G_\sigma(\tau'_{\rm new},\tau_{\rm new}) \quad (2.81)$$

$$= \sum_{q_k} |V|^{2n} \langle \mathrm{T}_\tau \hat{c}^\dagger(\tau'_k)\hat{c}(\tau_k)\ldots\hat{c}^\dagger(\tau'_1)\hat{c}(\tau_1)\rangle_{\rm c} \langle \mathrm{T}_\tau \hat{f}(\tau'_k)\hat{f}^\dagger(\tau_k)\ldots\hat{f}(\tau'_1)\hat{f}^\dagger(\tau_1)\hat{f}(\tau'_{\rm new})\hat{f}^\dagger(\tau_{\rm new})\rangle_{\rm f} \quad (2.82)$$

$$= \sum_{q_k} |V|^{2(n+1)} \langle \mathrm{T}_\tau \hat{c}^\dagger(\tau'_k)\hat{c}(\tau_k)\ldots\hat{c}^\dagger(\tau'_1)\hat{c}(\tau_1)\hat{c}^\dagger(\tau'_{\rm new})\hat{c}(\tau_{\rm new})\rangle_{\rm c}$$
$$\times \langle \mathrm{T}_\tau \hat{f}(\tau'_k)\hat{f}^\dagger(\tau_k)\ldots\hat{f}(\tau'_1)\hat{f}^\dagger(\tau_1)\hat{f}(\tau'_{\rm new})\hat{f}^\dagger(\tau_{\rm new})\rangle_{\rm f}$$
$$\times \frac{|V|^{2n}\langle \mathrm{T}_\tau \hat{c}^\dagger(\tau'_k)\hat{c}(\tau_k)\ldots\hat{c}^\dagger(\tau'_1)\hat{c}(\tau_1)\rangle_{\rm c}}{|V|^{2(n+1)}\langle \mathrm{T}_\tau \hat{c}^\dagger(\tau'_k)\hat{c}(\tau_k)\ldots\hat{c}^\dagger(\tau'_1)\hat{c}(\tau_1)\hat{c}^\dagger(\tau'_{\rm new})\hat{c}(\tau_{\rm new})\rangle_{\rm c}}. \quad (2.83)$$

From that point we move the new operators into the time ordered sequence of operators [6] . For every exchange of two neighbouring creators / annihilators we get an additional factor of $(-1)^3$ (for example: $\hat{c}^\dagger(\tau'_1)\hat{c}(\tau_1)\hat{c}^\dagger(\tau'_{\rm new})\hat{c}(\tau_{\rm new}) = (-1)^3\hat{c}^\dagger(\tau'_{\rm new})\hat{c}(\tau_1)\hat{c}^\dagger(\tau'_1)\hat{c}(\tau_{\rm new})$). The new positions of $\tau_{\rm new}$ / $\tau'_{\rm new}$ is called n / m, and we get an additional factor of $(-1)^{3(n/m-1)}$ for the new ordering within the expectation values. The fact, that the new operators have been moved into the existing set of operators, is symbolized by $\hat{\ldots}$.

$$= \sum_{q_k} |V|^{2(n+1)} \langle \mathrm{T}_\tau \hat{c}^\dagger(\tau'_k)\hat{c}(\tau_k)\ldots c^\dagger(\tau'_{\rm new})\ldots\hat{c}(\tau_{\rm new})\ldots\hat{c}^\dagger(\tau'_1)\hat{c}(\tau_1)\hat{\rangle}_{\rm c} \quad (2.84)$$

$$\times \langle \mathrm{T}_\tau \hat{f}(\tau'_k)\hat{f}^\dagger(\tau_k)\ldots\hat{f}(\tau'_{\rm new})\hat{.}\hat{.}\hat{.}f^\dagger(\tau_{\rm new})\ldots\hat{f}(\tau'_1)\hat{f}^\dagger(\tau_1)\rangle_{\rm f} \quad (2.85)$$

$$\times \frac{|V|^{2n}\langle \mathrm{T}_\tau \hat{c}^\dagger(\tau'_k)\hat{c}(\tau_k)\ldots\hat{c}^\dagger(\tau'_1)\hat{c}(\tau_1)\rangle_{\rm c}}{(-1)^{3(n-1)+3(m-1)}|V|^{2(n+1)}\langle \mathrm{T}_\tau \hat{c}^\dagger(\tau'_k)\hat{c}(\tau_k)\ldots\hat{c}^\dagger(\tau'_{\rm new})\ldots\hat{c}(\tau_{\rm new})\ldots\hat{c}^\dagger(\tau'_1)\hat{c}(\tau_1)\rangle_{\rm c}} \quad (2.86)$$

$$= \sum_{q_{k+1}(\tau_{\rm new},\tau'_{\rm new})} w(q_{k+1}(\tau_{\rm new},\tau'_{\rm new}))\frac{\det\left(\Delta^{q_k,\sigma}\right)}{\det\left(\Delta^{q_{k+1},\sigma(\tau_{\rm new},\tau'_{\rm new})}\right)}(-1)^{n+m} \quad (2.87)$$

Here $q_{k+1,\sigma}(\tau_{\rm new},\tau'_{\rm new})$ denotes a configuration with $k+1$ creators, $k+1$ annihilators in spin channel σ. In this configuration a particle is created on the impurity at imaginary time point $\tau_{\rm new}$ and annihilated at time point $\tau'_{\rm new}$. A configuration (eventually only one spin channel) as the upper right index of a matrix Δ or M denotes, that the matrix is constructed from that

[5] In general we would need to introduce spin indices, as the Green function is a spin dependent quantity as well. For simplicity we just drop them. The only point where the derivation changes, is at the definition of $q(\tau_{\rm new},\tau'_{\rm new})$ and $q(\tau)$, which considers only operators with the same spin index then. The result does not change because of this simplification.

[6] We remember from 2.2, that the $\tau_{\ldots}$'s are time ordered among themselves because of the integration borders. The same is valid for the $\tau'_{\ldots}$'s.

configuration. The index σ occurs in the ratio of the determinants because the determinant factorizes as shown in (2.69). With equation (3.35) it follows

$$G_\sigma(\tau'_{\text{new}},\tau_{\text{new}}) = -\frac{Z_0}{Z} \sum_{q_{k+1}(\tau_{\text{new}},\tau'_{\text{new}})} w(q_{k+1}(\tau_{\text{new}},\tau'_{\text{new}})) M_{n,m}^{q_{k+1,\sigma}(\tau_{\text{new}},\tau'_{\text{new}})}. \tag{2.88}$$

Now we go to the Green function with one imaginary time argument. The reader may note, that $\tau \in (0,\beta)$ and $G(\tau,\ldots) = -G(\tau-\beta,\ldots)$.

$$G_\sigma(\tau) \equiv \frac{1}{\beta}\int_0^\beta \mathrm{d}\tilde{\tau}\, G_\sigma(\tau+\tilde{\tau},\tilde{\tau}) \tag{2.89}$$

$$= \frac{1}{\beta}\int_0^{\beta-\tau} \mathrm{d}\tilde{\tau}\, G_\sigma(\tau+\tilde{\tau},\tilde{\tau}) + \frac{1}{\beta}\int_{\beta-\tau}^{\beta} \mathrm{d}\tilde{\tau}\, G_\sigma(\tau+\tilde{\tau},\tilde{\tau}) \tag{2.90}$$

$$= \frac{1}{\beta}\int_0^{\beta-\tau} \mathrm{d}\tilde{\tau}\, G_\sigma(\tau+\tilde{\tau},\tilde{\tau}) - \frac{1}{\beta}\int_{-\tau}^{0} \mathrm{d}\tilde{\tau}\, G_\sigma(\tau+\tilde{\tau},\beta+\tilde{\tau}) \tag{2.91}$$

$$= \frac{-\frac{1}{\beta}\sum\limits_{q_{k+1}^{\text{no wind}}(\tau)} w(q_{k+1}^{\text{no wind}}(\tau)) M_{n,m}^{q_{k+1,\sigma}^{\text{no wind}}(\tau)}}{\sum\limits_{q_k} w(q_k)} - \frac{-\frac{1}{\beta}\sum\limits_{q_{k+1}^{\text{wind}}(\tau)} w(q_{k+1}^{\text{wind}}(\tau)) M_{n,m}^{q_{k+1,\sigma}^{\text{wind}}(\tau)}}{\sum\limits_{q_k} w(q_k)} \tag{2.92}$$

$q_{\ldots}^{\cdots}(\tau)$ denotes a configuration , which has at least one creator (at τ_n) and one annihilator (at τ'_m) with distance

$$\tau = |\tau'_m,\tau_n| \equiv \begin{cases} \tau'_m - \tau_n & \text{for } \tau'_m > \tau_n (\text{no wind}) \\ \tau'_m + \beta - \tau_n & \text{for } \tau'_m < \tau_n (\text{wind}). \end{cases} \tag{2.93}$$

The indices n and m follow from the position of the operators compared to the other operators of the same kind.

To be able to sample over all possible configurations $\sum_{q_k}$, we use the β-antiperiodic delta function. [7] Further we use equation (2.70) to reduce the configuration space to one spin channel.

$$G_\sigma(\tau) = \frac{\sum_{q_k^{\text{no wind}}} -\frac{1}{\beta} \sum_{n,m} w(q_k^{\text{no wind}}) \delta\left(\tau - (\tau'_m - \tau_n)\right) M_{n,m}^{q_{k,\sigma}^{\text{no wind}}}}{\sum_{q_k} w(q_k)} \tag{2.94}$$

$$- \frac{\sum_{q_k^{\text{wind}}} -\frac{1}{\beta} \sum_{n,m} w(q_k^{\text{wind}}) \delta\left(\tau - (\tau'_m + \beta - \tau_n)\right) M_{n,m}^{q_{k,\sigma}^{\text{wind}}}}{\sum_{q_k} w(q_k)} \tag{2.95}$$

$$= \frac{\sum_{q_{k,\sigma}} -\frac{1}{\beta} \sum_{n,m} M_{n,m}^{q_{k,\sigma}} \, d(\tau, \tau'_m - \tau_n) w(q_{k,\sigma})}{\sum_{q_k} w(q_{k,\sigma})} \tag{2.96}$$

with

$$d(\tau, \tau'_m - \tau_n) = \begin{cases} \delta(\tau - (\tau'_m - \tau_n)) & \text{for} \quad (\tau'_m - \tau_n) > 0 \\ -\delta(\tau - (\tau'_m + \beta - \tau_n)) & \text{for} \quad (\tau'_m - \tau_n) < 0. \end{cases} \tag{2.97}$$

2.5. Susceptibility

The dynamic susceptibility χ is defined as:

$$\chi_{\sigma\sigma'}(\tau - \tau') = \langle \mathrm{T}_\tau \hat{n}_\sigma(\tau) \hat{n}_{\sigma'}(\tau') \rangle - \langle \hat{n}_\sigma \rangle \langle \hat{n}_{\sigma'} \rangle \tag{2.98}$$

$$= \frac{1}{\beta} \left\langle l_{\text{ov}}(q_{k,\sigma}^{\text{shifted:}+\tau}, q_{k,\sigma'}) \right\rangle - \langle \hat{n}_\sigma \rangle \langle \hat{n}_{\sigma'} \rangle \tag{2.99}$$

$$\chi_{\text{ch}} = \sum_{\sigma\sigma'} \chi_{\sigma\sigma'} \tag{2.100}$$

$$\chi_{\text{sp}} = \sum_{\sigma\sigma'} \sigma\sigma' \chi_{\sigma\sigma'} \tag{2.101}$$

$$\tag{2.102}$$

$q_{k,\sigma}^{\text{shifted:}+\tau}$ denotes a configuration of spin channel σ, which is basically $q_{k,\sigma}$ but every creator and annihilator shifted with $+\tau$. The dynamic susceptibility describes how the system in influenced in the future by the current configuration.

The static susceptibility follows from the zero frequency limit of the dynamic susceptibility. It is a scalar quantity. If the static susceptibility diverges, the system changes its behavior

[7] We use a delta function instead of a Koniker delta, as the Green function in imaginary time can numerically only be stored in an discrete way. We implement the delta function as a rectangular function with heigth $\frac{1}{\delta\tau}$ and width $\delta\tau$. $\delta\tau$ denotes the mesh distance in imaginary time domain.

qualitatively and hence undergoes a phase transition. In the following we will only investigate the dynamic susceptibility.

The dynamic susceptibility has the following symmetry property, which is the reason, why it is sufficient to show the 4 channels of χ in the interval $[0,\frac{\beta}{2})$.

$$\chi_{\sigma\sigma'}(\tau) = \chi_{\sigma'\sigma}(-\tau) = \chi_{\sigma'\sigma}(\beta - \tau) \tag{2.103}$$

For $U = 0$ we can compare the results of our simulation to the analytic solution

$$\chi_{\sigma\sigma'}(\tau) = \langle \mathrm{T}_\tau \hat{n}_\sigma(\tau)\hat{n}_{\sigma'}(0)\rangle - \langle \hat{n}_\sigma\rangle\langle \hat{n}_{\sigma'}\rangle \overset{wick}{=} -\delta_{\sigma\sigma'}G(\tau)G(-\tau). \tag{2.104}$$

proof of susceptibility formula

Starting by the definition

$$\chi_{\sigma,\sigma'}(\tau) = \frac{1}{\beta}\int_0^\beta \mathrm{d}\tilde{\tau}\ \langle \mathrm{T}_\tau \hat{n}_\sigma(\tau+\tilde{\tau})\hat{n}_{\sigma'}(\tilde{\tau})\rangle - \langle \hat{n}_\sigma\rangle\langle \hat{n}_{\sigma'}\rangle. \tag{2.105}$$

We need to look more carefully on the expectation value of the counting operators. By introducing the sum of all possible configurations q_k (q_k represents both spin channels σ and σ'), we get

$$\int_0^\beta \mathrm{d}\tilde{\tau}\ \langle \hat{n}_\sigma(\tau+\tilde{\tau})\hat{n}_{\sigma'}(\tilde{\tau})\rangle = \int_0^\beta \mathrm{d}\tilde{\tau}\ \frac{\sum_{q_k} \hat{n}_\sigma^{q_k}(\tau+\tilde{\tau})\hat{n}_{\sigma'}^{q_k}(\tilde{\tau})w(q_k)}{\sum_{q_k} w(q_k)}, \tag{2.106}$$

where $\hat{n}_{\sigma'}^{q_k}(\tilde{\tau})$ is 1, if q_k is a configuration with spin channel σ' occupied at imaginary time point $\tilde{\tau}$ and 0 otherwise. Then we exchange sum and integral and express the $\hat{n}$-operators by the overlap l_{ov} of the two spin channels, which is measurable directly:

$$= \frac{\sum_{q_k}\int_0^\beta \mathrm{d}\tilde{\tau}\ \hat{n}_\sigma^{q_k}(\tau+\tilde{\tau})\hat{n}_{\sigma'}^{q_k}(\tilde{\tau})w(q_k)}{\sum_{q_k} w(q_k)} = \frac{\sum_{q_k} l_{\mathrm{ov}}(q_{k,\sigma}^{\text{shifted:}+\tau}, q_{k,\sigma'})w(q_k)}{\sum_{q_k} w(q_k)} \tag{2.107}$$

$$\equiv \left\langle l_{\mathrm{ov}}(q_{k,\sigma}^{\text{shifted:}+\tau}, q_{k,\sigma'})\right\rangle. \tag{2.108}$$

3. Continuous-time quantum Monte Carlo (CT-QMC) method

As mentioned in the previous chapter Monte Carlo methods are used to evaluate averages of the type

$$\langle A \rangle = \frac{\sum\limits_{q_n} A w(q_n)}{\sum\limits_{q_n} w(q_n)}, \tag{3.1}$$

where $\sum\limits_{q_n}$ denotes the sum over all possible configurations (**phase space**), and $w(q_n)$ is the weighting factor of each configuration. [1]
As long as there is a limited number of possible configurations q_n, we can solve that problem exactly. But in real systems we get very quickly to such a large number of configurations, that this is not numerically tractable.

Monte Carlo methods are heuristics, which sample statistically through the configuration space. On the one side these methods do not consider every possible configuration [2]. On the other side they are quick for complex problems, and the precision is adjustable (by the number of samples). This sampling is performed by the Metropolis-Hasting algorithm.

After the application of the Metropolis-Hasting algorithm to our problem has been explained, we will derive the fast update procedure, as it provides an efficient speedup in the context of CT-QMC. The implementation and architecture of the CT-QMC code are presented to provide a guideline for the implementation of similar solvers.

3.1. Metropolis(-Hasting) algorithm

The idea of these algorithms is to produce a **Markov chain** [3] , which represents the appearance of each configuration according to its weight.

To achieve this we start with a simple example with a two configurations system: We have

[1] A physical example for this type of average is the partition function.
[2] Hence it might miss some (important) configuration with a high weight, if it is only accessible by passing configurations with low weights.
[3] For our purposes a Markov chain can be described as a sequence of statistically independent configurations.

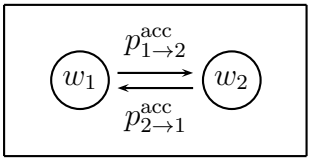

Figure 3.1.: simplest example: detailed balance condition for a two configurations system

a phase space with 2 possible configurations (which are denoted by index x and y), with a specific weight w. As we are doing a simulation to create a Markov Chain, we need to sample both configurations, according to they weights. Metropolis algorithms do that by proposing a transition from the one configuration to the other and accept that proposal with a certain probability p^{acc}. The tricky task is now to determine p^{acc} in such a way, that the occurrence of configurations x and y in the Markov chain mirrors their weights. For that we introduce the **detailed balance condition**. The idea is to establish some kind of equilibrium to the system, so that the number of transitions $1 \to 2$ is equal to the number of transitions $2 \to 1$, if one considers the whole Markov chain. From that requirement it follows the condition

$$w_1 p^{\text{acc}}_{1\to 2} = w_2 p^{\text{acc}}_{2\to 1}. \tag{3.2}$$

In this equation we already included the assumption, that the number of occurrences of configuration 1 / 2 is proportional to its weight. As w_1, w_2 are given by the physical system, we have one equation with two unknowns. One can resolve that by the so called Metropolis choice.

$$p^{\text{acc}}_{1\to 2} = \min\left(1, \frac{w_2}{w_1}\right). \tag{3.3}$$

The indices x and y can be exchanged to get the other acceptance probability. This is especially useful, because we can assign one formula to both acceptance probabilities. This makes the numerical implementation more straight forward.

This simple example can be generalized to a more complex system with (countable) [4] infinitely many configurations. In the new example there are many options to go from configuration x to another one. Because of this, we have to introduce the proposal probability $p^{\text{prop}}_{x\to y}$. If the system is in configuration x, $p^{\text{prop}}_{x\to y}$ is the probability to decide, to try a transition $x \to y$. If the transition is actually performed, depends on the acceptance probability $p^{\text{acc}}_{x\to y}$.

The detailed balance condition for 2 random configurations x and y is now

$$w_x p^{\text{prop}}_{x\to y} p^{\text{acc}}_{x\to y} = w_y p^{\text{prop}}_{y\to x} p^{\text{acc}}_{y\to x}, \tag{3.4}$$

because the proposal probabilities have to be considered as well. The reader may notice, that we do not consider circular transitions ($x \to y \to z \to x$), which may establish an equilibrium as well. The reason for this is, that things are getting more complicated without any additional benefit. So we keep things simple and use the most simple condition for a

[4] The reader may notice, that we are going to apply this method to the segment picture, which has an uncountable number of configurations. This is the reason for introducing the transformation (3.6) later.

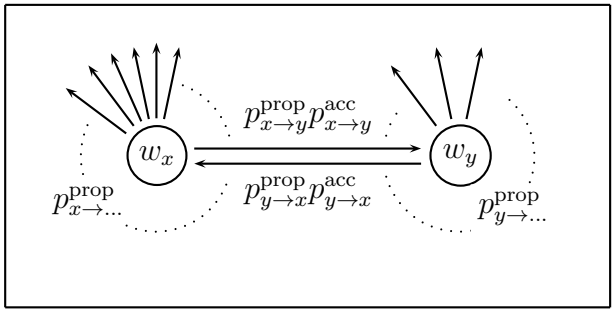

Figure 3.2.: detailed balance condition for a general system

Markov chain that mirrors the weights of the configurations. The Metropolis choice follows straight forward

$$p^{\text{acc}}_{x\to y} = \min\left(1, \frac{p^{\text{prop}}_{y\to x}}{p^{\text{prop}}_{x\to y}}\,\frac{w_y}{w_x}\right). \tag{3.5}$$

We can see, that the acceptance probability depends on the proposal probability and hence on the proposal process. This detail may cause some misunderstandings.

The difference between the Metropolis and the Metropolis-Hasting algorithm is the proposal probability:

- **Metropolis:** $p^{\text{prop}}_{x\to y} = p^{\text{prop}}_{y\to x}\ \forall x,y$
- **Metropolis-Hasting:** $\exists x,y : p^{\text{prop}}_{x\to y} \neq p^{\text{prop}}_{y\to x}$.

3.2. Update processes

As described in the previous chapter we will use the Metropolis-Hasting algorithm to cover the whole Hilbert space. Because the interval $[0,\beta)$ on the imaginary time axis is continuous, we have infinitely many possibilities to go from one configuration to another. As Metropolis-Hasting is designed for discrete problems, we discretize our interval. [5] When we evaluate the partition function (2.41), we use the following substitution for each integration in imaginary time

$$\int_0^\beta \mathrm{d}\tau_m \int_0^\beta \tau'_m w(\tau_m,\tau'_m,\ldots) \to \sum_{i=1}^{N}\frac{\beta}{N}\sum_{j=1}^{N}\frac{\beta}{N} w(i,j,\ldots) \tag{3.6}$$

From that, we get an additional factor of $\left(\frac{\beta}{N}\right)^2$ for every expansion order.

$$w(q_n) \to \left(\frac{\beta}{N}\right)^{2n} w(q_n) \tag{3.7}$$

[5] Later we will find out, that this discretization cancels out in the acceptance probabilities which are calculated according to (3.10), (3.11), (3.12), (3.13) and (3.15).

This prefactor has to be added to every w^{new} and w^{old} in this section.

To get from one segment configuration to another we use 5 different update processes (add segment, remove segment, add antisegment, remove antisegment, shift operator). For ergodicity (ability to reach every point of the Hilbert space) it would be enough to use just the processes add and remove segment. The others are just there to increase performance. The start configuration for the warm up process is $\langle 0|\hat{1}|0\rangle$, with no particle being present ($n = 0$). The update processes work as following:

add / remove segment (as / rs)

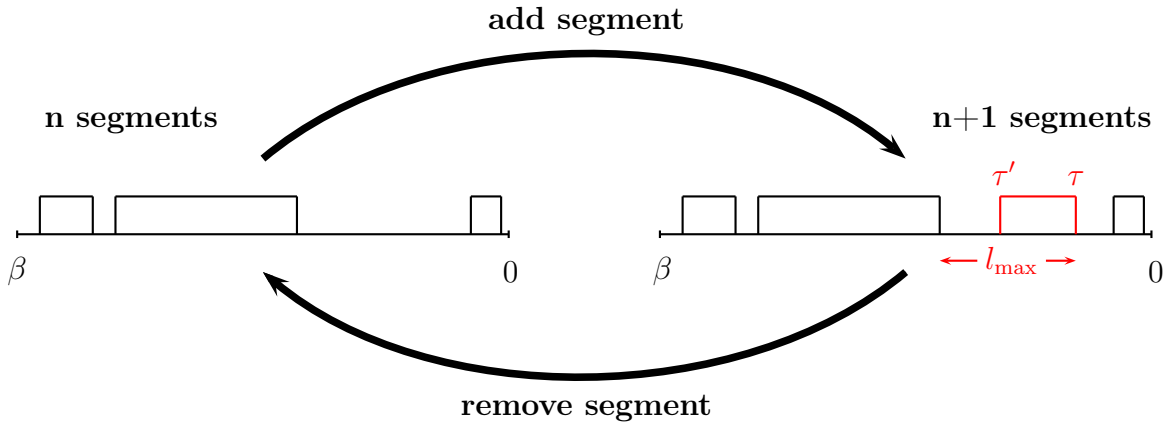

Figure 3.3.: Illustration of the add segment and the remove segment processes

After having decided to add a segment we use the following procedure. First we choose a random starting point $\in [0,\beta)$. If the starting point τ hits an existing segment, we cancel the process immediately. [6] If we hit no existing segment, we choose a random endpoint τ' from the interval of our starting point and the starting point of the next segment. The length of this interval is called $l_{\max}$. $\tau' \in (\tau, \tau + l_{\max}]$. Then we change the numeration of the segments (according to the way, it is described in section 2.2.3) and evaluate the new weight. To evaluate the proposal probability for this process we have to consider again the discretized imaginary time interval. We have a probability of $\frac{1}{N}$ of choosing τ and a probability of $\frac{1}{\frac{l_{\max}}{\beta}N}$ of choosing τ'. The probability for deciding to add a segment in the first place is $\frac{1}{4}$ (compare section 3.4). Therefore it follows

$$p_{\text{as}}^{\text{prop}} = \frac{\beta}{4 l_{\max} N^2} \tag{3.8}$$

The remove process simply consists of deciding to remove a segment (probability $\frac{1}{4}$) and of choosing the segment, which shall be removed (probability $\frac{1}{n+1}$).

$$p_{\text{rs}}^{\text{prop}} = \frac{1}{4(n+1)} \tag{3.9}$$

[6] This is equivalent of putting the weight of the new configuration to zero. $w^{\text{new}} = 0$

According to (3.5) and (3.7) it follows for the acceptance probabilities

$$p_{\text{as}}^{\text{acc}} = \min\left(1, \frac{p_{\text{rs}}^{\text{prop}} w_{n+1}}{p_{\text{as}}^{\text{prop}} w_n}\right) = \frac{l_{\max}\beta}{n+1}\frac{w_{n+1}}{w_n} \tag{3.10}$$

$$p_{\text{rs}}^{\text{acc}} = \min\left(1, \frac{p_{\text{as}}^{\text{prop}} w_n}{p_{\text{rs}}^{\text{prop}} w_{n+1}}\right) = \frac{n+1}{l_{\max}\beta}\frac{w_n}{w_{n+1}} \tag{3.11}$$

Here w_n denotes the weight of the configuration with n segments. Further we dropped the $\min(1, \ldots)$. Our convention from now on is to accept probabilities > 1 with probability 1.

add / remove antisegment (aa / ra)

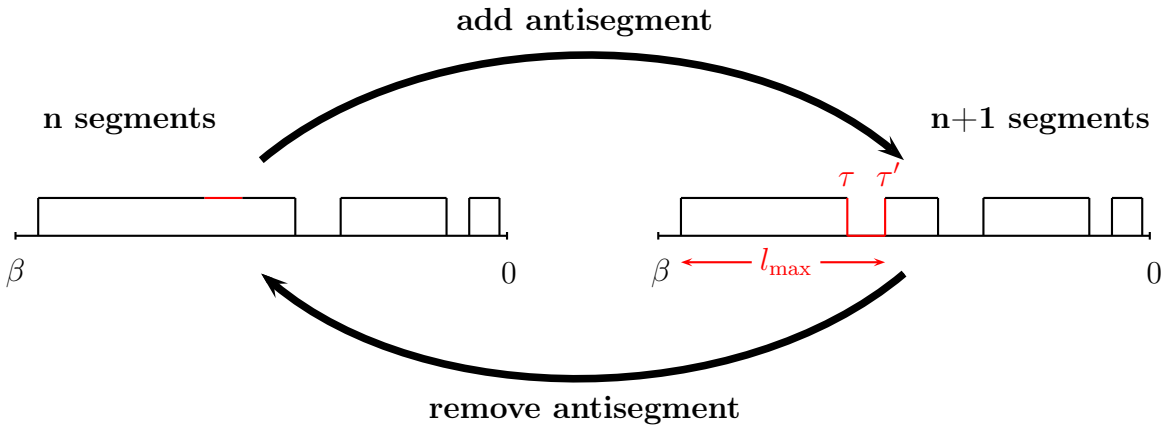

Figure 3.4.: Illustration of the add antisegment and the remove antisegment processes

The add and remove antisegment processes work corresponding to the segment processes. An antisegment is a not occupied area. In the add antisegment process we first decide to execute that process (prob. $\frac{1}{4}$). Then we choose a random point τ' (prob. $\frac{1}{N}$). If we did not hit a segment, we cancel the process immediately, otherwise we determine $l_{\max}$, which is the distance to the next annihilator in this case. From that interval we choose another point τ (prob. $\frac{1}{\frac{l_{\max}}{\beta}N}$). Now we add a hole into the segment, we hit, and change the numeration.

The reverse process of removing an antisegment consists of two steps; first to decide to remove a antisegment (prob. $\frac{1}{4}$) and then to choose the antisegment which shall be removed. The probability for that is $\frac{1}{n+1}$, because the number of segments is equal to the number of antisegments.

So the acceptance probabilities for the antisegent processes are:

$$p_{aa}^{\text{acc}} = \frac{\beta l_{\max}}{n+1}\frac{w_{\text{n+1}}}{w_{\text{n}}} \tag{3.12}$$

$$p_{ra}^{\text{acc}} = \frac{n+1}{\beta l_{\max}}\frac{w_{\text{n}}}{w_{\text{n+1}}}. \tag{3.13}$$

Here we used the discretization of the imaginary time according to equation (3.7).

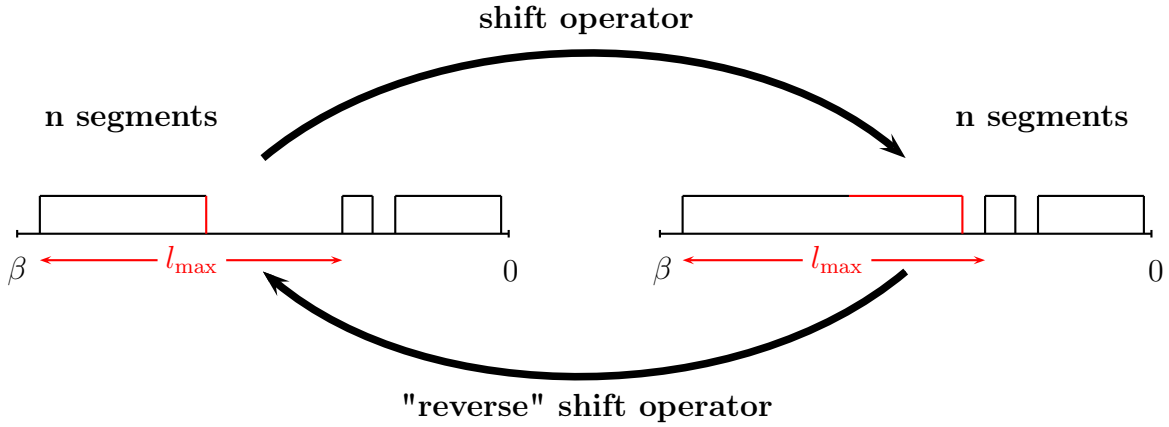

Figure 3.5.: Illustration of the shift operator process

shift operator (sh / rsh)

When shifting an operator we first choose a segment with a probability $\frac{1}{n}$. After that we decide if we shall shift the creator or the annihilator of this segment (probability $\frac{1}{2}$). The new position of the operator is bounded by the positions of the 2 surrounding operators of the opposite kind. The resulting interval, which is accessible for the new operator position is $l_{\max}$. This gives us an additional factor $\frac{1}{\frac{l_{\max}}{\beta}N}$.

The reverse process works exactly the same way. Even the length of $l_{\max}$ is equal. Therefore we get

$$p_{\text{sh}}^{\text{prop}} = p_{\text{rsh}}^{\text{prop}} = \frac{\beta}{2nl_{\max}N} \tag{3.14}$$

We see that it is not possible to make a distinction between shift and reverse shift processes.

The proposal probabilities cancel out of equation 3.5 and the acceptance probability yields

$$p_{n\to n}^{\text{acc}} = \frac{w^{\text{new}}}{w^{\text{old}}}. \tag{3.15}$$

increasing performance

To increase performance we replace the fraction of the weights by

$$\frac{w^{\text{new}}}{w^{\text{old}}} = \text{sign}_{\text{wind}} \frac{\det(\Delta^{\text{new}})}{\det(\Delta^{\text{old}})} \times e^{-\delta l\, \epsilon_{\text{f}} - \delta_{\text{ov}} U} \tag{3.16}$$

$$\lambda \equiv \frac{\det(\Delta^{\text{new}})}{\det(\Delta^{\text{old}})} \tag{3.17}$$

with $\text{sign}_{\text{wind}} = 1$, if the wind status is the same for the new and the old configuration and $\text{sign}_{\text{wind}} = -1$ otherwise. δl denotes the difference of the sum over the length of all segments $\delta l = \sum_{\text{segments new}} \text{length}_{\text{segment}} - \sum_{\text{segments old}} \text{length}_{\text{segment}}$. δ_{ov} denotes the change of l_{ov}, which is the imaginary time span of double occupation on the impurity.

3.3. Fast update scheme

The equations (2.68) and (2.75) are essentially for sampling through the phase space, for computing the Green function and hence for solving the SIAM. Unfortunately each contains a numerically very expensive step, which is the computation of the determinant / the inverse of a matrix. This costs at least of order $n^{\log_2 7}$ [26] substantial processes. Hence this is the speed-limiting part for the CT-QMC algorithm.

The fast update scheme offers a speed up for this. The basic idea is to consider an update process $q_n^{\text{old}} \to q_m^{\text{new}}$. Because we already evaluated the weight and the Green function of the configuration q_n^{old}, we already have the matrices Δ^{old} and M^{old}. After having evaluated Δ^{new} by adding/removing/changing a row and a column, there are now two options:

- We calculate M^{new} form Δ^{new} by matrix inversion.
- We evaluate M^{new} from the collective information which are provided by M^{old}, Δ^{old} and the new row and the new column. This is called the fast update scheme.

The later choice turns out to use only of order n^2 operations and hence offers an important speedup for the algorithm. The fast update scheme will be explained in this chapter.

We start with the following setup. We have a matrix Δ^{old} and its inverse transposed M^{old}. Both have dimension k. The indices on the upper left side of a matrix/vector have the following meaning: **t: top; b: bottom; l: left; r: right** and denote a part of the matrix, which is split because of the inserted row and column.

$$\Delta^{\text{old}} = \begin{pmatrix} {}^{\text{tl}}\Delta^{\text{old}} & {}^{\text{tr}}\Delta^{\text{old}} \\ {}^{\text{bl}}\Delta^{\text{old}} & {}^{\text{br}}\Delta^{\text{old}} \end{pmatrix}, \quad M^{\text{old}} = \begin{pmatrix} {}^{\text{tl}}M^{\text{old}} & {}^{\text{tr}}M^{\text{old}} \\ {}^{\text{bl}}M^{\text{old}} & {}^{\text{br}}M^{\text{old}} \end{pmatrix} \tag{3.18}$$

We add a column $\boldsymbol{c}$ and a row $\boldsymbol{r}^{\text{T}}$ to Δ^{old}, which are also k dimensional vectors. The intersecting element of the new row and the new column is called rc. The resulting matrix Δ^{new} has dimension $(k+1) \times (k+1)$.

$$\Delta^{\text{new}} = \begin{pmatrix} & & m & \\ & & c_1 & \\ & {}^{\text{tl}}\Delta^{\text{old}} & \vdots & {}^{\text{tr}}\Delta^{\text{old}} \\ & & c_{n-1} & \\ r_1 \quad \dots \quad r_{m-1} & & rc & r_m \quad \dots \quad r_k \\ & & c_n & \\ & {}^{\text{bl}}\Delta^{\text{old}} & \vdots & {}^{\text{br}}\Delta^{\text{old}} \\ & & c_k & \end{pmatrix} \begin{matrix} \\ \\ \\ \\ n \\ \\ \\ \\ \\ \end{matrix} \tag{3.19}$$

To make the new and the old matrices comparable we introduce $\tilde{\Delta}$ and $\tilde{M}$, which have a dummy row and column included. The dimension of those matrices is hence $(k{+}1){\times}(k{+}1)$.

$$\tilde{\Delta} = \begin{pmatrix} & & m & \\ & & 0 & \\ & {}^{\text{tl}}\Delta^{\text{old}} & \vdots & {}^{\text{tr}}\Delta^{\text{old}} \\ & & 0 & \\ 0 \quad \dots \quad 0 & & 1 & 0 \quad \dots \quad 0 \\ & & 0 & \\ & {}^{\text{bl}}\Delta^{\text{old}} & \vdots & {}^{\text{br}}\Delta^{\text{old}} \\ & & 0 & \end{pmatrix} \begin{matrix} \\ \\ \\ \\ n \\ \\ \\ \\ \\ \end{matrix} \tag{3.20}$$

$$\tilde{M} = \left(\tilde{\Delta}^{-1}\right)^{\text{T}} = \begin{pmatrix} & & m & \\ & & 0 & \\ & {}^{\text{tl}}M^{\text{old}} & \vdots & {}^{\text{tr}}M^{\text{old}} \\ & & 0 & \\ 0 \quad \dots \quad 0 & & 1 & 0 \quad \dots \quad 0 \\ & & 0 & \\ & {}^{\text{bl}}M^{\text{old}} & \vdots & {}^{\text{br}}M^{\text{old}} \\ & & 0 & \end{pmatrix} \begin{matrix} \\ \\ \\ \\ n \\ \\ \\ \\ \\ \end{matrix} \tag{3.21}$$

Further we calculate the difference between the new and the old Δ matrix

$$D = \Delta^{\text{new}} - \tilde{\Delta} = \begin{pmatrix} & & & m & & & \\ & & & c_1 & & & \\ & 0 & & \vdots & & 0 & \\ & & & c_{n-1} & & & \\ r_1 & \dots & r_{m-1} & rc-1 & r_m & \dots & r_k \\ & & & c_n & & & \\ & 0 & & \vdots & & 0 & \\ & & & c_k & & & \end{pmatrix} \begin{matrix} \\ \\ \\ \\ n \\ \\ \\ \\ \end{matrix} \tag{3.22}$$

From the definitions of $D = \Delta^{\text{new}} - \tilde{\Delta} = \left(M^{\text{new,T}}\right)^{-1} - \left(\tilde{M}^{\text{T}}\right)^{-1}$ follows

$$M^{\text{new}} = \left(\hat{1} + \tilde{M} D^{\text{T}}\right)^{-1} \tilde{M}. \tag{3.23}$$

This formula is the central formula for the derivation of the fast update scheme. It may look complicated at the first sight, but the matrix $\hat{1} + \tilde{M} D^{\text{T}}$ is a sparse matrix with very simple properties:

$$\hat{1} + \tilde{M} D^{\text{T}} = \begin{pmatrix} & & & n & & & \\ & & & \left(M^{\text{old}} \boldsymbol{r}\right)_1 & & & \\ & \hat{1} & & \vdots & & 0 & \\ & & & \left(M^{\text{old}} \boldsymbol{r}\right)_{n-1} & & & \\ c_1 & \dots & c_{n-1} & rc & c_n & \dots & c_k \\ & & & \left(M^{\text{old}} \boldsymbol{r}\right)_n & & & \\ & 0 & & \vdots & & \hat{1} & \\ & & & \left(M^{\text{old}} \boldsymbol{r}\right)_k & & & \end{pmatrix} \begin{matrix} \\ \\ \\ \\ n \\ \\ \\ \\ \end{matrix} . \tag{3.24}$$

To derive these properties we first define a general matrix of that kind

$$U \equiv \begin{pmatrix} & & & n & & & \\ & & & a_1 & & & \\ & \hat{1} & & \vdots & & 0 & \\ & & & a_{n-1} & & & \\ b_1 & \dots & b_{n-1} & x & b_n & \dots & b_k \\ & & & a_n & & & \\ & 0 & & \vdots & & \hat{1} & \\ & & & a_k & & & \end{pmatrix} \begin{matrix} \\ \\ \\ \\ n \\ \\ \\ \\ \end{matrix} . \tag{3.25}$$

The determinant follows by splitting into subdeterminants of dimension k and switching rows

$$\begin{aligned}\det(U) =& \det\begin{pmatrix} x & b_1 & \dots & b_k \\ a_1 & & & \\ \vdots & & \hat{1} & \\ a_k & & & \end{pmatrix} = x + \sum_{i=1}^{k}(-1)^i a_i \det\begin{pmatrix} b_1 & \dots & b_k \\ \hat{1}_{i\text{-th row missing}} & & \end{pmatrix} \\ =& x + \sum_{i=1}^{k}(-1)^i a_i (-1)^{i-1} b_i = x - \boldsymbol{b}^{\mathrm{T}}\boldsymbol{a}. \end{aligned} \tag{3.26}$$

The inverse of U is[7]

$$U^{-1} = \frac{1}{\det(U)} \begin{pmatrix} & & & n & \\ & & & -a_1 & \\ & \hat{1} + {}^{\mathrm{tl}}\left(\boldsymbol{a}\boldsymbol{b}^{\mathrm{T}}\right) & \vdots & \hat{1} + {}^{\mathrm{tr}}\left(\boldsymbol{a}\boldsymbol{b}^{\mathrm{T}}\right) & \\ & & & -a_{m-1} & \\ -b_1 & \dots & -b_{m-1} & 1 & -b_m \quad \dots \quad -b_k \\ & & & -a_m & \\ & \hat{1} + {}^{\mathrm{bl}}\left(\boldsymbol{a}\boldsymbol{b}^{\mathrm{T}}\right) & \vdots & \hat{1} + {}^{\mathrm{br}}\left(\boldsymbol{a}\boldsymbol{b}^{\mathrm{T}}\right) & \\ & & & -a_k & \end{pmatrix} \quad n \ . \tag{3.27}$$

Here $\boldsymbol{a}\boldsymbol{b}^{\mathrm{T}}$ denotes a Matrix with $\left(\boldsymbol{a}\boldsymbol{b}^{\mathrm{T}}\right)_{ij} = a_i b_j$. Now we have all the properties of $\hat{1} + \tilde{M} D^{\mathrm{T}}$ to derive the fast update scheme.

determinant ratio λ

First we handle the determinant ratio, which is

$$\lambda = \frac{\det\left(\Delta^{\mathrm{new}}\right)}{\det\left(\Delta^{\mathrm{old}}\right)} = \frac{\det\left(M^{\mathrm{old}}\right)}{\det\left(M^{\mathrm{new}}\right)} = \frac{(-1)^{n+m}\det\left(\tilde{M}\right)}{\frac{1}{\det\left(\hat{1}+\tilde{M}^{\mathrm{T}}D\right)}\det\left(\tilde{M}\right)} = (-1)^{n+m}\det\left(\hat{1} + D^{\mathrm{T}}\tilde{M}\right) \tag{3.28}$$

and we get

$$\lambda = (-1)^{n+m}\left(rc - \boldsymbol{c}^{\mathrm{T}} M^{\mathrm{old}} \boldsymbol{r}\right). \tag{3.29}$$

new inverse transposed matrix M^{new}

Next we derive the fast update formular for M^{new}. For that we define

$$\lambda' \equiv \det\left(\hat{1} + D^{\mathrm{T}}\tilde{M}\right) = (-1)^{n+m}\lambda. \tag{3.30}$$

[7],which can be verified by calculating $UU^{-1} = U^{-1}U = \mathbb{1}$

Hence it follows

$$M^{\text{new}} = \left(\hat{1} + \tilde{M} D^{\mathrm{T}}\right)^{-1} \tilde{M} \tag{3.31}$$

$$= \left[\hat{1} + \frac{1}{\lambda'} \begin{pmatrix} {}^{\text{tl}}\left(M^{\text{old}} \boldsymbol{r} \boldsymbol{c}^{\mathrm{T}}\right) & {}^{\text{t}}\left(-M^{\text{old}} \boldsymbol{r}\right) & {}^{\text{tr}}\left(M^{\text{old}} \boldsymbol{r} \boldsymbol{c}^{\mathrm{T}}\right) \\ {}^{\text{l}}\left(-\boldsymbol{c}^{\mathrm{T}}\right) & 1 - \lambda' & {}^{\text{r}}\left(-\boldsymbol{c}^{\mathrm{T}}\right) \\ {}^{\text{bl}}\left(M^{\text{old}} \boldsymbol{r} \boldsymbol{c}^{\mathrm{T}}\right) & {}^{\text{b}}\left(-M^{\text{old}} \boldsymbol{r}\right) & {}^{\text{br}}\left(M^{\text{old}} \boldsymbol{r} \boldsymbol{c}^{\mathrm{T}}\right) \end{pmatrix} \begin{matrix} \\ n \\ \\ \end{matrix} \right] \begin{matrix} \\ n \\ \\ \end{matrix} \tag{3.32}$$

$$\times \begin{pmatrix} & & & m & & & \\ & & & 0 & & & \\ & {}^{\text{tl}}\left(M^{\text{old}}\right) & & \vdots & & {}^{\text{tr}}\left(M^{\text{old}}\right) & \\ & & & 0 & & & \\ 0 & \cdots & 0 & 1 & 0 & \cdots & 0 \\ & & & 0 & & & \\ & {}^{\text{bl}}\left(M^{\text{old}}\right) & & \vdots & & {}^{\text{br}}\left(M^{\text{old}}\right) & \\ & & & 0 & & & \end{pmatrix} \begin{matrix} \\ \\ \\ \\ n \\ \\ \\ \\ \end{matrix} \tag{3.33}$$

$$= \tilde{M} + \frac{1}{\lambda'} \begin{pmatrix} {}^{\text{tl}}\left(\boldsymbol{L}\boldsymbol{R}^{\mathrm{T}}\right) & {}^{\text{t}}\left(-M^{\text{old}} \boldsymbol{r}\right) & {}^{\text{tr}}\left(\boldsymbol{L}\boldsymbol{R}^{\mathrm{T}}\right) \\ {}^{\text{l}}\left(-\boldsymbol{c}^{\mathrm{T}}\right) & 1 - \lambda' & {}^{\text{r}}\left(-\boldsymbol{c}^{\mathrm{T}}\right) \\ {}^{\text{bl}}\left(\boldsymbol{L}\boldsymbol{R}^{\mathrm{T}}\right) & {}^{\text{b}}\left(-M^{\text{old}} \boldsymbol{r}\right) & {}^{\text{br}}\left(\boldsymbol{L}\boldsymbol{R}^{\mathrm{T}}\right) \end{pmatrix} \begin{matrix} \\ n \\ \\ \end{matrix} \tag{3.34}$$

with $\boldsymbol{L} \equiv M^{\text{old}} \boldsymbol{r}$; $\boldsymbol{R}^{\mathrm{T}} \equiv \boldsymbol{c}^{\mathrm{T}} M^{\text{old}}$.
In the last step we made use of the relation $\left[\left(M^{\text{old}} \boldsymbol{r}\right) \boldsymbol{c}^{\mathrm{T}}\right] M^{\text{old}} = \boldsymbol{L}\boldsymbol{R}^{\mathrm{T}}$.

Further we see the relation

$$M^{\text{new}}_{n,m} = \frac{1}{\lambda'} = (-1)^{n+m} \lambda = (-1)^{n+m} \frac{\det\left(\Delta^{\text{old}}\right)}{\det\left(\Delta^{\text{new}}\right)}. \tag{3.35}$$

3.4. Code architecture

The general mechanism of the Metropolis-Hasting algorithm has been explained in 3.1. This section is about the specific implementation of this kind of algorithm.

The first problem we face, when implementing the algorithm is the question: What is the configuration we start with? There are two concepts of choosing a start configuration. In the

cold start [20] we use with the simplest possible configuration. In our case is this an empty segment picture. The alternative option is a **hot start**. This is done, by either choosing a random start configuration or by constructing it in such a way, that it has a high weight compared to the other configurations [20]. We perform a cold start in our simulation.

Independent of what start we choose, we face the problem, that the starting configuration and the first configurations in the Markov chain might be overweighted, because they appear at least once. To prevent this issue we use a **warm up phase**, which consists of $\sim 10^5$ randomly chosen as/rs/aa/ra processes and $\sim 10^5/4$ shift operator processes. We first perform four as/rs/aa/ra processes and afterwards the shift process, because it might happen otherwise, that we would remove a segment, which had been just modified by the shift process. The shift process would have costed time then, without any computational use.

In this phase we do not measure any observables, but only the following quantities:

- average expansion order $\langle k \rangle$
- average probability to accept a as/rs/aa/ra process
- average probability to accept a shift process

With these quantities we can calculate an estimate for the average number of processes, which are necessary to change the whole segment picture. This is called the **Monte Carlo step** size for the further simulation. In the main part of the Monte Carlo procedure we measure the observables after each Monte Carlo step, because it ensures a certain degree of independence of the measurements and avoids the computational effort, which is connected to the measurement process. In general it would be also correct to measure after every process, but because of the high correlation of the measurements we would not achieve any improvement. A rule of thumb for the size of a Monte Carlo step is $n_i^{\mathrm{MC}} \propto \frac{\langle k \rangle}{\langle p_i^{\mathrm{acc}} \rangle}$ with $i = 1$ denoting the as/rs/aa/ra processes and $i = 2$ denoting the shift operator process.

A further issue shows, that Monte Carlo methods are a statistical measurement. This is compareable of performing a numerical experiment, which has a certain probability to return the right result, but there are also derivations possible. Like other statistical measurements the probability for the different possible results is a Gauss distribution around the right result (expectation value). [8] In figure 3.6 we can see a schematic description of this problem.

To improve the measurement, we can perform more Monte Carlo steps, but we still have no indication, how precise our result is. To get a quantity for that we just perform several independent measurements and calculate the average and the standard derivation. So if

[8] To ensure, that the data is indeed Gaussian distributed, we protocol the distribution of our measurements.

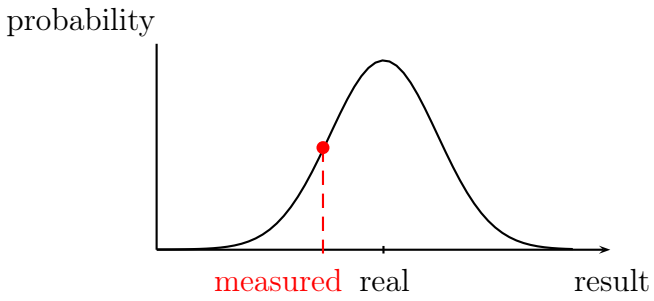

Figure 3.6.: result of a statistical Monte Carlo measurement

we measured an observable A before directly, we measure now a set of A_1,A_2,...,A_N in N independent measurements. From that we can calculate the average

$$\langle A \rangle = \frac{1}{N} \sum_{i=1}^{N} A_i \tag{3.36}$$

and the standard derivation

$$\sigma_A = \sqrt{\langle A^2 \rangle - \langle A \rangle^2}. \tag{3.37}$$

By this the precision of the measurement stays the same, because it consists of the same number of independent samples, but we have an additional indicator for the quality of the result. A schematic description of this new way of measureing can be found in figure 3.7. There is a further big advantage of this way of computing. Because of the independence of

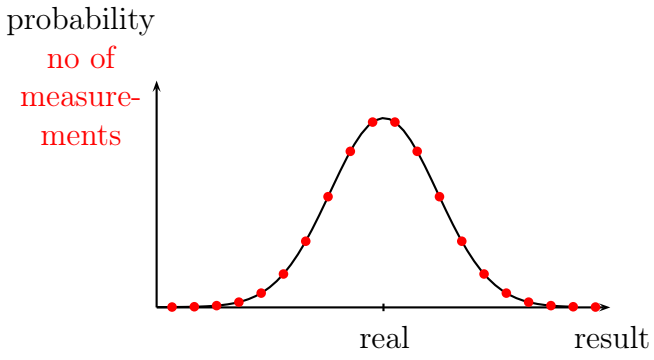

Figure 3.7.: resulting statistic of serveral independent measurements

the measurement process we can parallelize the simulation to N cores. The communication footprint is very small, because we get communication only after the warm up and at the end of the simulation. Further we do not need shared memory and hence are not restricted to the maximum number of core per node on a cluster. The tool I used to implement the parallelization is the current **MPI 3.0** standard with the collective communication routines.

The full architecture of the Monte Carlo process can be seen in figure 3.8.

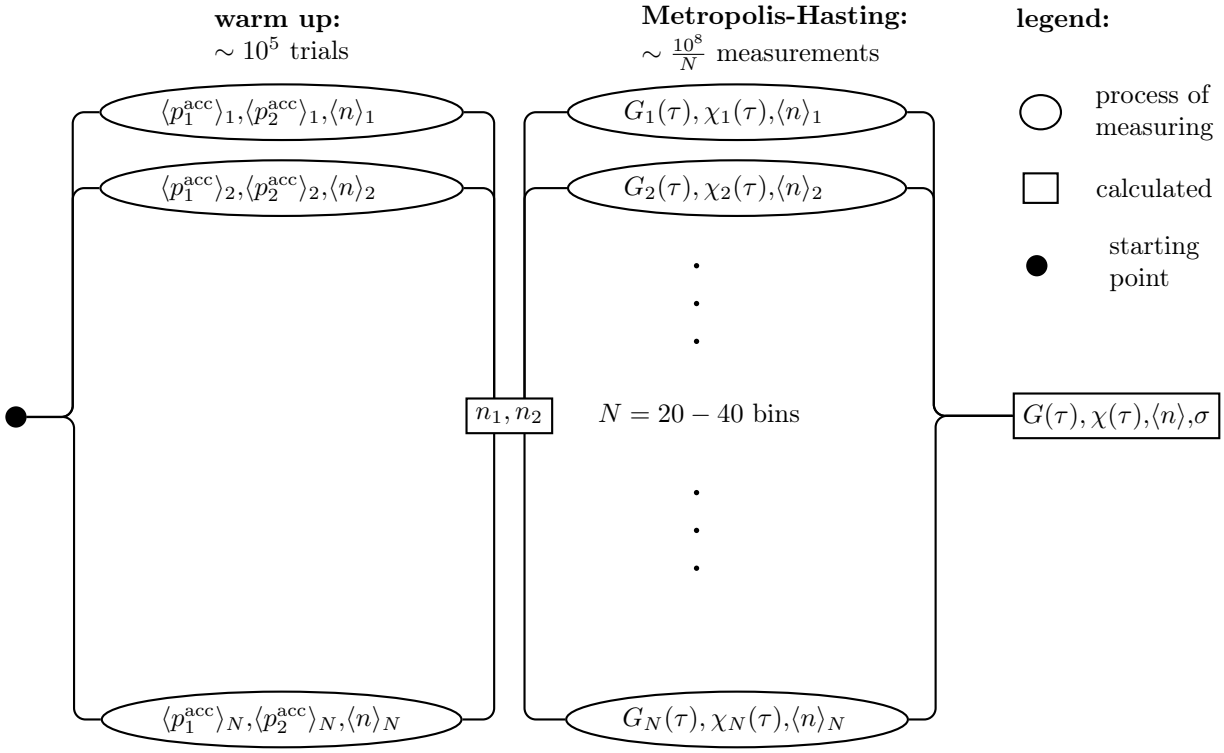

Figure 3.8.: architecture of the CT-QMC process

3.5. Analytic continuation

The purpose of analytic continuation is to calculate the spectral function from the impurity Green function. There are two different methods available: the maximum entropy method (maxent) and the pade method. In this work an existing maxent code based on [5, 19, 27] was used, which calculates the spectral function in real energy domain from the impurity Green function in imaginary time domain.

A necessary precondition to use maxent is, that the input data is Gaussian distributed. To ensure that, the code, which was written for this thesis, produces statistical protocols of the numerical data. In table 3.9 we look at the statistical protocol of the Green function, which was used to produce figure 4.7. We count therefore all measurements $x(\tau)$ of the impurity Green function in imaginary time domain τ, which are smaller then the average value of the data$\langle X(\tau)\rangle$ plus/minus an integer multiple of the standard derivation $\sigma_{x,\tau}$. This is done for each τ mesh point independently. The $\langle X(\tau)\rangle$ were computed by 20 parallel processes. To increase the precision of our analysis we sum up the distributions over all 512 τ mesh points.

We can see a good agreement of the expected and the measured distribution. Derivations result from the low sample size of $20 * 512$ (not independent) points. This check was also performed on 200 parallel processes, which gave a better agreement of the measured and expected distribution. The distribution of each τ mesh point was also Gaussian there. We did not look at this statistics here, because it does not represent the quality of the maxent input data, which was used in this work.

$$\sum_{\tau} \#x(\tau) : x(\tau) < \langle X(\tau) \rangle + j\sigma_{x,\tau}$$

$j =$	-3	-2	-1	0	1	2	3
expected (in %)	0.2	2.3	15.8	50	84.2	97.7	99.8
h=0.0 (in %)	0.2	2.5	15.8	49.4	84.5	97.9	99.8
h=0.1 (in %)	0.0	1.5	16.9	50.7	83.0	97.7	100.0
h=0.175 (in %)	0.1	2.5	15.0	51.3	83.9	97.6	100.0
h=0.2 (in %)	0.0	1.5	16.9	50.4	84.4	97.8	100.0

Figure 3.9.: quality of the Gaussian distributed input data for the maximum entropy method used to produce the results, shown in figure 4.7

Attention: Maxent cannot reproduce functions with sharp turning point features such as the top and the bottom of a semi-circular spectral function. Occurring artefacts are a flattening / smoothening and an oscillating structure on top of the results in the effected area. We will observe these features on the spectral functions presented in section 4.

3.6. Problems during implementation

When implementing the CT-QMC algorithm some unexpected problems might occure. Some of those are very difficult to detect, because they appear very rarely. [9]

Double precision

The error of double precision occures due to numerical rounding, after approximately 7 hours on 16 cores. The fundamentel mechanism, that produces that error is, that in numerics the following equation is valid:

$$1 + 10^{-16} = 1 \tag{3.38}$$

This results from the maximum span of digits, which can be stored is about 15. When we already stored 1 in a variable, we can not add 10^{-16}, because it is 16 powers of 10 smaller.

If we create a segment, we first choose a creator position τ in the whole interval $\tau \in [0,\beta)$. Then we determin the interval length $l_{\max}$ and choose a annihilator position τ'. We do that by producing a random number $r \in (0, l_{\max}]$ according to figure 3.10. Then we add it to the creator position $\tau' = \tau + r$.

If $l_{\max}$ is too small, we might end up with choosing a number of order $\mathcal{O} = 10^{-16}$. Together with $\mathcal{O}(\tau) = 1$ we end up with equation (3.38). This means, that instead of getting a τ' sightly larger than τ, we get a $\tau' = \tau$. According to section 2.2.3 this corresponds to a

[9] A typical runtime for detection is about 100 CPU hours.

```
double getRandomDouble(const double l_max=beta){
  /*
   * returns a random double between 0 and l_max
   */
  double out=rand()*l_max/RAND_MAX;
  return out;
}
```

Figure 3.10.: Simple c++ implementation of finding a random number $\in [0, l_{\max}]$. The constant RAND_MAX is of order $\mathcal{O} = 10^{10}$.

segments covering the whole imaginary time interval instead of a very short segment (which we intended to create). By this we created a not allowed segment picture (compare also 3.11).

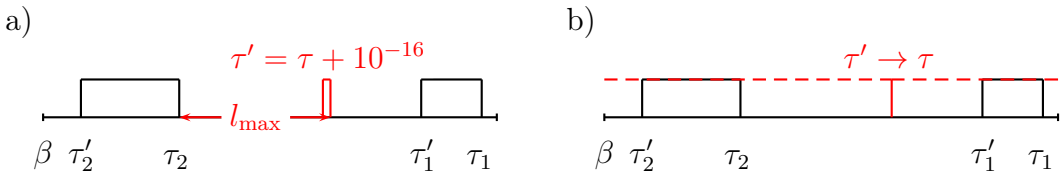

Figure 3.11.: Rounding errors can change a segment configuration qualitatively:
a) annihilator is chosen, which is slightly larger than the creator
b) due to numerical rounding, the annihilator becomes equal to the creator. This segment is interpreted differently (compare "note: half open segments" in section 2.2.3) and results in a forbidden segment configuration.

We can prevent this problem by defining a function in c++, which chooses a random number from a given interval. In this function we can include some asserts to ensure, that the number we choose is really element of the interval.

Precision of the analytic solution

A further point, which might lead to confusion, is the "precision of the analytic solution". We keep in mind, that the analytic solution of the SIAM according to (2.24) is only given in Matsubara domain. Hence, if we want to compare our results according to (2.75), we have to perform a (Fast) Fourier Transformation. For CT-QMC results with a high precision, the precision of the FFT has a not neglectablerole, as can be seen in figure 3.12. So if one does not get results in agreement with the analytic solution, the number of Matsubara frequencies may be the (non obvious) reason. A high number of Matsubara frequencies has no relevant influence on the runtime of the code, as the main computational effort derives from the fast update procedure and in the computation of the susceptibility.

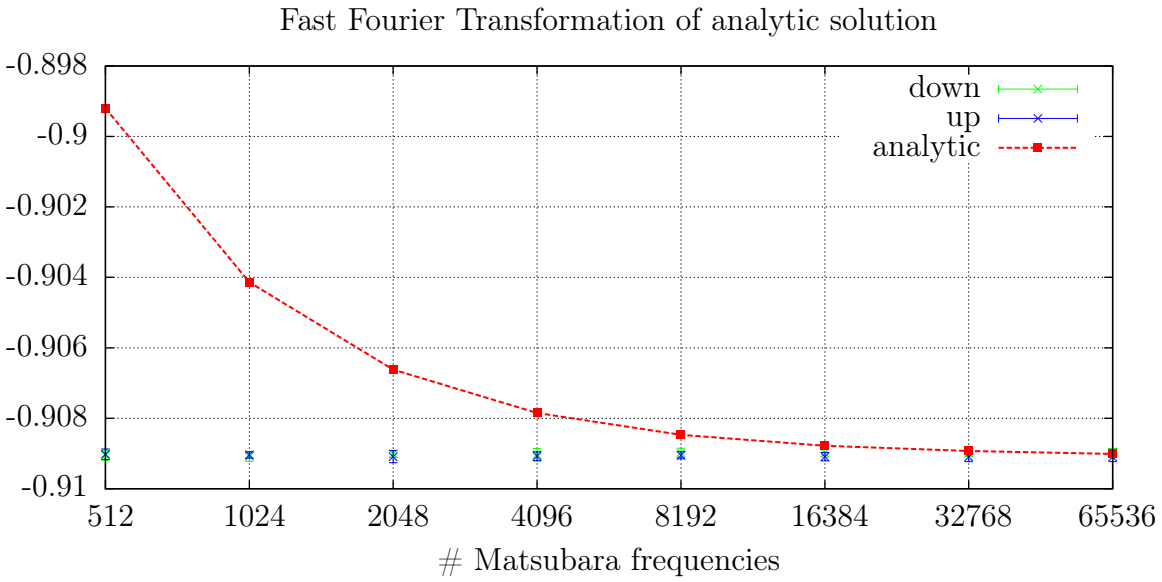

Figure 3.12.: Change of the analytic solution with the number of mesh points due to Fourier Transformation: The CT-QMC results stay basically the same, while the analytic solution moves into the error bars of the CT-QMC results with an increasing number of Matsubara frequencies.

3.7. Debugging

Fixed seeds

One problem of debugging a Monte Carlo simulation is the disability to reproduce certain errors, because we choose random numbers. This means, that problems, which occurred one run before cannot be investigated further and hence can not be repaired properly. To avoid that, we can work with **fixed seeds**. Fixing the seed means, that the initialisation point of the sequence of random numbers is fixed. Usually one uses an initialisation point, which depends on the current system time, but in this case we can just set it to the rank of the process. This helps a lot in finding current problems.

Segment antisegment symmetry

A very important property of the CT-QMC algorithm is the antisymmetric [10] handling of segments and antisegments. For debugging we can run the simulation twice with the same seed and input parameters $U = 0$ and $\epsilon_f = 0$. One time we start with an empty segment configuration and allow only the processes add / remove segment, the other time we start with a full occupied configuration and allow only add / remove antisegment processes. The

[10] meaning segments / antisegments have the same position in an unoccupied / occupied environment.

```
  #define SEED //switches on the fixed seed mode

  //some code

  seed=time(NULL)+noOfProc*rank; //usual way of seed finding
#if defined(SEED)
  if(rank==0){seed=1382954071;}//chrashed in 28long1, 29long1
  if(rank==1){seed=1384856893;}//chrashed without output in 2013_11_19-2
  if(rank==2){seed=419;}//chrashed in 23b1
  //ranks 3 to N-1 are still generated randomly
#endif
  srand(seed);

  //simulation
```

Figure 3.13.: Keeping track of the occurred errors, and provoking them by using fixed seeds. Rank denotes the index of the parallel MPI processes.

code will handle both runs exactly antisymmetric during the whole simulation, so we expect two antisymmtric pictures after **every** update..

To show this property, we look at the differen parts of the update probabilities from section 3.2: The proposal probabilities are always $\frac{1}{4}$. The acceptance probabilities does not differ as well. The determinant of Δ will stay the same, because the matrix Δ is just the transposed compared to the other run. The quantities ϵ_f and U, which affect the acceptance probabilities differently for segments and antisegments are set to zero.

4. Results: Hubbard model in a magnetic field

In this chaper we will present DMFT results using a CT-QMC solver for the Hubbard model with a magnetic field on a Bethe lattice in infinite dimensions. We investigate how the spectral function, the self energy and the **quasiparticle weight** (or **effective mass enhancement**) depend on an external magnetic field. The magnetic field shifts the chemical potential of spin $\uparrow$ with $+h$ and the chemical potential of spin $\downarrow$ with $-h$. The corresponding Hamiltonian reads:

$$\hat{H} = -\sum_{<i,j>,\sigma} t_{i,j}\hat{c}^{\dagger}_{i,\sigma}\hat{c}_{j,\sigma} + \sum_{i} U\hat{n}_{i,\uparrow}\hat{n}_{i,\downarrow} - \sum_{i,\sigma}\hat{n}_{i,\sigma}\left(\mu + \sigma h\right). \tag{4.1}$$

We expect a spin dependent change in the spectral function and the effective mass. In strongly correlated systems, the effective mass enhancement is exceptionally large. Local interactions may cause spin fluctuations; the application of a magnetic field can suppress these fluctuations and hence give rise to a neutralizing of this mass enhancement [3].

4.1. Testing the SIAM

This section describes some CT-QMC test-results. These have only minor physical meaning but a significant impact, concerning the validity and the performance of the CT-QMC code.

As we pointed out in section 2.1, the analytic solution (2.24) of the spinless Anderson model can be used to check large parts[1] of the code. The only point, where the interaction enters the CT-QMC simulation is the determination of the ratio between the weights of the old and the new configuration (3.16). If we look at the results shown in figure 4.2, we see a very good agreement of our results with the analytic solution even at $\tau = 0$. With a very high number of meshpoints for the Green function, the analytic solution is in the errorbars of the numeric result (compare section 3.6).

A further important test (comp. figure 4.3) is to go to high β (i.e. low temperatures), meaning high expansion orders (average number of segments). As described in 3.3, the expansion order determines the dimension of the fast update matrices. Hence a high expansion order

[1] estimation of the author: 95%

figure	expansion order	runtime
4.2	6	20min
4.3	92	20h

Figure 4.1.: expansion order vs runtime

leads to a significant increase of the runtime, as can be seen in tabular 4.1 . The results show, that an expansion order ≈ 90 is still accessible. Considering that CT-QMC is only one step of a DMFT loop with 10 - 100 iterations (from experience), we hit the limits of practicality [2]. An idea to increase the expansion order even more is to go to bigger computational resources. For the Augsburger Linux Computer Cluster (ALCC) 20 cores for 10 days are in general the maximum job size.

[2]These calculations were performed on the Augsburger Linux Computer Cluster (ALCC)

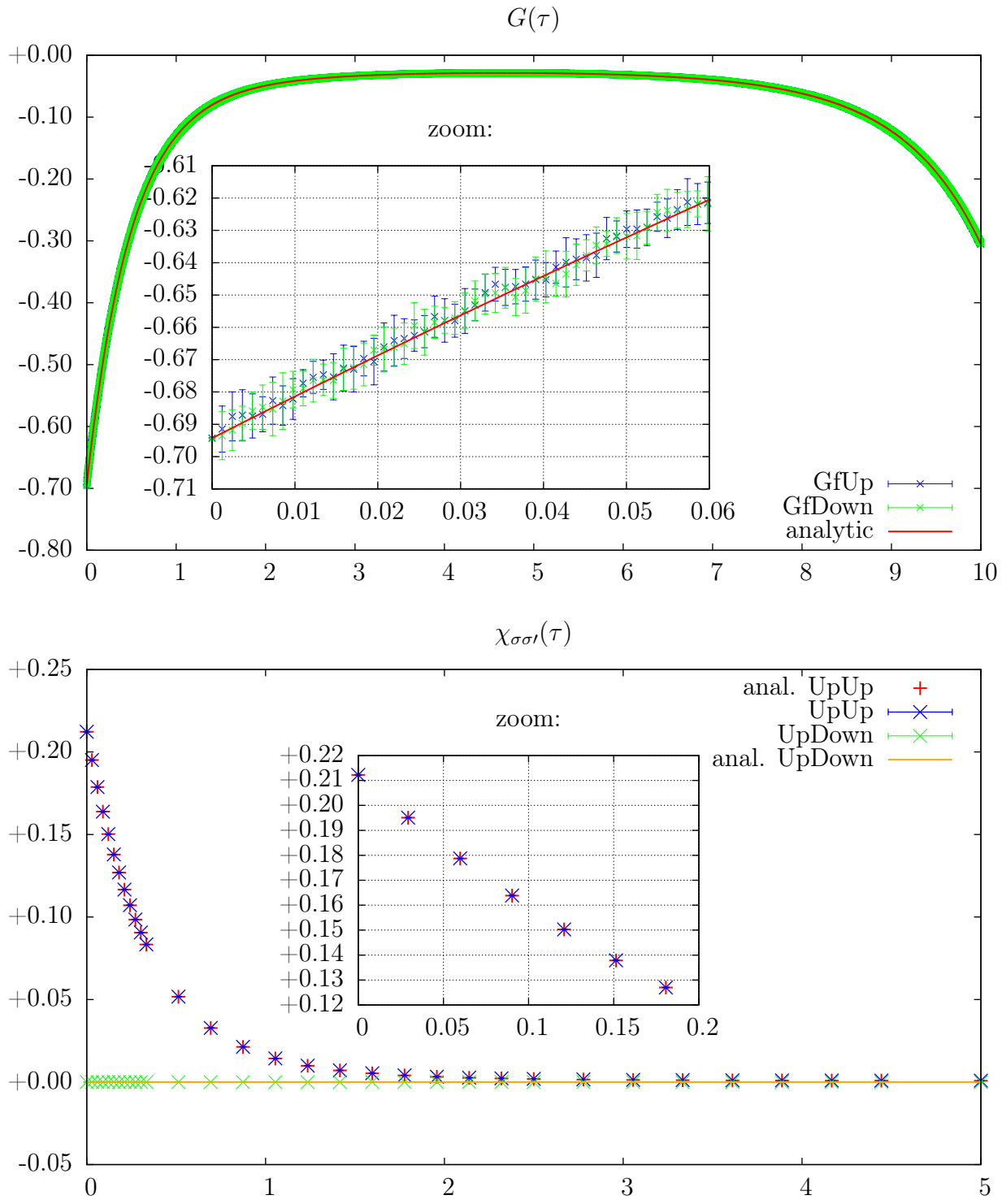

Figure 4.2.: **comparison with the analytic results:**
We observe a very good accordance with the analytic solution.
input parameters:
$U = 0; \beta = 10; |V|^2 = 2; \epsilon_f = 1;$
NoMeshp Gf=8192; NoMeshp Chi=32;
WarmUps=0.3mio; Measurements=20bins * 2mio
execution parameters:
average expansion order≈6; runtime=70min

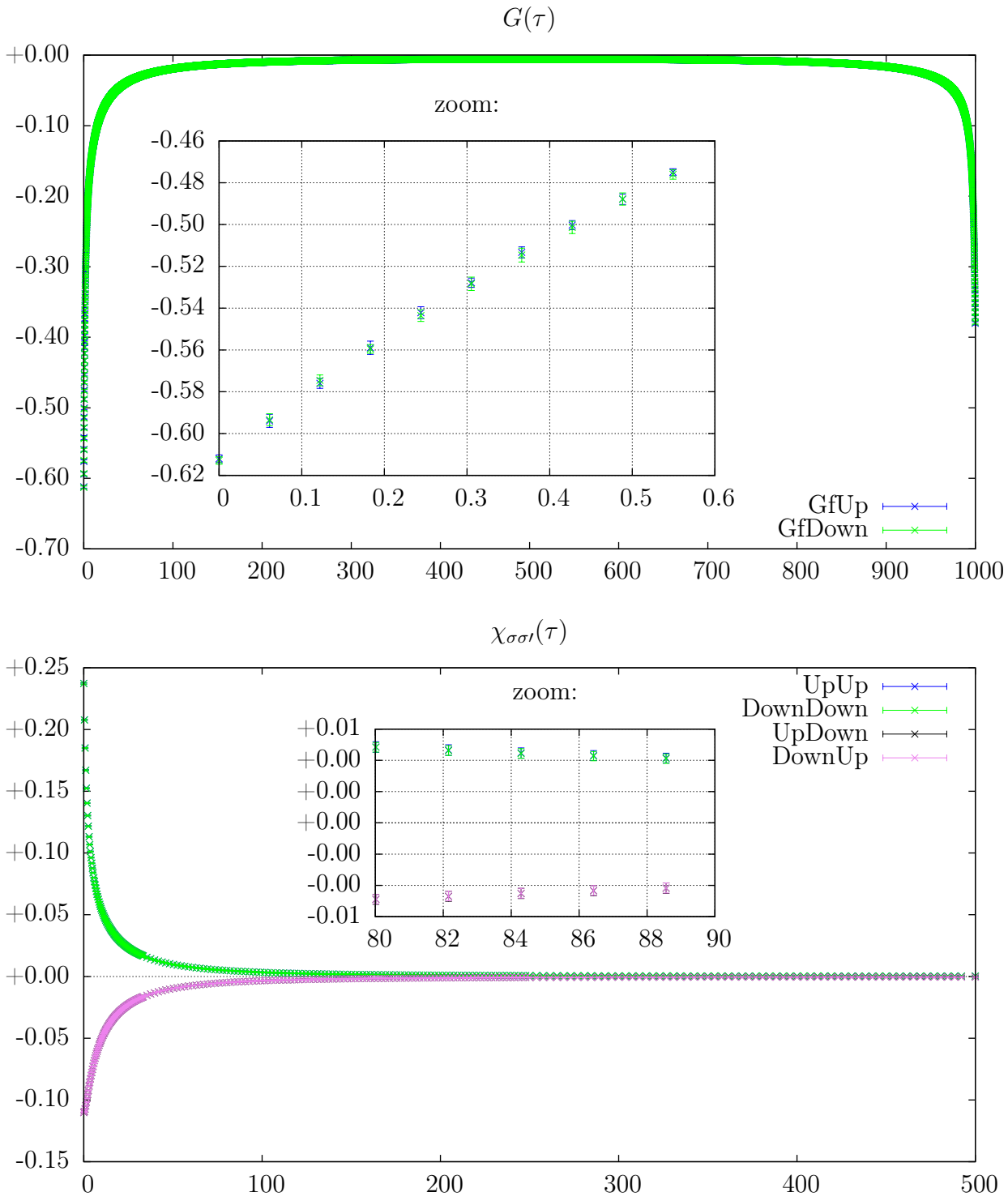

Figure 4.3.: **computational limits:**
We can increase beta up to 1000.
input parameters:
$U = 1; \beta = 1000; |V|^2 = 0.1; \epsilon_f = -0.2;$
NoMeshp Gf=16384; NoMeshp Chi=256;
WarmUps=0.3mio; Measurements=20bins * 0.1mio
execution parameters:
average expansion order≈92; runtime=20h

4.2. Comparison to NRG results

We use a semicircular non interacting density of states (Dos)

$$\mathrm{Dos}(\epsilon) = \frac{2}{\pi D^2}\sqrt{D^2 - (\epsilon+\mu)^2}, \tag{4.2}$$

as described in chapter 1. In the following we investigate the dependence of the spectral function for spin up electrons with respect to a magnetic field. The spin down spectral function $\rho_\downarrow$ is symmetric to $\rho_\uparrow$ with respect to 0 in the half filled case:

$$\rho_\downarrow(\omega) = \rho_\uparrow(-\omega). \tag{4.3}$$

Hence, for reasons of simplicity we do now plot the spin down quantities for the cases of half filling. Further we examine the effective mass of the particles at the Fermi surface.

We compare our results to the NRG results presented in [3]. The difference between the two used methods is, that NRG operates on the real energy axis at zero temperature, whereas CT-QMC operates in imaginary time domain for finite temperature. Hence we expect some distortion due to maxent [21] and some temperature dependent broadening of the spectral function in the CT-QMC results. We compare the spectral function and the inverse quasiparticle weight for different interaction strengths and different magnetic fields. The inverse quasiparticle weight describes the enhancement of the effective mass due to electronic correlation [3] and is computed according to the following formula [22], [3], [2]

$$z^{-1} = \frac{m^*}{m} = 1 - \frac{\partial \mathfrak{Re}\left\{\Sigma(\omega)\right\}}{\partial\omega}. \tag{4.4}$$

As we work in Matsubara domain, we have to rewrite this formula. The self-energy is an analytic quantity, so the Cauchy Riemann equations hold and we can perform the differentiation in Matsubara frequencies.

$$z^{-1} = 1 - \frac{\partial \mathfrak{Im}\left\{\Sigma(i\omega_n)\right\}}{\partial i\omega_n}\Big|_{z=0} = 1 - \frac{\mathfrak{Im}\left\{\Sigma(i\omega_0\right\}}{\omega_0} \tag{4.5}$$

$$\tag{4.6}$$

with

$$\omega_n = \frac{(2n+1)\pi}{\beta}. \tag{4.7}$$

In the second step we used that $\mathfrak{Im}\left\{\Sigma(z=0)\right\} = 0$.

In the following we will compare the CT-QMC and the NRG results for different magnetic fields in different parameter regimes.

We used the same input parameters as presented in paper [3]:

$$U = \ldots; \quad \beta = 30; \quad D = 2; \quad \mu = \frac{U}{2} \text{ (at half filling)}; \tag{4.8}$$

$$\mathfrak{m} = 0.15; \quad \text{MC warm ups} = 20\text{mio}; \quad \text{MC Steps} = 900\text{mio}. \tag{4.9}$$

[3] A high inverse quasiparticle weight hence indicates a strong influence by correlation.

4.3. Weak interaction strength

The weak interacting regime is simulated at $U = 2$. 100 mio MC Steps were used for these results. Without a magnetic field, we see a spectral function, which is similar to the non

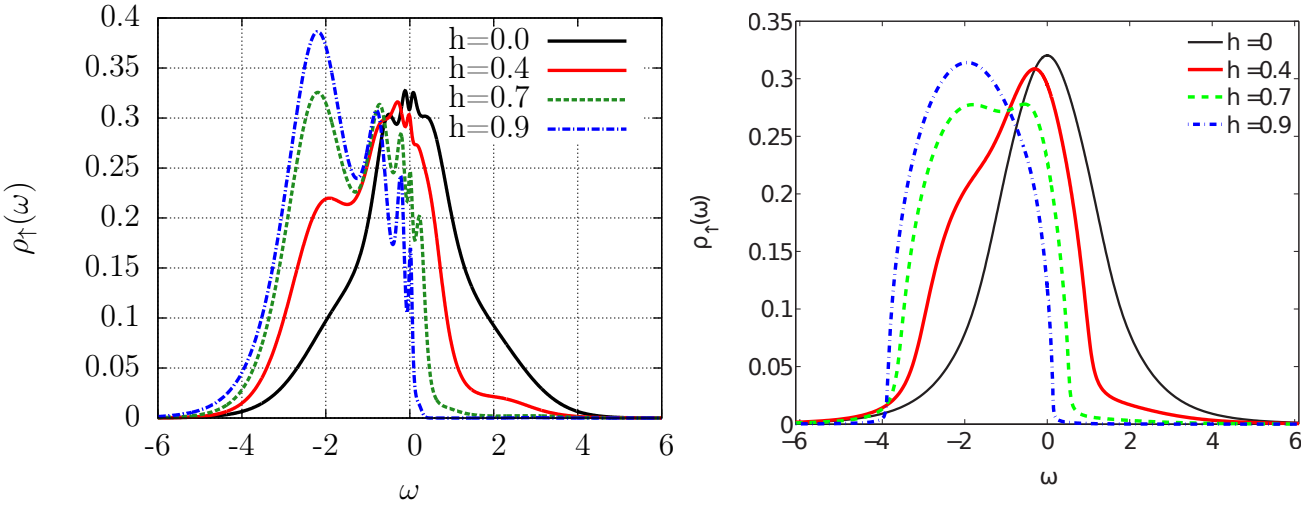

(a) CT-QMC results

(b) NRG results [3]

Figure 4.4.: spectral function for $U = 2$

interacting density of states. The interaction smooths out the edges but the general shape is the same. With increasing magnetic field the band gets broadened. For $h \approx 0.7$ the spectral density shows a weak two peak structure. For higher magnetic fields they loose it again. The oscillations on top of the CT-QMC results may origin from the attempt to reproduce sharp turning point features[4], which can be found in the NRG results. We notice, that these oscillations are stronger for the regime of high magnetic fields. These spectral functions exhibit a sharper turning point feature in the NRG results.

As can be seen in fig. 4.5, the effective mass is enhanced with a factor 1.5 ($m^* = 1.5m$) in the absence of a magnetic field ($h = 0$) and Coulomb interaction $U = 2$. For an increasing magnetic field this value decreases towards 1, which means a very small mass enhancement. This origins exactly from the mechanism of suppressed spin fluctuations described in the introduction of this chapter.

To illustrate the computation of the effective mass enhancement and to convey a better impression of the quantities of the DMFT loop, the self-energies are shown for the strongest and weakest magnetic field in figure 4.6.

We see very good agreement between the results of this work and the results of [3]. For the inverse quasiparticle weight it would be nice to compare more meshpoints to see if smaller details like the kink at $h = 0.9$ are reproduced as well.

[4] compare section 3.5

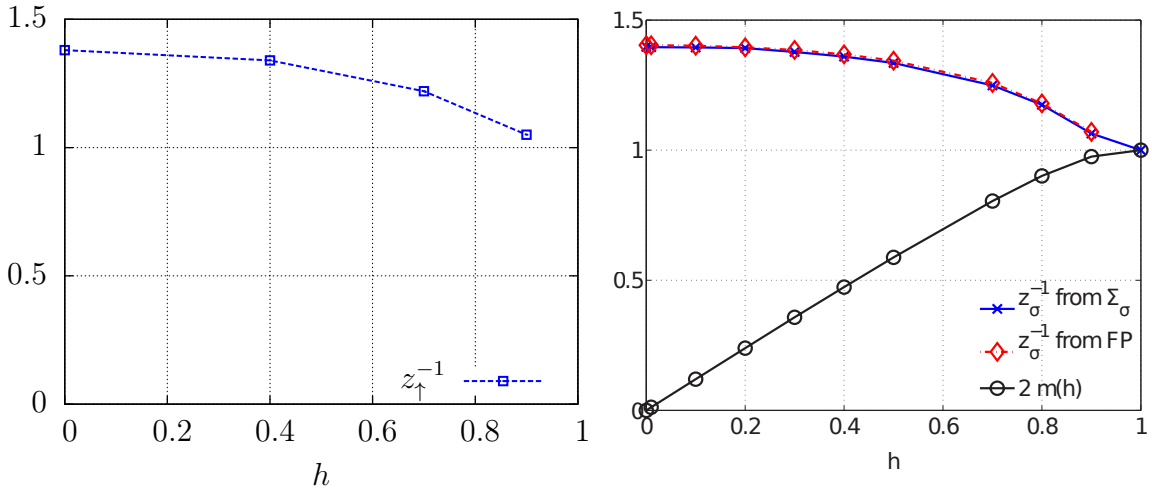

(a) CT-QMC results (b) NRG results [3]

Figure 4.5.: quasi particle weight for $U = 2$

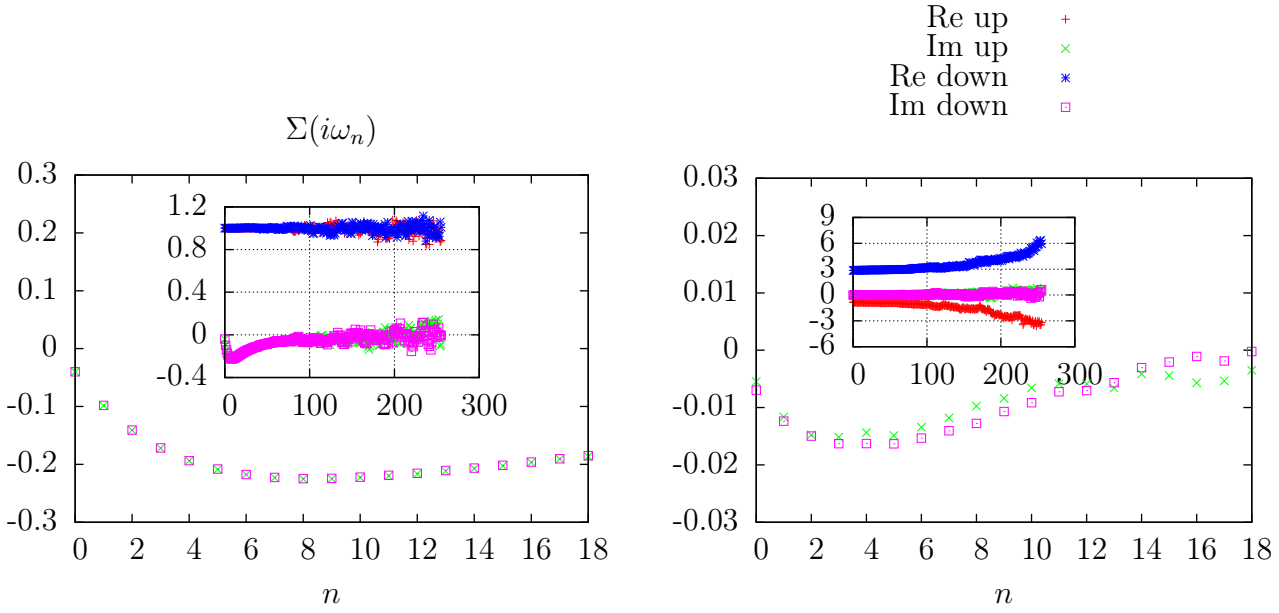

(a) h=0.0 (b) h=0.9

Figure 4.6.: Self-energies used for the calculation of the inverse quasiparticle weight in CT-QMC.

4.4. Intermediate interaction strength

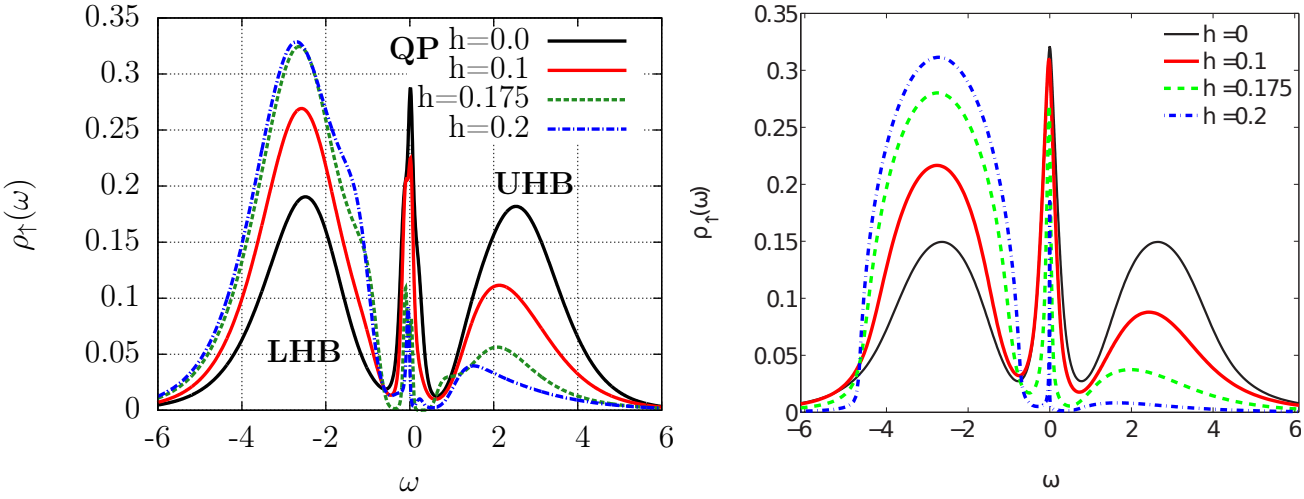

(a) CT-QMC results

(b) NRG results [3]

Figure 4.7.: spectral function for $U = 5$

For the intermediate regime an interaction strength of $U = 5$ has been chosen. We see a three peak structure in the spectral functions (figure 4.7) for all magnetic field strengths. With increasing magnetic field, more and more states are shifted towards the lower Hubbard band (LHB). The inverse quasiparticle weight (figure 4.8) starts with a value of ≈ 10 for $h = 0$ and is much lower for $h \approx 0.2$.

In the spectral function the comparison of the CT-QMC results with [3] show a quantitative good agreement. The CT-QMC result exhibits a broadening in the LHB for $h \geq 0.175$ at $\omega = -5$ and a peakier top region. These effects origin from the analytic continuation and the finite temperature. There are no oscillations on top of the CT-QMC spectral functions and no sharp turning points in the NRG results. The quasiparticle peak (QP) or Kondo peak at $\omega = 0$ differs slightly but shows the same features. NRG is the only solver, which can get the Kondo peak accurately, as it works on the real energy axis. Hence one is able to use a very dense mesh around $\omega = 0$, to produce highly accurate results in this region.

The results of the inverse quasiparticle weight capture only the same tendency as the results from [3]. Both results increase slowly with rising magnetic field, reach some maximum and decrease drastically for higher magnetic fields. The obvious distinction is, that the divergence of the inverse quasiparticle weight is not present in the CT-QMC data. We can see some features around $h = 0.12$ in the CT-QMC data, which indicate that the data in this region might not be reliable. According to (4.4), the quasiparticle weight strongly depends on self-energy around $\omega = 0$. As the spectral function differs at the Kondo peak, the other quantities in the self-consistency loop will differ as well. Hence the moderate agreement is not surprising. The convergence factor of the DMFT loop for these results is at $\mathcal{O}(10^{-4})$. Usually it is of order $\mathcal{O}(10^{-5})$. An further increase of the convergence factor was to expansive from a computational point of view.

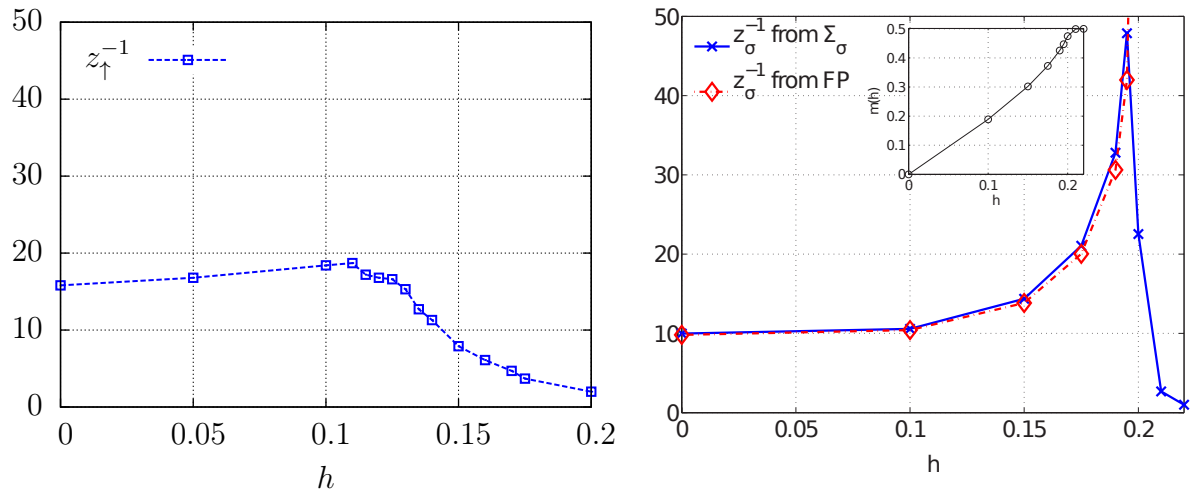

(a) CT-QMC results (b) NRG results [3]

Figure 4.8.: inverse quasiparticle weight for $U = 5$

4.5. Quarter filling

The interaction is again at intermediate interaction strength ($U = 5$) but the system is now at quarter filling ($n = 0.5$). As we are away from half filling now, the spin symmetry (4.3) is broken now. For this reason we show all quantities for both spin channels. Only 70 mio MC Steps were used to produce the results. To achieve quarter filling the chemical potential has to be set to the values listed in table 4.9.

magnetic field: h	chemical potential: μ
0.0	-0.2194
0.1	-0.2292
0.25	-0.2881
0.4	-0.3998

Figure 4.9.: chemical potential for different magnetic fields to establish quarter filling

In the case of quarter filling the non interacting density of states is only little modified. Some of the lower states are shifted to an energy $\omega \approx 7$ and form a small upper Hubbard band band (UHB) there. With increasing magnetic field, this effect is getting weaker / stronger for the spin up / down channel. For the up channel and $h = 0.4$ there are no more states shifted to $\omega \approx 7$. We hence yield the uncorrelated-like density of states in the spin up channel and a two peak structure in spin down channel. There is a two peak structure present in this spectral function (LHB and UHB). The oscillations for spin up ($h = 0.0$ at $\omega = -1$) and for spin down ($h = 0.1; 0.25; 0.4$ at $\omega = -1$) are artificial features due to the analytic continuation and do **not** indicate a three peak structure. We can observe a good agreement of the spectral functions of both spin channels. The oscillations on top of the

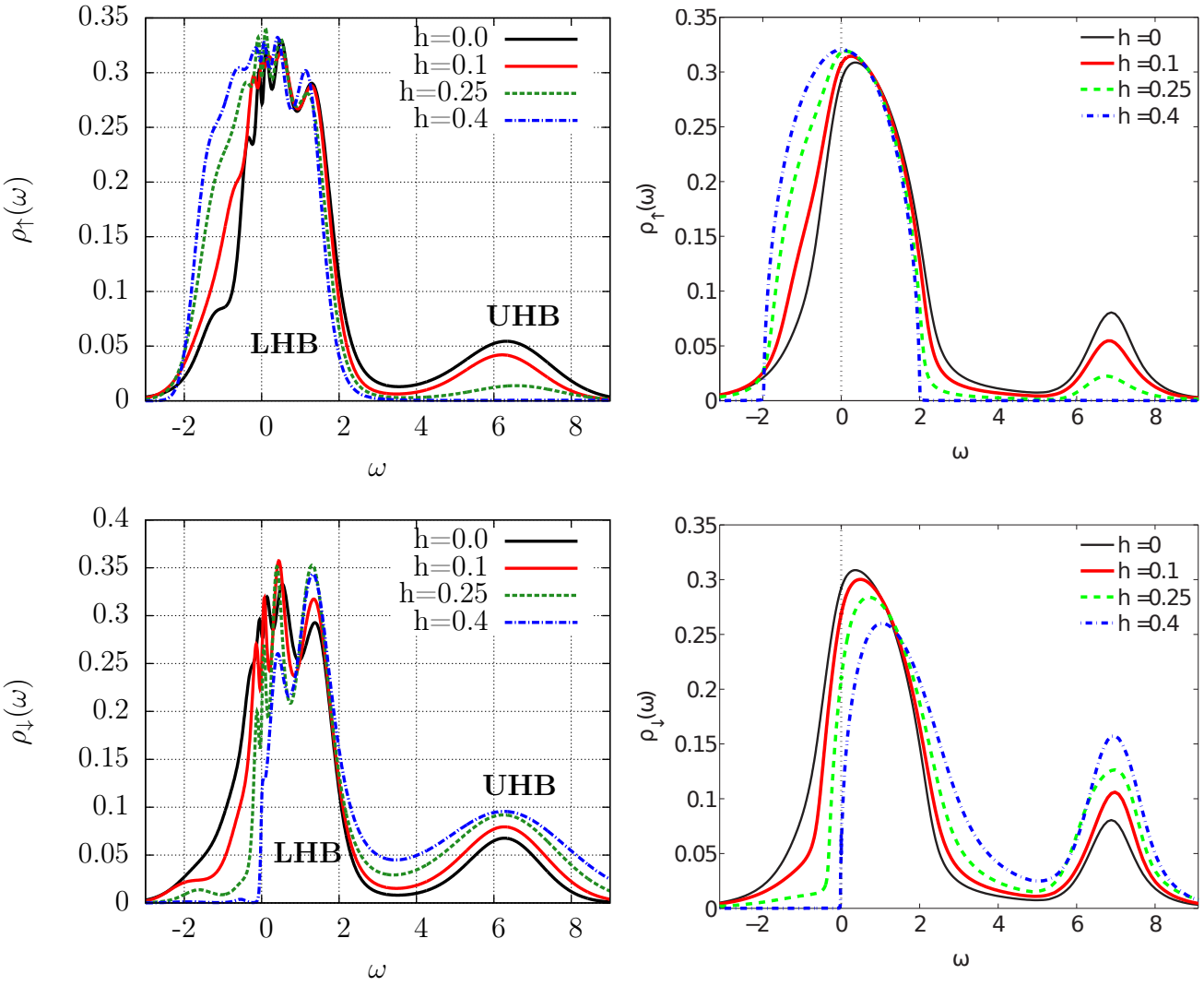

(a) CT-QMC results

(b) NRG results [3]

Figure 4.10.: spectral function for $U = 5; n = 0.5$

CT-QMC results may origin from the attempt to reproduce sharp turning point features[5], as argued in section 4.3. In contrast to this section we see stronger oscillations for $h = 0.0$ and $h = 0.1$ in the spin down channel, which correspond to the sharp turning point features at the top of the NRG spectral function at $\omega = 1$.

The inverse quasiparticle weight is in a range between 1 and 1.5 and is thereby much smaller than in the regime of intermediate interaction. It is very interesting to notice, that in the range $h \in [0.0; 0.1]$ the effective mass is decreasing for spin up and increasing for spin down at the same time. The inverse quasiparticle weight coincides very well with the results from [3]. The spin up channel is monotonic decreasing from 1.5 to 1, while the spin down channel is always approximately 1.5 and has a maximum at $h \approx 0.15$. This is the expected

[5] compare section 3.5

effect announced in the introduction of this chapter. More meshpoints would increase the comparability with [3].

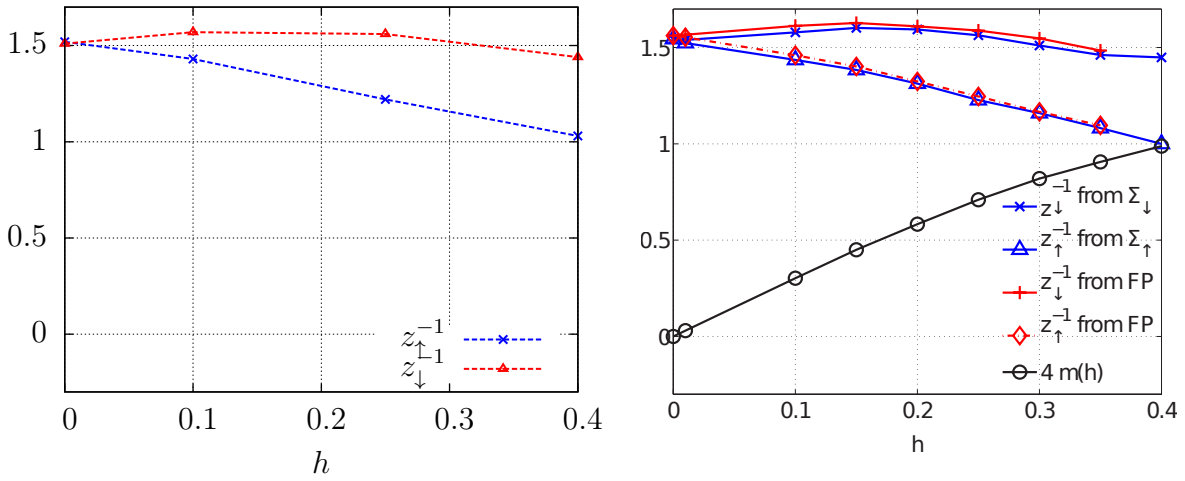

(a) CT-QMC results

(b) NRG results [3]

Figure 4.11.: quasi particle weight for $U = 5; n = 0.5$

Conclusion

To summarize the results of this work we repeat the key messages of each chapter.

In **Chapter 1** we presented the DMFT self consistence scheme in such a way, that it can be implemented easily. We gave an effective way of measuring the lattice occupation in Matsubara domain. Further we proofed that half filling can always be established by setting $\mu = \frac{U}{2}$.

The **2. Chapter** we solved the non-interacting Single Impurity Anderson Model analytically. This is a key feature for debugging, as approximately 95% of the CT-QMC code can be tested by that. Further we explained the segment picture and how the one- (Green function) and two- particle (susceptibility) correlation functions are measured in the hybridisation expansion of the interacting SIAM. The analytic derivations of this chapter are generalized to a SIAM with spin and an external magnetic field.

Chapter 3 explains how the CT-QMC algorithm works from a practical point of view. The Metropolis-Hasting algorithm can be used to handle a broad class of problems by sampling statistically trough indefinite configurations spaces. Further this algorithm is highly parallel, which plays a crucial role on todays high performance computing architectures. In the section about the Fast update procedure we introduce a highly effective speedup, which is a necessary foundation for every CT-QMC simulation. Further we pointed out some numerical difficulties and tricks suitable for debugging. People who are eager to implement similar concepts like the ones presented in this chapter are strongly encouraged to read this part.

In **Chapter 4** the CT-QMC results, which were produced by the CT-QMC code written in the context of this thesis, for the Hubbard model in a magnetic field are presented. We see how the Hubbard model behaves, in different interaction regimes and at different fillings under the influence of an increasing magnetic field. We see clear examples

- how the analytic continuation influences the quality of the results,
- how a spin polarisation can take place: fig. 4.4,
- a reduction of the effective mass enhancement with rising magnet field: fig. 4.11,

- and how the spectral function of one spin channel evolves back to the non-interacting DOS, while the spectral function of the other spin channel forms into a two-peak structure: fig. 4.10.

In most cases we see a good agreement of the numeric data compared with the NRG based results presented in reference [3]. Differences origin from the characteristics of used solvers and pointed out clearly.

A. Appendix: Poster

Results of this work were presented by Markus Dutschke on the ¨Frühjahrstagung der Deutschen Physikalischen Gesellschaft, Sektion kondensierte Materie, 30. März - 4. April 2014 in Dresden¨ in cooperation with Prof. Liviu Chioncel and Prof. Junya Otsuki [7].

Signatures of electronic correlation in half-metals

Markus Dutschke [1], Liviu Chioncel [1,2] and Junya Otsuki [1,3]

[1]Theoretical Physics III, Center for Electronic Correlations and Magnetism, Institute of Physics, University of Augsburg, Germany

[2]Augsburg Center for Innovative Technologies, University of Augsburg, D-86135 Augsburg, Germany

[3] Department of Physics, Tohoku University, Sendai 980-8578, Japan

Half-metalls

A new class of materials: metals and insualtors in the same time [1].

Magnets with an expected 100% spin polarization

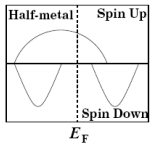

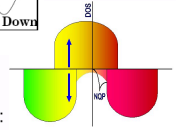

Within Dynamical Mean Field Theory [2] we address:

the interplay of ferromagnetism, electronic correlations and spin-polarization

Models: I. One band Hubbard model on the Bethe lattice [3]

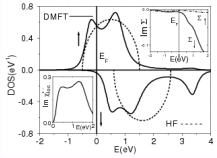

$$\hat{H} = -\sum_{i,j,\sigma} t_{i,j}\hat{c}^{\dagger}_{i,\sigma}\hat{c}_{j,\sigma} + \sum_{i} U\hat{n}_{i,\uparrow}\hat{n}_{i,\downarrow}$$

DMFT with Hirsch-Fye QMC

$$S^{eff} = -\int_0^{\beta} d\tau \int_0^{\beta} d\tau' c_{\sigma}(\tau)^{\dagger}\mathcal{G}_{\sigma}c_{\sigma}(\tau') + \frac{1}{2}\int_0^{\beta} d\tau n_{\sigma}(\tau)Un_{\sigma}(\tau)$$

$$S^{eff} \rightarrow QMC \rightarrow G_{\sigma} \rightarrow \mathcal{G}_{\sigma} = i\omega + \mu - t^2 G_{\sigma} - \frac{1}{2}\sigma\Delta$$

Models: II. The ground state of the Saturated Ferromagnet [4]

$$H = \sum_{k,\sigma} t_{k\sigma}c^{\dagger}_{k\sigma}c_{k\sigma} - I\sum_{q} S_q c^{\dagger}_{k+q\alpha}\sigma_{\alpha\beta}c_{k\beta} - \sum_{q} J_q S_{-q}S_q; \quad S_q = \sum_{k} c^{\dagger}_{k\sigma}c_{k+q\,-\sigma}$$

$$G^{\sigma}_{k}(E) = << c_{k\sigma}|c^{\dagger}_{k\sigma} >>_E = [E - t_k - \Sigma^{\sigma}_{k}(E)]^{-1}$$

- s-d Ferromagnet
- Eq. of motion for Green's Function
- Half-metallic ferromagnet n~0
- Analytic expression for the self-energy electron-magnon scattering

$$\Sigma^{\downarrow}_{k}(E) \approx \sum_{q} \frac{1 + N_q - n_{k-q\uparrow}}{E - t_{k-q\uparrow} - \omega_q}$$

$$N_{\sigma}(E) = \rho^{(MF)}_{\sigma}(E) - \sum_{\mathbf{k}} Re\Sigma_{k\sigma}(E)\delta'(E - t_{\mathbf{k}\sigma}) - \frac{1}{\pi}\sum_{\mathbf{k}} \frac{Im\Sigma_{k-\sigma}(E)}{(E - t_{\mathbf{k}\sigma})^2}$$

Models: III. Electronic structure calculation with DMFT

LDA+DMFT: Realistic electronic structure input: ab-initio calculation
Correlation effect: many body calcualtions [5]

$$\mathcal{H} = \mathcal{H}^{dc}_{\mathrm{LDA}} + \tfrac{1}{2}\sum_{i\{\sigma m\}} U^{i}_{m_1m_2m_1'm_2'} c^{+}_{im_1\sigma}c^{+}_{im_2\sigma'}c_{im_2'\sigma'}c_{im_1'\sigma}$$

$$\mathcal{H}^{dc}_{\mathrm{LDA}} = \sum_{ij\sigma\{m\}} h^{ij}_{m_1m_2}c^{+}_{im_1\sigma}c_{jm_2\sigma} - E^{dc}$$

$$W^{\sigma\sigma'}(i\omega) = \begin{pmatrix} W_{\uparrow\uparrow} & W_{\uparrow\downarrow} \\ W_{\downarrow\uparrow} & W_{\downarrow\downarrow} \end{pmatrix}$$

$$\Sigma_{12\sigma} = \sum_{34\sigma} W^{\sigma\sigma'}_{1342}G^{\sigma'}_{34}$$

$\Phi = \sum_{\boldsymbol{n}} \frac{1}{\boldsymbol{n}}$

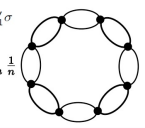

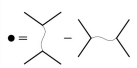

NiMnSb the prototype HMF [1,6]

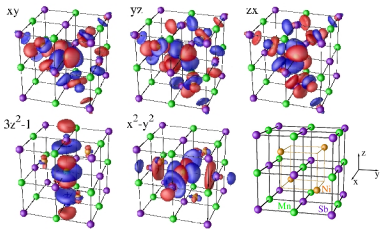

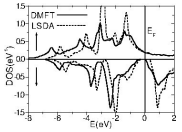

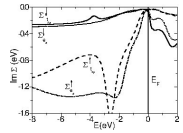

Magnetisation / Polarization at finite temperatures. [7]

$P(E,T) = \frac{N_{\uparrow}(E) - N_{\downarrow}(E)}{N_{\uparrow}(E) + N_{\downarrow}(E)} \propto < S_z >$

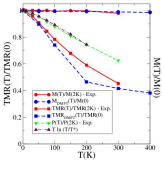

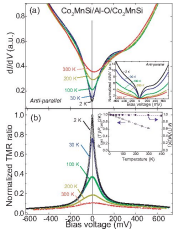

$\mathrm{Im}\Sigma_{\uparrow}(E) \propto (E - E_F)^2$

$\mathrm{Im}\Sigma_{\uparrow}(E) \sim (E - E_F)^2$

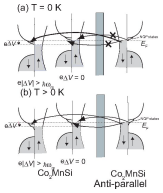

The CT-QMC (HYB-EXP) solver of DMFT [8,9]:

SIAM: $\hat{H} = \epsilon_f\hat{f}^{\dagger}\hat{f} + \sum_{k}\epsilon_k\hat{c}^{\dagger}_{k}\hat{c}_{k} + \frac{1}{\sqrt{N}}\sum_{k} V\hat{f}^{\dagger}\hat{c}_{k} + \frac{1}{\sqrt{N}}\sum_{k} V^{*}\hat{c}^{\dagger}_{k}\hat{f}$

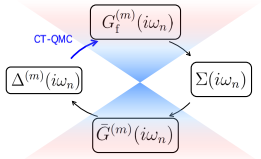

Hubbard model: $\hat{H} = -\sum_{i,j,\sigma} t_{i,j}\hat{c}^{\dagger}_{i,\sigma}\hat{c}_{j,\sigma} + \sum_{i} U\hat{n}_{i,\downarrow}\hat{n}_{i,\downarrow}$

Continuous time methods:

1. Eliminates the systematic errors associated with time discretization and the Suzuki-Trotter decomposition.
2. Allow in some cases to reduce significantly the sign problem .
3. Can be used to efficiently compute four-point correlation functions

Partition function and weights

$$\frac{Z}{Z_0} = \frac{1}{Z_0}\mathrm{Tr}\left\{\mathrm{T}_{\tau}e^{-\beta\hat{H}_0}\frac{1}{(2n)!}\sum_{n=0}^{\infty}\int_0^{\beta} d\tilde{\tau}_{2n}\ldots d\tilde{\tau}_1\left(\hat{H}_V(\tilde{\tau}_{2n}) + \hat{H}^1_V(\tilde{\tau}_{2n})\right)\ldots\left(\hat{H}_V(\tilde{\tau}_1) + \hat{H}^1_V(\tilde{\tau}_1)\right)\right\}$$

$$\frac{Z}{Z_0} = \sum_{n=0}^{\infty}\int_0^{\beta} d\tau_1\int_{\tau_1}^{\beta} d\tau_2\ldots\int_{\tau_{n-1}}^{\beta} d\tau_n\int_0^{\beta} d\tau_1'\int_{\tau_1'}^{\beta} d\tau_2'\ldots\int_{\tau_{n-1}'}^{\beta} d\tau_n' w(q_k)$$

$$w(q_k) = -|V|^{2n}\left\langle \mathrm{T}_{\tau}c^{\dagger}(\tau_1')c(\tau_1)\ldots c^{\dagger}(\tau_n')c(\tau_n)\right\rangle_{f_c}\left\langle \mathrm{T}_{\tau}f(\tau_1')f^{\dagger}(\tau_1)\ldots f(\tau_n')f^{\dagger}(\tau_n)\right\rangle_{f}$$

$$w(q_n) = \frac{\det(\Delta)}{1 + e^{-\beta\epsilon_f}}\prod_{n=1}^{n} e^{-(\tau_n' - \tau_n)\epsilon_f} \times \begin{cases} 1 & \text{for no wind case} \\ -e^{-\beta\epsilon_f} & \text{for wind case} \end{cases}$$

Segment picture

$$w(q_n) = \mathrm{sign}_{\mathrm{wind}}\det(\Delta)\frac{e^{-L\epsilon_f}}{1 + e^{-\beta\epsilon_f}}e^{-L_{ct}U}$$

Metropolis-Hasting algorithm

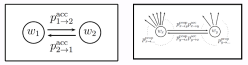

(Detailed) Balance Condition:

$$w_1 p^{acc}_{1\to 2} = w_2 p^{acc}_{2\to 1} \qquad w_x p^{prop}_{x\to y} p^{acc}_{x\to y} = w_y p^{prop}_{y\to x} p^{acc}_{y\to x}$$

Metropolis choice:

$$p^{acc}_{1\to 2} = \min\left(1, \frac{w_2}{w_1}\right) \qquad p^{acc}_{x\to y} = \min\left(1, \frac{p^{prop}_{y\to x}}{p^{prop}_{x\to y}}\frac{w_y}{w_x}\right)$$

CT-QMC results [10]

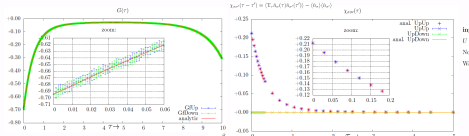

- Analytic solution of the non-interacting SIAM within the errorbars of CT-QMC
- G(0) has smaller errorbars, as determined differently (<n>)
- Expensive computation: high expansion order, susceptibility

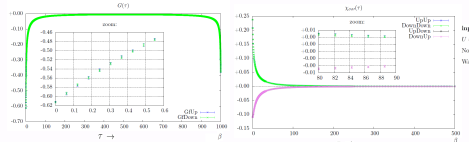

- Low temperatures possible

Preliminary Results:

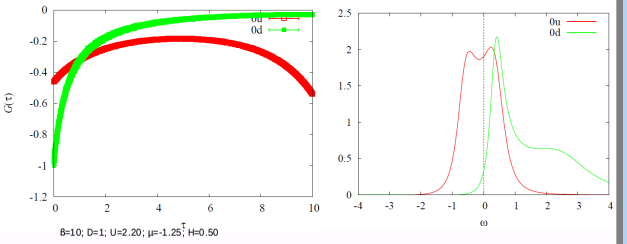

Further studies about different parameter settings are about to be done ...

References:

[1] R. A. de Groot, F. M. Mueller, P. G. van Engen, and K. H. J. Buschow Phys. Rev. Lett. 50, 2024 (1983)
[2] W. Metzner and D. Vollhardt Phys. Rev. Lett. 62, 324 (1989); G. Kotliar and D. Vollhardt Phys. Today 57, 53 (2004)
[3] L. Chioncel, M. I. Katsnelson, R. A. de Groot, and A. I. Lichtenstein Phys. Rev. B 68, 144425 (2003)
[4] M. I. Katsnelson, V. Yu. Irkhin, L. Chioncel, A. I. Lichtenstein, and R. A. de Groot Rev. Mod. Phys. 80, 315 (2008)
[5] A. I. Lichtenstein and M. I. Katsnelson Phys. Rev. B 57, 6884 (1998)
[6] A. Yamasaki, L. Chioncel, A. I. Lichtenstein, and O. K. Andersen Phys. Rev. B 74, 024419 (2006)
[7] L. Chioncel, Y. Sakuraba, E. Arrigoni, M. I. Katsnelson, M. Oogane, Y. Ando, T. Miyazaki, E. Burzo, and A. I. Lichtenstein Phys. Rev. Lett. 100, 086402 (2008)
[8] A. N. Rubtsov and A. I. Lichtenstein JETP Letters 80, 61 (2004)
[9] Emanuel Gull, Andrew J. Millis, Alexander I. Lichtenstein, Alexey N. Rubtsov, Matthias Troyer, and Philipp Werner Rev. Mod. Phys. 83, 349 (2011)
[10] M. Dutschke – Continuous Time – Quantum Monte Carlo impurity solver for the Hubbard model

Acknowledgements:

This research was supported in part by the Deutsche Foruschungsgemeinschaft through FOR1346.

Bibliography

[1] A. Abrikosov, L. Gorkov, and I. Dzyaloshinski, *Methods of Quantum Field Theory in Statistical Physics*, Pergamon Press Ltd., 2nd ed., 1965.

[2] R. Asgari, B. Davoudi, M. Polini, G. F. Giuliani, M. P. Tosi, G. Vignale, and W. Lafayette, *Quasiparticle self-energy and many-body effective mass enhancement in a two-dimensional electron liquid*, Phys. Rev. B3, 71 (2005), pp. 1–41.

[3] J. Bauer and A. Hewson, *Field-dependent quasiparticles in the infinite-dimensional Hubbard model*, Physical Review B, 76 (2007), p. 035118.

[4] H. Bruus and K. Flesberg, *Many-body Quantum Theory in Condensed Matter Physics*, vol. 7, Oxford University Press, Oct. 2002.

[5] R. K. Bryan, *European Biophysics Maximum entropy analysis of oversampled data problems*, Eur. Biophys J, (1990), pp. 165–174.

[6] P. Coleman, *Indroduction to Many Body Physics*, no publisher, 2012.

[7] M. Dutschke, L. Chioncel, and J. Otsuki, *Signatures of electronic correlation in half-metals*, in Verhandlungen der Deutschen Physikalischen Gesellschft: DPG Spring Meeting of the Condensed Matter Section, 2014, p. 440.

[8] A. L. Fetter and J. D. Walecka, *Quantum theory of many-particle systems*, Dover Publications, Inc., 2003.

[9] F. Gebhard, *The Mott Metal-Insulator Transition*, Springer, 1997.

[10] A. Georges, *Strongly Correlated Electron Materials: Dynamical Mean-Field Theory and Electronic Structure*, Lectures on the Physics of Highly Correlated Electron Systems VIII, (2004), p. 71.

[11] A. Georges, P. Cedex, W. Krauth, and M. J. Rozenberg, *Dynamical mean-field theory of strongly correlated fermion systems and the limit of infinite dimensions*, Rev. Mod. Phys., 68 (1996), pp. 13–125.

[12] A. Georges and G. Kotliar, *Hubbard model in infinite dimensions*, Phys. Rev. B, 45 (1992).

[13] C. Gramsch, *The mapping problem in nonequilibrium dynamical mean-field theory, M.Sc. Thesis.* 2013.

[14] R. Greiner, *Field Quantization*, Verlag Harri Deutsch, 1996.

[15] E. Gull, *Continuous-Time Quantum Monte Carlo Algorithms for Fermions*, PhD thesis, ETH Zurich, 2008.

[16] E. Gull, A. J. Millis, A. I. Lichtenstein, A. N. Rubtsov, M. Troyer, and P. Werner, *Continuous-time Monte Carlo methods for quantum impurity models*, Rev. Mod. Phys., 83 (2011), p. 349.

[17] K. Haule, *Diagrammatic Theory of Strongly Correlated Electron Systems*, PhD thesis, University of Ljubljana, 2002.

[18] P. Hohenberg and W. Kohn, *Inhomogeneous electron gas*, Physical Review, 136 (1964).

[19] M. Jarrell and J. E. Gubernatis, *Bayesian inference and the analytic continuation of imaginary-time quantum Monte Carlo data*, Physics Reports, 269 (1996), pp. 133–195.

[20] R. H. Landau, M. J. Paez, and C. C. Bordeianu, *A Survey Of Computational Physicas*, Princeton University Press, 2008.

[21] F. Mancini, *Lectures on the Physics of Strongly Correlated Systems XII: Twelfth Training Course in the Physics of Strongly Correlated Systems, Salerno, Italy, 1-12 October 2007*, American Institute of Physics, 2008.

[22] R. D. Mattuck, *A Guide to Feynman Diagrams in the Many-Body Problem*, Dover Publications, Inc., 2nd ed., 1992.

[23] W. Metzner, *Linked-cluster expansion around the atomic limit of the Hubbard model*, Physical Review B, 43 (1991), pp. 8549–8563.

[24] W. Metzner and D. Vollhardt, *Correlated Lattice Fermions in d =infinity Dimensions*, Physical Review Letters, 62 (1989), pp. 324–327.

[25] E. Mueller-Hartmann, *The Hubbard model at high dimensions: some exact results and weak coupling theory*, Z. Phys. B, 76 (1989), pp. 211–218.

[26] H. Press, S. A. Teukolsky, W. Vetterling, and B. P. Flannery, *Numerical Recipes in C: The Art of Scientific Computing*, vol. 29, Cambridge University Press, 2. ed., Nov. 2002.

[27] J. Skilling and R. Bryan, *Maximum Entropy Image Reconstruction - General Algorithm*, Monthly Notices of the Royal Astronomical Society, 211 (1984), p. 111.

[28] D. Vollhardt, *Dynamical Mean-Field Theory of Electronic Correlations in Models and Materials*, arXiv:1004.5069v3, (2010), pp. 339–403.

[29] P. Werner, A. Comanac, L. de Medici, M. Troyer, and A. Millis, *Continuous-Time Solver for Quantum Impurity Models*, Physical Review Letters, 97 (2006), p. 076405.

[30] P. Werner and A. Millis, *Hybridization expansion impurity solver: General formulation and application to Kondo lattice and two-orbital models*, Physical Review B, 74 (2006), p. 155107.

[31] G. C. Wick, *The Evaluation of the Collision Matrix*, Phys. Rev., 80 (1950).

Acknowledgements

Thanks to Junya Otsuki for teaching me the concept of CT-QMC. It was a pleasure to learn from you! I admire your ability to take a wrong question from me, explain to me why it is wrong and how it should be asked the right way and then answering it.

Thanks to Christian Gramsch for the stuff he taught me during the past 3 years, for great motivation and the pursuit to evolve further every single day.

Thanks to Michael Sekania. The discussions we had from time to time (usually after 10 PM and on the weekends :D) helped me a lot and made some things much simpler.

Thanks to Ivan Leonov for an open ear for my problems and numerical data for comparison.

Thanks to Christian Gramsch, Michael Stark, Johannes Thiele and Leonard Wossnig for a great time we had together on ¨theo3¨.

Thanks to Ralf Utermann, Marcus Kollar and Michael Stark for the technical support on the cluster, on our local machines and on the printer.

Thanks to Willhelm Appelt and Jaromir Panas. Thanks to Willi about being so interested about every physics topic (including my one) and to Jaro who does the same like me - "but for bosons". After about 1 hour of discussion the two of you helped me understanding / solving all problems I discussed with you.

Thanks to my supervisor Liviu Chioncel, for several lectures especially held for his Master students, for the journal club you initiated, for sending me to very useful workshops (MPI workshop Stuttgart, DFT workshop Jülich) and giving me the opportunity to present my work in the ¨Tagung der Deutschen Physikalischen Gesellschaft, Fachbereich Condensierte Materie¨ in Dresden [7]. I am looking forward to further projects with you!